Study of Multiphase Flows Through Different Geometries

By:

FAROOQ HUSSAIN
58-FBAS/PHDMA/F15

Department of Mathematics and Statistics
Faculty of Basic and Applied Sciences
International Islamic University, Islamabad
Pakistan
2019

surfaces
Geometry, Projective

Study of Multiphase Flows Through Different Geometries

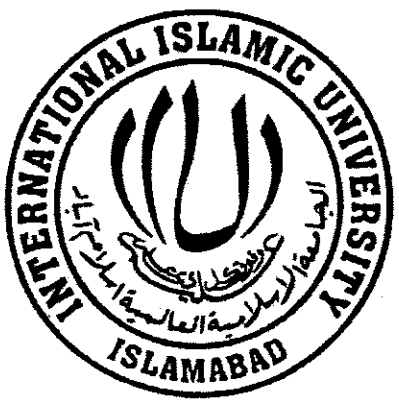

By:

FAROOQ HUSSAIN
58-FBAS/PHDMA/F15

Supervised By:

DR. RAHMAT ELLAHI

Co-Supervised By:

DR. AHMED ZEESHAN

Department of Mathematics and Statistics
Faculty of Basic and Applied Sciences
International Islamic University, Islamabad
Pakistan
2019

Study of Multiphase Flows Through Different Geometries

By:

FAROOQ HUSSAIN
58-FBAS/PHDMA/F15

A Thesis

Submitted in the Partial Fulfillment of the

Requirements for the Degree of

DOCTOR OF PHILOSOPHY IN MATHEMATICS

Supervised By:

DR. RAHMAT ELLAHI

Co-Supervised By:

DR. AHMED ZEESHAN

Department of Mathematics and Statistics
Faculty of Basic and Applied Sciences
International Islamic University, Islamabad
Pakistan
2019

Author's Declaration

I, **Farooq Hussain** Reg. No. **58-FBAS/PHDMA/F15** hereby state that my Ph.D. thesis titled: **Study of Multiphase Flows Through Different Geometries** is my own work and has not been submitted previously by me for taking any degree from this university, **International Islamic University, Sector H-10, Islamabad, Pakistan** or anywhere else in the country/world.

At any time if my statement is found to be incorrect even after my Graduation the university has the right to withdraw my Ph.D. degree.

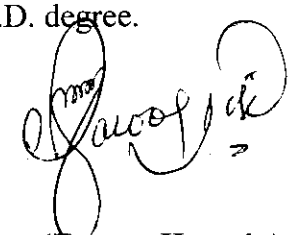

Name of Student: ***(Farooq Hussain)***
Reg. No. **58-FBAS/PHDMA/F15**
Dated: **13/11/2019**

Plagiarism Undertaking

I solemnly declare that research work presented in the thesis titled: **Study of Multiphase Flows Through Different Geometries** is solely my research work with no significant contribution from any other person. Small contribution/help wherever taken has been duly acknowledged and that complete thesis has been written by me.

I understand the zero tolerance policy of the HEC and University, **International Islamic University, Sector H-10, Islamabad, Pakistan** towards plagiarism. Therefore, I as an Author of the above titled thesis declare that no portion of my thesis has been plagiarized and any material used as reference is properly referred/cited.

I undertake that if I am found guilty of any formal plagiarism in the above titled thesis even after award of Ph.D. degree, the university reserves the rights to withdraw/revoke my Ph.D. degree and that HEC and the University has the right to publish my name on the HEC/University Website on which names of students are placed who submitted plagiarized thesis.

Student/Author Signature: _____

Name: **(Farooq Hussain)**

Certificate of Approval

This is to certify that the research work presented in this thesis, entitled: **Study of Multiphase Flows Through Different Geometries** was conducted by **Mr. Farooq Hussain,** Reg. No. **58-FBAS/PHDMA/F15** under the supervision of **Dr. Rahmat Ellahi** no part of this thesis has been submitted anywhere else for any other degree. This thesis is submitted to the **Department of Mathematics & Statistics, FBAS, IIU, Islamabad** in partial fulfillment of the requirements for the degree of **Doctor of Philosophy in Mathematics, Department of Mathematics & Statistics, Faculty of Basic & Applied Science, International Islamic University, Sector H-10, Islamabad, Pakistan.**

Student Name: Farooq Hussain **Signature:** _____

Examination Committee:

a) **External Examiner 1:**
Name/Designation/Office Address **Signature:** _____

Prof. Dr. Muhammad Ayub
Professor of Mathematics,
Department of Mathematics,
Hitech University, Taxilla.

b) **External Examiner 2:**
Name/Designation/Office Address) **Signature:** _____

Dr. Faisal Shazad
Associate Professor and Head of Department,
College of Aeronautical Engineering,
NUST, PAF Academy Risalpur, Pakistan.

c) **Internal Examiner:**
Name/Designation/Office Address) **Signature:** _____

Prof. Dr. Muhammad Sajid T.I
Professor

Supervisor Name:
Dr. Rahmat Ellahi **Signature:** _____ 13/11/19

Co-Supervisor Name:
Dr. Ahmed Zeeshan **Signature:** _____

Name of Dean/HOD:
Prof. Dr. Muhammad Sajid, T.I **Signature:** _____

Dedicated

"Death Leaves a Heartache No One Can Heal"

To My

Youngest and Loveliest

Sister (Deceased)

MARIA BANO

"Love Leaves a Memory No One Can Steal"

Acknowledgements

No word or phrase serves as the best alternate to express my humble gratitude to The Almighty Allah (SWT) for enabling me to complete my thesis well in time. I feel lucky for being the very first who coming off Balochistan and finishes Ph.D (Mathematics) from International Islamic University, Islamabad.

I offer my sincere thanks and appreciations to a person for his selfless cooperation, unconditional help and expertise guidance which assisted me to achieve this goal in time. I also take this opportunity to thank him for granting me the facility of his personal office, and feel honored to be trusted and counted on. Being a kind-hearted person, his commitment and devotion to his job are highly regarded by each student and staff. Above all, he is extremely diligent, punctual, sincere and an ideal supervisor. By all means one must accept that he is truly a blessing of Allah (SWT) for students and especially for research scholars. A man of all these and more such attributes is no one, but my respected supervisor **Dr. Rahmat Ellahi.**

Similarly, there is one more name that contributed a lot in fulfillment of my degree. His innovative ideas and research skills introduced me to some new field of study and equipped me to work with a different perspective. I really thank my co-supervisor **Dr. Ahmed Zeeshan** whose friendly and amicable nature made even difficult tasks easily achieved.

I also thank chairperson department of Mathematics and Statistics **Prof. Dr. Muhammad Sajid (T.I)** for his sincere efforts to provide better facilities and suitable atmosphere to PhD scholars so that they can fully focus on their research.

I thank all my research fellows seniors and juniors for sharing useful ideas, suggestions and timely assistance such as **Nasir Shehzad, Mudassar Maskeen, Shahid Nadeem,**

Bilal Arain, Aftab Gul, Zeehan Pervaiz, Fehid Ishtiq, Zeeshan Saith. Special thanks to **Imtiaz Ali Shah** and **Afraz Ahmad** for sparing time for me whenever i needed them. Finally, acknowledge the cooperation of my roommates **Umer Khattab** and **Shah Zahir Shah.**

I must be grateful to **Higher Education Commission (HEC)** of Pakistan for awarding me the most prestigious **"Indigenous 5000 PhD Fellowship"** for the pursuance of my Ph.D studies. This definitely, is not possible for a person having a very limited sources to pursuit his academic goals. I term the provision of such scholarships by the government of Pakistan as a blessing for poor students.

How i can forget the struggles and scarifies of my parents. It is very difficult for parents with low income to embellish their offspring with the trinket of education. My heart feels very heavy when i think of my beloved father **Mehmood Khan (Late)** at this joyous occasion who was a devotee of education, despite being a Truck driver. But, i console my heart by praying for his high ranks in "Jannat-ul-Firdos".

I would also like to thank my family members including my siblings, nieces and nephews for their sincere prayers, support and care. Last but not least, thanks to **Sabir Hussain** (my eldest brother) for everything that he has done for us and who keeps the family together. He is not only my foundation but, my inspiration and my champion. For, he solely brought us to the light when darkness was prevailing all around. May he live hale and healthy, Ameen.

(FAROOQ HUSSAIN)

58-FBAS/PHDMS/F15

Preface

To think about a flow diverse types of flows start striking one's mind, and most of such flow are *"Multiphase flows"*. Natural flows are of great importance and special kinds of flows that evolve the planet, for these all are comprising of more than one phase. Most commonly encountered such flows, is a granular flow which takes place in the form of floods, streams, avalanches, rain and dust storm etc. In practical point of view chemical and pharmaceutical processes along with the treatment of industrial waste involve the application of multiphase through different compositions of structures, such as by Farooq et al. [1]. They have analyzed a non-Newtonian fluid through a horizontal plates, placed at some distance. In order to examine the shear thinning effects, Reynolds model is brought under consideration. Mahabaleshwar et al. [2] use power series solution for the analysis of Couples stress fluid. The flow dynamics are studied over a plane sheet. Additional contributions of radiation and magnetic fields are also applied. A numerical solution for an unsteady flow is reported by Saad and Ashmway [3]. The Couette flow between the horizontal plates go through under the application of slip. The modeled differential equations are obtained by introducing suitable transformation. Akhtar and Shah [4] provide a routine solution for three different types of flows by taking Couple stress liquid. An MHD and Couette flow of Couple stress fluid are presented in [5,6] by employing uniform and non-uniform magnetic effects. An upper moving wall generating the flow of Maxwell fluid in [7-8] by different authors applying separate mathematical techniques. Some relevant individual and joint investigations of researchers provide analytical and numerical solutions given in the listed [9-15].

Shearing thinning effects due to temperature are reported by Poply et al. [16] on a magnetized flow. The work by Ellahi et al. [17] is regarding a closed form solution of

nanoflow of third-grade fluid. They designed two different flow problems by taking different viscosity models. A non-symmetric porous channel is considered of two-dimensional flow in [18]. Heating effects at the boundary varies the physical property of the liquid, besides the radiation. A comparative examination of fourth-grade fluid is performed by Nadeem and Ali [19]. A cylinder of uniform in structure contains steady flow. Ellahi et al. [20] give a numerical solution solid-liquid flow in a channel. The role of a constant pressure gradient and slippage at the boundary change the dynamics of magnetized flow. The help of numerical method such as Runge–Kutta with shooting is used for temperature depended viscosity. Chemical reactions also effectively bring change in the dynamics of viscoelastic fluid as shown in [21]. Makinde [22] presents the contribution of gravity on a steady flow. Viscosity gets affected by external source of heat placed adjacent to the surface of geometry. Similar kinds of investigation pertaining to the attenuation of fluid viscosity can also been seen in [23,24].

It is a recognized that nano size particles of metals are promising agent of heat enhancement. Normally, such particles are of size ranging from 1-100 nano-meter for various practical reasons. Such of these particles are considered by Karimipour et al. [25] in their survey. In which authors made analysis of heat and mass transfer incorporated with MHD.

Zeeshan et al. [26] form a multiphase flow with nanoparticles to transport bio-liquid. Jeffrey fluid being a main carrier transport the particles by following the peristaltic phenomena. Nasiri et al. [27] successfully analyzed two-phase flow model. The hydrodynamics of tiny particles and liquid are studied with a great skill. In [28] researcher examined a turbulent flow of silver-water nanofluid. Since, silver has the highest thermal conductivity. Some relevant references which highlight the significance of nanoparticles in thermal enhancement are [29-34].

In view of fore going above literature a multiphase flow of Hafnium-Couple stress fluid is investigated. Viscosity of base liquid is attenuated due to heating effects at the upper wall which reduces exponentially. A symmetric horizontal channel with confines the bi-phase flow with effects of uniform and constant externally applied magnetic fields. The source of motion of solid-liquid suspension is the uniform movement of upper sheet of the channel. A suitable numerical scheme yields an approximated solution which is vetted through parametric survey as well. The presented innovation provides in depth look of mechanical flows that follow multiphase phenomenon. The contents of this chapter have been published in the journal of **"Symmetry", 11 (2019) 647-659.**

Fluid flows go through rapid morpho-hydrodynamics changes subject to gravitational effects. Authors in [35,36] successfully study the thermal radiation effects over an inclined planes and isothermal permeable surface. The concerned boundary layer flow with the free convection thermophoretic is numerically investigated under the application of external magnetic fields. Ramesh et al. [37] studied a two-phase boundary layer flow over a stretching sheet. Dusty particles comprising the particulate flow is solved analytically under the influence of non-uniform heat sink/source. Different types of flows such as nanofluids in presence of chemical reactions etc., mainly generated by the inclination of steep channels have been examined by various researchers as enlisted in [38-40].

Magnetohydrodynamics flows are of great interest in fluid dynamics. There is much literature available in which researchers utilize magnetic fields to see the changing behavior of the fluid pattern. Peristaltic transport of fourth-grade fluid through a curved channel is focused by Khan et. al. [41]. Flow is disturbed by the externally applied magnetic fields. The presence of chemical reactions on the flow makes the investigation much more different and reveals some distinct findings. However, MHD flows of

nanofluid and ferrofluid, respectively, are discussed in [42-45]. Hakeem et al. [46] gives a comparative analysis of two types of fluids. He considers a Newtonian and non-Newtonian fluid over a horizontal plate with heat flux. Further, the reported involves, respectively magnetic and non-magnetic particles of nano-size.

Similarly, a nanofluid in a vertically resting annulus is addressed by Malvandi et al. [47]. Water serves as a base fluid suspended with aluminum oxide is studied under the influence of MHD and mixed convection. Ellahi et al. [48] give an analytic solution of nano Ferro-fluid over a rotating disk. The boundary layer flow is caused by the oscillation of and stretching of the disk. Prakash and Tripathi [49] focused on electroosmotic flow of nanofluid. They examined their findings in a tapered channel. In the same way in [50] authors came with the solution of non-Newtonian fluid through a wavy channel. However, An approximated solution of an unsteady Couple stress fluid is offered by Reddy et al. [51]. They chose a vertical plate for their analysis.

With the passage of time new flow problems are emerging containing tiny size of particles. The major application of nano particles gain high level of heat conductivity [52-57]. Esfe and Rostamian [58] considered engine oils and nanoparticles bearing the size 30nm for their empirical investigation. Their findings state that that the composed nano-lubricants display the non-Newtonian fluid behavior much similar to that of Power-law fluid model. Goshayeshi et al. [59] an experimentally study ferrofluid in a closed loop inside the pipe. Unlike, nano reports Hussain et al. [60] is relevant to a two-phase flow working with Newtonian fluid. Exact solutions are obtained and compared with each other by considering the particulate flow through three different physical geometries.

Very less attention has been to a special kind of non-Newtonian fluid such as Magma. Since, these flows are involving very high temperature therefore, the viscosity of such

fluid highly depend upon the temperature. Nichols [61] formally comes up with some calculations by determining the viscosity of Alika flow of Hawaii. His findings state that the viscosity of lave flow was fifteen times that of water. Melnik and Sparks [62] conclude that the crystallization causes strong mechanism to intensify the effects on extrusion of lava. Basaltic flow of Mauna Loa Hawaii is studied in literature [63]. Moore et al. have empirically gathered and reported the physical properties of then highly thick magmatic flow. In recent past, Diniega et al. [64] reveals a great variation in viscosity corresponds to a little variation in the temperature. And this results in a dynamic instability and this instability causes the formation of low-viscosity pathways. Above-mentioned literature reveals that a two-phase supercritical flow down a steep channel is still missing. Couple stress fluid serves as base fluid which drifts down with crystal and Hafnium through the channel. The simultaneous effects of magnetic and gravitations fields are taken into account. This investigation has been published in the **"Journal of Molecular Liquids", 286 (2019): Article No. 110898.**

The existence of multiphase fluid flows encountered in daily routine such as natural flows, mechanical or industrial flows. These flows comprise of Newtonian or non-Newtonian fluid as the main flow carrier. Consequently, there is a freedom of choice to investigate and analyze multiphase flows with respect to any kind of fluid even suspended with different types of particles. A reasonable amount of research related to, semi-infinite plans by considering such types of fluid flows under various conditions can be found in available literature, for example, the transversely applied magnetic field on the flow of Newtonian fluid is investigated by Palani and Srikanth [65]. The magnetized mass transfer is carried out on a vertical semi-infinite plate. Kumar [66] has given an analytic expression for the velocities in different directions, pressure gradient and skin friction. He has considered peristaltic flow of the Couple stress fluid through

an inclined channel in which long wavelength and low Reynold' number assumption restricts the nonlinear hydromagnetic fluid flow. A steady viscous flow through a porous medium is examined by Kumar et al. [67]. The flow over the inclined plate is influenced by chemical reaction involving mass transfer is tackled analytically. Murti et al. [68] have reported the flow along a semi-infinite plate which is positioned vertically while a heat mass transfer flow experiences the effects of chemical and double dispersion by means of Range-Kutta method. Ghosh and Usha [69] came up with quite different idea by considering two different fluids. Fluids are assumed to be miscible ones having different viscosities and indifferent densities whereas the flow is purely due the effects of gravity on the slippery tilted plane. The Chebyshev spectral collocation approach is applied to get the desired results for nonlinear model. Bognar et al. [70] have examined the velocity profile solely for non-Newtonian fluid at plane which is not up-right in position. The modeled flow of Power-law fluid is solved analytically under boundary layer assumptions. Variations caused by the rheological properties and positioning of the plane are investigated for sand-water and bentonite mixtures. Ganguly et al. [71] have presented two-dimensional power law fluid drifting down the slope. Boundary thickness of the flow is assumed to be very thin besides taking lubrication approximation to cope with governing equations. The MHD flow of micropolar fluid moving in two dimensions along with the heat flux is investigated by Uddin [72]. Flow is considered to be laminar and free from the influence of time. Resulting equations are numerically solved with the help of Range-Kutta method of order six. Among the various few most noteworthy efforts on nanoparticles, inclined plane and numerical techniques related to this problem are listed in [73-91].

A particulate flow over semi-infinite inclined plate has not been studied. Therefore, a fruitful effort flourished some useful findings of a particulate flow over a semi-infinite

inclined plane. Bi-phase flow comprises of Couple stress fluid and metallic particles of Hafnium. Findings of this chapter have been accepted for the publication in **"International Journal of Numerical Methods of Heat and Fluid Flow", DOI 10.1108/HFF-11-2018-0677 (2019).**

Among many scientific blessings nano-technology is one of them. It depends upon the special particles having size within range of between 1 nanometer to 100 nanometer, such particles are called "Nanoparticles". Similarly, a liquid which drifts any quantity of nanoparticles, is called "Nanofluid". The concept of nanofluid does not date back very long. Formally, the last witnessed the application of nanotechnology in various fields. Basic, utility of nano particle is to enhance thermal conductivity Choi and Eastman [92]. However, later engineers and scientists work out some other application of these tiny particles to benefit and make life easy [93,94]. Most prominently, [95,96] contains highly regarded proposed models of Buongiorno that relates mutual movement of nanoparticles and base fluid. Xu et al. [97] performed a nanofluid study in a vertical channel by considering the Buongiornio under the influence of mixed convection. They performed their investigation by taking a vertical channel.

One has to admit that peristaltic movement in living things is one of the most significant process and source of life. Different types of Newtonian and non-Newtonian fluid through esophagus to kidney or bladder obey peristatic motion. Because, grinded particles of food and quantity of liquid (such as water and blood) are pushed forward due to the flexible composition of veins and arteries [98-100]. Nabil et al. [101] have explained the significant contribution of nanofluids in peristalsis. They produced their results for flexible wall properties, lubrication, MHD, and porosity. Similarly, transport through two coaxial tubes affirms the application of endoscope or catheterized artery in medical sciences.

In the connection to the above-mentioned useful information it was perceived to focus on the physical application of gold nanoparticle (GNPs). Therefore, a physiological phenomenon such as peristalsis transport of blood through annulus is examined. The nanofluid made-up of blood (Couple stress fluid) suspended with gold particles provides a remedy for a fatal disease. The homotopy analysis method (HAM) base solution confirms the credibility of the solution which further verified by parametric study and found to be in great agreement. This endeavor has been published in the **"Journal of Molecular Liquids", 268 (2018) 149-155.**

In any living organism peristaltic motion is mainly caused by the contraction and expansion of some flexible organs. This applies a pressure force to drive fluids, for example, blood in veins, urine to bladder, and transport of medicines to desired locations are a few common biological examples. The rapid developments in nano-science have noticeably revolutionized almost every field of life, particularly in medical sciences. The advent of nano-technology in medicines has brought miraculous changes by reshaping the primitive methods of treatment. Nowadays, in developed countries operations are preferably performed without involving any prunes and cuts, which was once thought to be very complex and menacing for cancer treatment, brain tumors, lithotripsy, etc. Regardless of many other uses of nanofluids in industrial and practical settings, the primary objective of nanoparticles is the enhancement of heat transfer. It is mainly due to their high conductivity. In addition to the size and type of nanoparticles, other factors, such as temperature, volume fraction, and thermal conductivity are also very important to maximize the thermal conductivity. In pursuit of attaining such enhancement in the system, with the passage of time many useful models based on the physical properties of the matter have been developed. On the said topic, scholars have made full use of these models in their analyses, experiments, and conditions, which

have been discussed here very briefly. For instance, the investigation of Tripathi and Beg [102] explains the application of peristaltic micropumps and novel drug delivery systems in pharmacological engineering. They formulated their study with the help of the Buongiornio nanofluid model and treated blood as Newtonian fluid. The effects of channel inclination are studied by Shit and Roy [103]. The Couple stress fluid influenced by constant application of magnetic fields is used as the base fluid. Jamalabadi et al. [104] reported the effects of biomagnetic blood flow through a stenosis artery by means of non-Newtonian flow of a Carreau-Yasuda fluid model. They carried out a numerical simulation of an unsteady blood flow problem. Hosseini et al. [105] have presented the thermal conductivity of a nanofluid model. To perform this investigation, the nanofluid model is considered as the function of thermal conductivity of nanoparticles, base fluid, and interfacial shell properties by considering temperature as the most effective of parameters involved in the study. The most noteworthy contributions on the matter can be seen in the list of references [106–117]. Furthermore, activation energy has a key role in industries, in particular, effectively aggravating slow chemical reactions in chemistry laboratories to improve the efficiency of various mechanisms by adding activation energy to respective physical and mechanical processes. A few of the latest works related to this present work have been listed in [118,119].

In view of the existing literature, one can feel the application of nanotechnology in medical science opens a new dimension for researchers to turn their attention towards the effective role of chemical reaction and activation energy. Since, nanoparticles help in treating different diseases by means of the peristaltic movement of blood. Such biological transport of blood helps to deliver drugs or medicine effectively to the damaged tissue or organ. As a matter of fact, this effort is devoted to inspecting the

simultaneous effects of chemical reaction and activation energy for the peristaltic flow of Couple stress nanofluids in a single model, which is yet not available in literature, and could have dual applications in expediting the treatment process. The contents of this study have been published in the journal of **"Symmetry", 11 (2019) 276-292.**

Nomenclatures

A^*	Reaction rate constant	a_1	Dimensional radius of the inner tube (m)
a_2	Dimensionless radius of the outer tube (m)	b	Amplitude ratio
B_d	Brownian diffusion constant	B_0	Magnetic strength (Tesla)
B_r	Brinkman number	C	Concentration of the particles
$\tilde{c}$	Constant speed of the wave frame (ms^{-1})	E^*	Activation energy (J)
f	Body force (N)	f'	Similarity velocity of the fluid (ms^{-1})
F_D	Drag force coefficient	Fr	Froude number
F'	Similarity velocity of the particle (ms^{-1})	g	Dimensional gravitational force (ms^{-2})
g^*	Dimensionless gravitational force	G_r	Grashof number
h	Width of the channel (m)	k_1	Thermal conductivity of the fluid $(Wm^{-1}K^{-1})$
k_2	A constant ratio	k_3	Viscosity variation index
k_4	Constant ratio	k_5	Constant ratio
k^*	Boltzmann constant $(8.61 \times 10^{-5} eV/K)$		
M	Hartman number	N_b	Brownian motion parameter
N_t	Thermophoresis parameter	n^*	Fitted rate constant
P	Constant pressure dimensionless	p	Pressure $(Pa.s)$ or $(kgm^{-1}s^{-2})$
R	Dimensional radial coordinate (m)	Re	Reynolds number

r	Dimensionless radial coordinate	r_1	Radius of the particle (m)
r_2	Dimensionless radius of the inner tube	r_3	Dimensionless radius of the outer tube
S	Stokes drag force $(kgm^{-3}s^{-1})$	T	Temperature in fixed frame (K)
t	Time (s)	U	Dimensional radial velocity component (ms^{-1})
U_1	Constant/reference velocity (ms^{-1})	u_m	Free stream velocity (ms^{-1})
u	Dimensionless radial velocity component (ms^{-1})	u_f	Axial velocity of the fluid (ms^{-1})
u_p	Axial velocity of the particle (ms^{-1})	$\boldsymbol{V}$	Velocity in vector form (ms^{-1})
v_f	Lateral velocity of the fluid (ms^{-1})	v_p	Lateral velocity of the particle (ms^{-1})
W	Dimensional vertical velocity component (ms^{-1})	w	Dimensionless vertical velocity component (ms^{-1})
x	Similarity variable	Z	Dimensional vertical coordinate (m)
z	Dimensionless vertical coordinate (m)		

Greek symbols

α	Inclination of the plane $(radian)$	β	Viscosity parameter
β^*	Temperature ratio	η	Lateral coordinate (m)
ϵ	Embedding parameter	ϵ_1	A constant ratio
ϵ_2	Ratio of heat capacity of particle to heat capacity of fluid	ϵ_3	A ratio defined as $\frac{k^*}{(\rho c)_f}$

γ	Dimensionless Couple stress parameter	γ_1	Material constant associated with Couple stress fluid $(kgms^{-1})$
γ_c	Local Couple stress parameter (Dimensionless)	λ	Wave length (m)
λ'	Particulate fraction/number density of the particles	μ_0	viscosity of the base liquid $(kgm^{-1}s^{-1})$
μ_s	viscosity of solid-liquid suspension $(kgm^{-1}s^{-1})$	ν	Kinematic viscosity (m^2s^{-1})
ϕ	Concentration of nanoparticles (kgm^{-3})	ϕ_1	Concentration at lower inner tube (kgm^{-3})
ϕ_2	Concentration at outer tube (kgm^{-3})	ρ_{rel}	Relative density (kgm^{-3})
ρ_p	Density of the particle (kgm^{-3})	ρ_f	Density of the fluid (kgm^{-3})
c_f	Heat capacity of fluid $(m^2s^{-2}k^{-1})$	c_p	Heat capacity of particle $(m^2s^{-2}k^{-1})$
$\bar{\bar{\psi}}$	Stream function	σ	Electric conductivity of the fluid (Sm^{-1})
Θ	Dimensionless temperature	θ_1	Lower wall temperature (K)
θ_2	Upper wall temperature (K)	ξ	Axial coordinate (m)
τ_T	Thermal equilibrium time (s)		

Subscript

f	Fluid	p	Particle
nf	Nanofluid		

Table of contents

Chapter 1

Introduction

1.1 Preliminaries

This chapter defines and explains the phenomenon of *"Multiphase flows"*. In doing so, basic and very useful informations are given with suitable examples for the readers. This effort will enable readers to comprehend the fundamental concept of dissertation, as elaborated in the title. In the same way some basic definitions serve as the prerequisite for the facts given in the subsequent chapters.

1.2 Matter

Anything which has a mass and occupies space is called matter. For instance, water, iron and oxygen etc.

1.3 Phase

It is defined as a distinctive state of matter such as solid, liquid and gas. Phase can be the combination of same or different form of matters. For instance, combination of ice-cubes in the glass of water, dust particles in air, globs of oil in liquid etc.

1.4 Phase transition

One of the main attributes of matter is to change from one phase to another. It can be comprehended by the transition of dry-ice from solid phase to liquid or gas phase. similarly, the water from liquid phase to ice or vapors. The following are the two general topologies of phase which are identified as:

1.4.1 Continuous phase

A main carrier such as liquid and gas, is known as continuous phase. Water and air are the simplest and most commonly encountered continuous phases.

1.4.2 Disperse phase

Transport of finite number of particles; droplets; or gas bubbles in continuous phase is called the disperse phase. Some general examples of disperse phase includes:

- Globs of oil or grease in water.
- Droplets of liquid in gas.
- Dust particles in the air.
- Sand particles liquid.

1.5 Flow

A material which deforms subject to various forces acting upon. If this process of deformation continues to increase boundlessly, then the phenomenon is known as flow. For brevity, mostly a flow is the transport of continuous phase. However, the existence of flows suggests that there are major two types of phase-flows which are generally encountered in daily life.

1.5.1 Single phase flow

A flow which is solely of continuous phase is termed as single phase. Such phase flows are usually either of liquid-phase or gas phase. Examples include flow of water, honey and oxygen etc.

1.5.2 Multiphase flow

A flow which consists of two or more phases but of different kinds, is called multiphase flow. The existence of multiphase flows that are a significant feature of our environment. In this type of flow main carries is always of continuous phase. Few of

such ubiquitous multiphase flows are:

- Slurry flow
- Bubbly flow
- Water globs in oil

1.6 Spin

This is an intrinsic property of the charge particles. From fluid mechanics point of view, this may appreciably be termed as orientation or positioning of fluid particle. Einstein suggested two major orientations known as *"Spin-up"* and *"Spin-down"* of electrons going through the vicinity of magnetism.

1.7 Spin density

The difference between the total density of spin-up electrons and total density of spin-down electrons, is called spin density. Moreover, different electron belonging to different families have different spins, such as Fermion having half spin.

1.8 Angular momentum

The motion of an object having some mass in a circular or curved path is called angular momentum. Mathematically, it is the cross product of linear momentum and the radius of a curved path.

1.9 Dipole

A charge (i.e., positive or negative) on molecules is called Pole. Molecules with unlike charges attract each other. A molecule of liquid with such charge difference is called dipole. A dipole helps to identify fluids as to be of polar or nonpolar nature.

1.10 Fluid

Most generally fluid is defined as a substance which is capable of flowing. It has no

defined shape, but it takes the shape of its container. however, form technical point of view a substance that offers on or very little, resistance to externally applied stress or force. A fluid can be liquid, vapor or gas.

Among all physical properties of fluid, viscosity is the most significant which mechanically partitions fluid in to major two kinds.

1.10.1 Polar fluid

Polar nature is an important feature of any fluid molecules. Polar molecules are not aligned in a straight line, but enjoy the freedom to rotate and swing around before they start pointing in the direction of applied field. In this case net forces on a dipole don't cancel out each other. This property makes such fluids to be a great solvent such as water. Because it is a 'Y-shaped' molecule. Other examples include ethanol, methanol and sulphuric acid etc.

1.10.2 Non-polar fluid

This feature of fluid molecules chains them in a straight line due to the application of uniform field and yields the resultant net force to be zero. Such non-polar liquids are benzene, ethylene, and carbon dioxide etc.

1.11 Fluid microstructure

As a region wherein, the compositions or densities of a fluid change over the distance of order of magnitude of the range of molecular forces is called fluid microstructure. Fluid-solid interfaces, liquid-liquid interfaces, multiphase contact regions, gels, bubbles, drops and thin films etc. are some common example of fluid microstructure.

1.12 Couple-stress fluid

The rheology of non-Newtonian fluids explains that an inherent force in fluids, resists the additive force (i.e., force due to the inclusion of some additives) which results in a

Couple force. This newly emerged interaction of forces induces a supplementary Couple stress in the fluid. The fluid which display such intrinsic properties/features is termed as "*Couple-stress*" fluid. The most significant contribution of Couple stresses is to emerge a length-dependent effects that were not described in non-polar theories.

1.13 Stress tensor for the Couples-stress fluid

In 1984 Stokes [120] presented the basic theory and constitutive equations of Couple stress fluid. In the proposed theory he considered the couple stress besides classical Cauchy stresses. One of the two fundamental equations which have a great significance in fluid dynamics, for balancing the net flow through an open or closed conduit; is known as "Conservation of mass". Mathematically, it is denoted as:

$$\frac{\partial \rho}{\partial t} + \rho\, v_{k,k} = 0. \tag{1.1}$$

The other most commonly used is the well-known Navier-Stokes equation. This equation in a tensor form for a viscous, incompressible and with externally applied body force is expressed as:

$$\rho a_i = \tau_{ki,k} + \rho f_i. \tag{1.2}$$

Constitutive equations for the polar fluid in tensor notation form are given as:

$$\tau_{ij}^{S} = \tau_{(ij)} = -p\,\delta_{ij} + \lambda d_{kk}\delta_{ij} + 2\mu d_{ij}, \tag{1.3}$$

$$m_{ij}^{D} = 4\gamma_1 k^*{}_{ij} + 4\gamma' k^*{}_{ji}. \tag{1.4}$$

Where λ, μ, γ_1 and γ' are material constants. (This theory is co special case of general theories. And results predicted by this theory are of grater interests). It is noticeable that Couple stress (i.e., $\mathbf{M} = m$) depends on the vorticity gradient $\mathbf{K} = k^*$, from Eq. (1.3), it is clear that the skew symmetric part of $\mathbf{T}$ which is $\mathbf{T}^A$ cannot be determined. Which can be determined with the help of equation of motion provided m is known. The quantity trace $(\mathbf{M}) = m_{rr} = m$ can be determined by boundary condition in many

cases, due to symmetry in the geometry, $m = 0$. However, if $"m"$ remains undetermined through boundary condition, then it is assumed to be zero without any loss of generality. $\tau^{S}_{ki,k}$ can also be expressed by using constitutive equation for a polar fluid in tensor is given below

$$\tau^{S}_{ki,k} = -p_{,k}\,\delta_{ki} + \lambda d_{ss,k}\,\delta_{ki} + 2\mu\, d_{ki,k}. \tag{1.5}$$

In term of velocity the above equation can be expressed as:

$$\tau^{S}_{ki,k} = -p,i + (\lambda + \mu)\, v_{k,ki} + \mu\, v_{i,kk}. \tag{1.6}$$

Consider Cauchy's second law of motion

$$m_{ki,k} + \rho l_i + e_{iks} + \tau_{ks} = 0. \tag{1.7}$$

Taking curl on both side gives

$$e_{kis} m_{ts,t} + \rho\, e_{kis}\, l_i + e_{kis} e_{spq} + \tau_{pq} = 0. \tag{1.8}$$

This can be expressed as:

$$e_{kis} m_{ts,t} + \rho e_{kis} l_i + 2\left(\frac{\tau_{ki} - \tau_{ik}}{2}\right) = 0. \tag{1.9}$$

This can be deduced that $\tau^{A}_{ik} = \frac{\tau_{ki} - \tau_{ik}}{2}$, is an anti-symmetric, then Eq. (1.7) becomes

$$e_{kis} m_{ts,t} + \rho e_{kis} l_i + 2\tau^{A}_{ik} = 0. \tag{1.10}$$

This implies that

$$\tau^{A}_{ik} = -\frac{e_{kis}}{2}\left(m_{ts,t} + \rho l_i\right). \tag{1.11}$$

This is mandatory for this polar theory of fluid that the stress tensor to be non-zero. However, if the (body moments per unit mass) $l_i \neq 0$, then the Couple stress m_i are assumed to zero. Because Cauchy law of motion can only be satisfied by assuming

$\frac{m_{ij}}{\mathbf{M}_{ij}} = 0$ and $\frac{\tau_{ij}}{\mathbf{T}_{ij}} \neq 0$. As Eq. (1.11) involves Couple stress m which depend on vorticity gradient R as given below:

$$m_{ts} = m\delta_{ts} + 4\gamma_1 k^*_{ts} + 4\gamma' k^*_{st}, \tag{1.12}$$

$$\mathbf{K}_{ks} = \mathbf{W}_{s,k}, \tag{1.13}$$

$$\mathbf{W}_k = \frac{e_{kis} v_{s,i}}{2}, \tag{1.14}$$

$$d_{ks} = \frac{1}{2}(V_{s,k} + V_{k,s}). \tag{1.15}$$

It is important to note that

$$\mathbf{K}_{kk} = 0. \tag{1.16}$$

Because the average twist rate per unit lengths. If three mutually perpendicular lines elements is zero. In view of Eqs. (1.12) – (1.13) then Eq. (1.11) takes the following form

$$\tau^A_{ki} = -\frac{1}{2}\{e_{kis} m_{,s} + 4\gamma_1 e_{kis}\omega_{s,tt}\} + \rho e_{kis} l_s. \tag{1.17}$$

As

$$\omega_{t,t} = 0. \tag{1.18}$$

Therefore

$$e_{kis}\omega_s = \omega_{ki}. \tag{1.19}$$

Using Eq. (1.19)in Eq. (1.17), it is obtained as:

$$\tau^A_{ki} = -2\gamma_1 \omega_{ki,tt} + \frac{1}{2} e_{iks}(m_{,s} + \rho l_s). \tag{1.20}$$

We know that

$$e_{kis} m_{,sk} = 0. \tag{1.21}$$

Thus Eq. (1.20) can be transformed into the following

$$\tau_{ki}^{A} = -2\gamma_1 \omega_{ki,tt} + \frac{1}{2} e_{iks}(\rho l_s)_{,k}. \tag{1.22}$$

Since ω is anti-symmetric part and which is defined as:

$$\omega_{ki} = \frac{(v_{i,k} - v_{k,i})}{2}. \tag{1.23}$$

$$\tau_{ki,k}^{A} = -\gamma_1 v_{i,kktt} + \gamma_1 v_{k,kitt} + \frac{1}{2} e_{iks}(\rho l_s)_k. \tag{1.24}$$

Now, both $\tau_{ki,k}^{S}$ and $\tau_{ki,k}^{A}$ have been determined. Therefore, adding Eq. (1.6) and Eq. (1.24) yields

$$\tau_{ki,k} = \left.\begin{matrix} [-\rho_{,i} + (\lambda + \mu) v_{k,ki} + \mu v_{i,kk}] + \\ \left[-\gamma_1 v_{i,kktt} + \gamma_1 v_{k,kitt} + \frac{1}{2} e_{iks}(\rho l_s)_k\right] \end{matrix}\right\}. \tag{1.25}$$

Substituting Eq. (1.25) in Eq. (1.2), then the governing equation takes the following form

$$\rho a_i = \left.\begin{matrix} -\rho_{,i} + (\lambda + \mu) v_{k,ki} + \mu v_{i,kk} - \gamma_1 v_{i,kktt} + \gamma_1 v_{k,kitt} + \\ \frac{1}{2} e_{iks}(\rho l_s)_k + \rho f_i. \end{matrix}\right\}. \tag{1.26}$$

Using Gibbs's notation, then Eq. (1.1)and Eq. (1.26), finally in vector form give the following look

$$\frac{\partial \rho}{\partial t} + \rho\, (\nabla . \boldsymbol{V}) = 0, \tag{1.27}$$

$$\rho \boldsymbol{a} = \left.\begin{matrix} -\nabla \mathrm{p} + (\lambda + \mu) \nabla\, \nabla . \boldsymbol{V} + \gamma_1 \nabla^2 \nabla \nabla . \boldsymbol{V} + \mu \nabla^2 \boldsymbol{V} - \gamma_1 \nabla^4 \boldsymbol{V} + \\ \frac{1}{2} \nabla \times (\rho \mathbf{I}) + \rho \boldsymbol{f} \end{matrix}\right\}. \tag{1.28}$$

In the absence of body moments (i.e., $\mathbf{I} = 0$) the above equation transforms as:

$$\rho \boldsymbol{a} = -\nabla \mathrm{p} + (\lambda + \mu) \nabla\, \nabla . \boldsymbol{V} + \gamma_1 \nabla^2 \nabla \nabla . \boldsymbol{V} + \mu \nabla^2 \boldsymbol{V} - \gamma_1 \nabla^4 \boldsymbol{V} + \rho \boldsymbol{f}. \tag{1.29}$$

Where $\boldsymbol{a}$ is defined as:

$$\boldsymbol{a} = \frac{\partial \boldsymbol{V}}{\partial t} + (\boldsymbol{V}.\nabla)\mathbf{V}. \tag{1.30}$$

Since, the fluid is instinctively incompressible in nature, then

$$\nabla.\boldsymbol{V} = 0. \tag{1.31}$$

This yields to viscous, incompressible Couple stress fluid momentum equation under the influence of applied external body force

$$\rho\left(\frac{\partial \boldsymbol{V}}{\partial t} + (\boldsymbol{V}.\nabla)\mathbf{V}\right) = -\nabla p + \mu\nabla^2\boldsymbol{V} - \gamma_1\nabla^4\boldsymbol{V} + \rho\boldsymbol{f}. \tag{1.32}$$

1.13.1 Boundary conditions for Couple stress fluid

Six boundary condition are needed, three of six can be obtained by assuming no-slip at boundary. The remaining three can be obtained by the given below two sets of assumptions.

1.13.1.1 Couple stresses are zero at the boundary

This assumption declares that the Couple stress at the wall vanish. This show that mechanical interactions at the wall are equivalent to the force distribution only. This condition essentially restricts the gradient of ω at the wall or boundary.

1.13.1.2 Vorticity at boundary is equal to the rate of rotation of boundary

According to this assumption the effects of boundary walls do not allow fluid elements /particles to rotate relative to the boundary. This can be turned as the vorticity at the boundary is equal to rate of rotation of boundary. Moreover $\omega = \omega_B$ at the boundary is same as Couple stress ($\gamma \to 0$) tend to zero, and the solution approaches to that of Navier-Stoked equations. Whereas, earlier it was thought differently if vorticity were equal angular velocity of the boundary at the wall.

1.13.2 Couple stress parameter

This dimensionless constant or number which is denoted as γ, distinguishes Couple stress fluid. The Couple stress fluid parameter is identified by containing a new material constant i.e., which is denoted as γ_1 responsible for Couple stress and lubricant viscosity.

1.13.3 Engineering and practical applications of Couple stress fluid

Among all non-Newtonian fluids, Couple stress fluid model enjoys a special status due to the spin field which produces anti-symmetric stresses. And, these stress are called couple stress. Common examples of such fluid includes liquid crystals, colloidal fluids, liquids containing long chain molecules such as polymer suspensions, blood and lubrications etc. These fluids have great significance natural, mechanical as well as many physical phenomenon such as peristalsis etc.

1.14 Governing equations (For solid-liquid flows)

The main governing equations which deal with the two-phase flow suspension having Couple stress fluid as the base fluid are given as:

1.14.1 Continuity equation

1.14.1.1 For fluid phase

$$\frac{\partial \rho_f}{\partial t} + \nabla.(\rho_f \boldsymbol{V}_f) = 0, \tag{1.33}$$

1.14.1.2 For particle phase

$$\frac{\partial \rho_p}{\partial t} + \nabla.(\rho_p \boldsymbol{V}_p) = 0. \tag{1.34}$$

1.14.2 Momentum equation

1.14.2.1 For fluid phase

$$\rho_f(1-C)\left(\frac{\partial}{\partial t}+\boldsymbol{V}_f.\nabla\right)\boldsymbol{V}_f=\left.\begin{matrix}(1-C)\nabla p+(1-C)\mu_s\nabla^2\boldsymbol{V}-\\ \gamma_1(1-C)\nabla^4\boldsymbol{V}_f+CS(\boldsymbol{V}_p-\boldsymbol{V}_f)+\\ \boldsymbol{J}\times\boldsymbol{B}+g\rho_f\sin\alpha\end{matrix}\right\}. \tag{1.35}$$

1.14.2.2 For particle phase

$$\rho_p C\left(\frac{\partial}{\partial t}+\boldsymbol{V}_p.\nabla\right)\boldsymbol{V}_p=-C\nabla p+CS(\boldsymbol{V}_f-\boldsymbol{V}_p). \tag{1.36}$$

1.14.3 Energy equation

1.14.3.1 For fluid phase

$$\rho_f c_f(1-C)\left(\frac{\partial}{\partial t}+\boldsymbol{V}_f.\nabla\right)\theta_f=\left.\begin{matrix}(1-C)k_1\nabla^2\theta_f+(1-C)(\boldsymbol{T}:\boldsymbol{L})+\\ \frac{C(\rho_p c_p)}{t_T}(\theta_p-\theta_f)\end{matrix}\right\}. \tag{1.37}$$

1.14.3.2 For particle phase

$$\rho_p c_p C\left(\frac{\partial}{\partial t}+\boldsymbol{V}_p.\nabla\right)\theta_p=\frac{C(\rho_p c_p)}{t_T}(\theta_f-\theta_p). \tag{1.38}$$

1.15 Governing equations (For Nano fluid flows)

The main governing equations which deal with the nanofluid flow suspension having Couple stress fluid as the base fluid are given as:

1.15.1 Continuity equation

$$\frac{\partial\rho_{nf}}{\partial t}+\nabla.(\rho_{nf}\boldsymbol{V})=0. \tag{1.39}$$

1.15.2 Momentum equation

$$\rho_{nf}\left(\frac{\partial}{\partial t}+\boldsymbol{V}.\nabla\right)\boldsymbol{V}=\left.\begin{matrix}\left[\varphi\rho_{np}+(1-\varphi)\{\rho_{nf}(1-\beta_T(T-\theta_w))\}\right]\boldsymbol{g}-\\ \nabla p+\mu_{nf}\nabla^2\boldsymbol{V}-\gamma_1\nabla^4\boldsymbol{V}\end{matrix}\right\}. \tag{1.40}$$

1.15.3 Energy equation

$$(\rho c)_{nf}\left(\frac{\partial}{\partial t}+\boldsymbol{V}.\boldsymbol{\nabla}\right)T = k_1\nabla^2 T + (\rho c)_{np}\left[D_b\boldsymbol{\nabla}\varphi\boldsymbol{\nabla}T + \frac{D_T}{\theta_w}\boldsymbol{\nabla}T.\boldsymbol{\nabla}T\right]. \qquad 1.41$$

1.15.4 Concentration of nanoparticles

$$\left(\frac{\partial}{\partial t}+\boldsymbol{V}.\boldsymbol{\nabla}\right)\varphi = D_b\nabla^2\varphi + \frac{D_T}{\theta_w}\nabla^2 T. \qquad 1.42$$

1.16 Conduit

Conduit is a physical structure in which liquid flows (or contains). The different conduits separate shape and configuration plausible to demand and scenario. But, the transport of fluids is mainly, in two types of conduits:

1.16.1 Open conduit

A conduit with one free surface, is called an open conduit. Most common examples of open channels include rivers, canals, streams etc. Fluid flows in such conduit is known as *"open channel or conduit flow"*. Flow transport in such conduits is caused by the influence of gravity in addition to free surface open to atmospheric pressure.

1.16.2 Closed conduit

A conduit which does not a free surface is called closed conduit. Pipes, circular cylinders and converging-diverging nozzles are few daily encountered specimens of closed conduits. A closed conduit is also known as *"Pressurized conduit"*. For, the longitudinal pressure difference (or *Hydraulic pressure*) causes the fluid motion along the channel. Therefore, such fluid flows are called "*closed conduit*".

Chapter 2

Two-phase Couette flow of Couple stress fluid with temperature dependent viscosity

This chapter provides a numerical survey of two-phase flow between two horizontal flat plates. The constant motion of the upper sheet generates the flow. However, the contribution of axial pressure gradient is also brought under consideration. The suspension of base fluid with particles is further influenced by heating at the wall. The temperature dependent viscosity model, namely Reynolds' model is utilized. The Runge-Kutta scheme with shooting method is used to tackle nonlinear system of equations. It is observed that the velocity decreases by increasing the values of Hartman number. However, due to the influence of heating wall weakens viscous forces and causes shear thinning effects. This leads to increase the velocity of the fluid for greater values of viscosity parameter and as a result temperature profile also declines.

2.1 Mathematical formulation

A particulate flow of Couple stress fluid is considered between two plates which are separated by the distance 2 h, such that upper wall moves with the uniform velocity U_1 which is only source of concerned bi-phase flow, as shown in Figure (2.1).

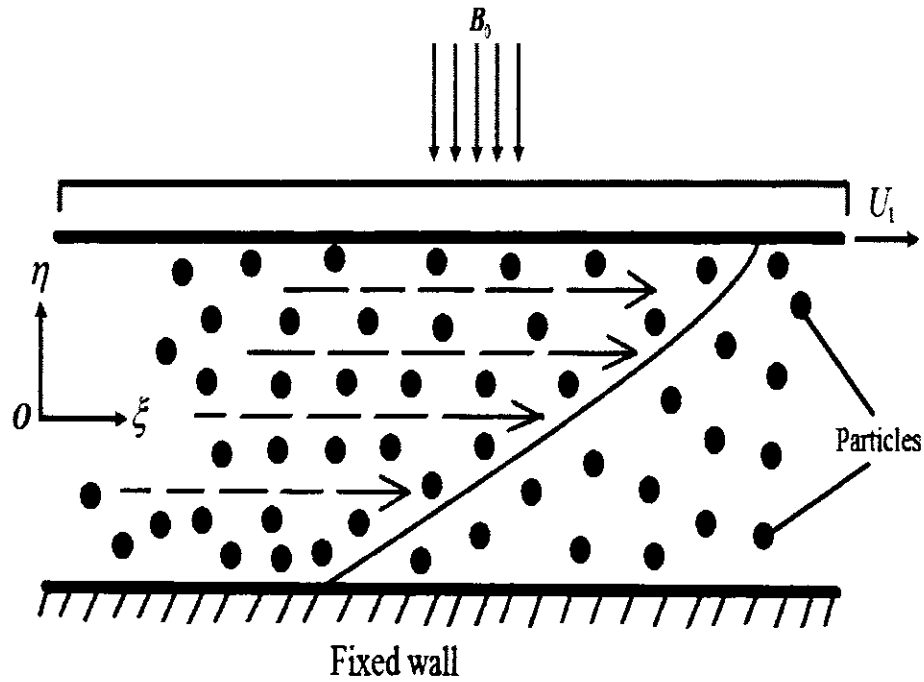

Figure 2.1: Configuration of the flow.

If $\boldsymbol{V} = [u,\ 0,\ 0]$ be the velocity components [121] of a uni-directional flow describing only axial disturbance while there is no disturbance in the lateral direction. However, the heating effects on the upper moving wall attenuates the viscosity of the base fluid. under these assumptions the governing Eqs. $(1.31) - (1.33)$ in components form [122] are given as:

2.1.1 For fluid phase

$$\frac{\partial u_f}{\partial \xi} + \frac{\partial v_f}{\partial \eta} = 0, \tag{2.1}$$

$$\frac{\partial}{\partial \eta}\left(\mu_s \frac{\partial u_f}{\partial \eta}\right) - \gamma_1 \left(\frac{\partial^4 u_f}{\partial \eta^4}\right) + \frac{CS}{(1-C)}\left(u_p - u_f\right) - \frac{\sigma B_0^2}{(1-C)} u_f = \frac{\partial p}{\partial \xi}. \tag{2.2}$$

2.1.2 For particle phase

$$\frac{\partial u_p}{\partial \xi} + \frac{\partial v_p}{\partial \eta} = 0, \tag{2.3}$$

$$u_f = u_p + \frac{1}{S}\left(\frac{\partial p}{\partial \xi}\right). \tag{2.4}$$

2.1.3 Energy equation

$$\frac{\partial^2 \theta}{\partial \eta^2} + \frac{\mu_s}{k_1}\left(\frac{\partial u_f}{\partial \eta}\right)^2 = \frac{\gamma_1}{k_1}\left(\frac{\partial u_f}{\partial \eta}\right)\left(\frac{\partial^3 u_f}{\partial \eta^3}\right). \tag{2.5}$$

In above equations S, represents the classical Stokes which can be obtained by finite particulate fractional volume as proposed by Tam [123] which are defined below:

$$S = 4.5\left(\frac{\mu_0}{r_1^2}\right)\lambda'(C), \tag{2.6}$$

$$\lambda'(C) = \frac{4 + 3\sqrt{8C - 3C^2} + 3C}{(2 - 3C)^2}. \tag{2.7}$$

The corresponding momentum and thermal boundary conditions at opposite wall are listed below:

(i). At lower wall

$$\left.\begin{aligned} &(i).\, u_f(\eta) = 0, \\ &(ii).\, \frac{\partial^2 u_f}{\partial \eta^2} = 0, \\ &(iii).\, \theta(\eta) = \theta_1. \end{aligned}\right\};\ \text{When } \eta = -h. \tag{2.8}$$

(ii). At upper wall

$$\left.\begin{aligned}(iv).u_f(\eta) &= U,\\ (v).\ \frac{\partial^2 u_f}{\partial \eta^2} &= 0,\\ (vi).\theta(\eta) &= \theta_2.\end{aligned}\right\};\ \text{When } \eta = h. \tag{2.9}$$

Considering the Eq. (10) which contains the pertinent parameters and variables which help to nondimensionalize the concerned governing equations and boundary equations.

$$\left.\begin{aligned}&\frac{u_f}{U_1} = u_f^*;\ \frac{u_p}{U_1} = u_p^*;\ \frac{\eta}{h} = \eta^*;\ \frac{\xi}{h} = \xi^*;\ \frac{\mu_s}{\mu_0} = \mu^*;\\ &B_r = \frac{U^2\mu_0}{k_1(\theta_2-\theta_1)};\ \beta = k_3(\theta_2-\theta_1);\ M = \sqrt{\frac{\sigma}{\mu_0}}hB_0;\\ &\frac{hp}{\mu_0 U_1} = p^*;\ \gamma = \sqrt{\frac{\mu_0}{\gamma_1}}h;\ k_2 = \frac{\mu_0}{h^2 S};\ \theta^* = \frac{\theta-\theta_1}{\theta_2-\theta_1};\end{aligned}\right\}. \tag{2.10}$$

Eqs. (2.1) – (2.5) are converted by ignoring asterisk into dimensionless form as:

$$\frac{dp}{d\xi} = \frac{d}{d\eta}\left(\mu\frac{du_f}{d\eta}\right) - \frac{1}{\gamma^2}\left(\frac{d^4u_f}{d\eta^4}\right) + \frac{C}{k_2}\frac{(u_p-u_f)}{(1-C)} - \frac{M^2}{(1-C)}u_f, \tag{2.11}$$

$$u_p = u_f - k_2\frac{dp}{d\xi}, \tag{2.12}$$

$$\frac{d^2\theta}{d\eta^2} + \mu B_r\left(\frac{du_f}{d\eta}\right)^2 = \frac{B_r}{\gamma^2}\left(\frac{du_f}{d\eta}\right)\left(\frac{d^3u_f}{d\eta^3}\right). \tag{2.13}$$

2.1.4 Variable viscosity

As the viscosity of the fluid depends upon the variation in temperature which is analyzed with the help of Reynolds' model [124] as expressed below:

$$\mu_s(\theta) = \mu_0 e^{-k_3(\theta-\theta_1)}. \tag{2.14}$$

In view of expression given in Eq. (2.10), final form of Eq. (2.14) provides the following look:

$$\mu(\theta) = e^{-k_3(\theta_2-\theta_1)\theta} = e^{-\beta\theta}. \tag{2.15}$$

For the convergence of above expression requires if viscosity parameter is chosen such that $\beta \in [0\ \ 1]$. Expanding Maclaurin' series and employing Walter's lemma one can obtain the linearized form of Eq. (2.15) as:

$$\mu(\theta) = 1 - \beta\theta. \tag{2.16}$$

Using Eqs. (2.12) and (2.16) in Eq. (2.11) and Eq. (2.13) provide dimensionless form of momentum and thermal differential equations having the contribution of constant pressure gradient such that (i.e., $\frac{dp}{d\xi} = P$). Then one can obtain the following expressions:

$$\left.\begin{aligned}\frac{d^4u_f}{d\eta^4} + \gamma^2\beta\left(\frac{d\theta}{d\eta}\right)\left(\frac{du_f}{d\eta}\right) + \gamma^2(\beta\theta - 1)\left(\frac{d^2u_f}{d\eta^2}\right) + \\ \left(\frac{M^2\gamma^2}{(\ )}\right)u_f - \left(\frac{\gamma^2 P}{C-1}\right) = 0\end{aligned}\right\}, \tag{2.17}$$

$$\frac{d^2\Theta}{d\eta^2} + B_r(1-\beta\theta)\left(\frac{du_f}{d\eta}\right)^2 = \frac{B_r}{\gamma^2}\left(\frac{du_f}{d\eta}\right)\left(\frac{d^3u_f}{d\eta^3}\right). \tag{2.18}$$

On the same contrast, Eqs. $(2.8) - (2.9)$, in view of Eq. (2.10), are transformed as:

$$\left.\begin{aligned}(i).\, u_f(\eta) = 0, \\ (ii).\ \frac{\partial^2 u_f}{\partial\eta^2} = 0, \\ (iii).\, \theta(\eta) = 0.\end{aligned}\right\};\ \text{When } \eta = -1, \tag{2.19}$$

$$\left.\begin{aligned}(iv).\, u_f(\eta) = 1, \\ (v).\ \frac{\partial^2 u_f}{\partial\eta^2} = 0, \\ (vi).\, \theta(\eta) = 1.\end{aligned}\right\};\ \text{When } \eta = 1. \tag{2.20}$$

2.2 Solution of the problem

For an approximate solution of Eqs. (2.17) and (2.18) using Eq. (2.19) and Eq. (2.20) Runge-Kutta method incorporated with shooting scheme [125] is preferred because

this iterative method is very efficient and converts BVP into first order initial value problem which is solved applying o -order method. Some mandatory substitutions to reduce higher order derivatives are explained below.

$$u_f = f_1, \tag{2.21}$$

If above equation describes the substitution of fluid's velocity, then following set of equations are used to convert higher derivatives of u_f.

$$f_2 = \frac{du_f}{d\eta} = f_1', \tag{2.22}$$

$$f_3 = \frac{d^2u_f}{d\eta^2} = f_2', \tag{2.23}$$

$$f_4 = \frac{d^3u_f}{d\eta^3} = f_3', \tag{2.24}$$

$$\theta = f_5, \tag{2.25}$$

$$f_6 = \frac{d\theta}{d\eta} = f_5'. \tag{2.26}$$

One can identify that prime (′) denotes differentiation w.r.t "η". In view of Eqs. (2.22) – (2.26) reduce to:

$$f_4' = \gamma^2(1-\beta(f_5))f_3 - \gamma^2\beta(f_2)(f_6) - \left(\frac{\gamma^2M^2}{1-C}\right)f_1 - \left(\frac{\gamma^2}{1-C}\right)P, \tag{2.27}$$

$$f_6' = \frac{B_r}{\gamma^2}(f_2)(f_4) + B_r(\beta(f_5)-1)(f_2)^2. \tag{2.28}$$

Set of new obtained conditions that help to seek the solution, at both plates respectively, are listed as:

$$\left.\begin{array}{l}(i).f_1 = 0,\\ (ii).f_2 = m_1,\\ (iii).f_3 = 0,\\ (iv).f_4 = m_2,\\ (v).f_5 = 0,\\ (vi).f_6 = m_3\end{array}\right\};\ \text{When } \eta = -1, \tag{2.29}$$

$$\left.\begin{array}{l}(i).\ f_1 = 1,\\ (ii).\ f_2 = m_4,\\ (iii).\ f_3 = 0,\\ (iv).\ f_4 = m_5,\\ (v).\ f_5 = 1,\\ (vi).\ f_6 = m_6\end{array}\right\};\ \text{When } \eta = 1. \tag{2.30}$$

Where m_1, m_2, m_3, m_4, m_5 and m_6 are unknowns to be calculated.

2.3 Analysis

2.3.1 Graphical illustration

As the graphical study provides a visual proof of the contribution of the pertinent variable and helps to infer what factors really bring such variations in the flow. To serve the purpose, a parametric study is performed in this section in order to examine the impact of involved physical factors such as Hartmann number M, concentration of the particles C, Couple stress parameter γ, viscous parameter β and the Brinkman number B_r as shown in Figures $(2.2) - (2.6)$.

Figure (2.2) explains the role of Hartmann number on particulate flow. For higher values of M, further the velocity is affected due Lorentz force. this which emerges when electric field and magnetic field interact and results to impede the moving flow. Therefore, fluid velocity declines in the given graph. Whereas increase in the number of particle alters the previous flow pattern as shown in Figure. (2.3). This can be referred as moving wall attenuates the particle drag force [126] causes the velocity of base fluid to rise. In Figure (2.4) offers the contribution of Couple stress parameter [127] on base

liquid which keeps on increasing. This is due to weak the rotational field of base fluid reducing the friction force to impart its influence on the flow. Figure (2.5) shows how viscous parameter β support the flow. Form Eq. (2.14), it is understandable that due change in temperature reduces shear thickening effects which promotes the velocity of the fluid. Role of Brinkman number B_r on the temperature is sighted in Figure (2.6). By increasing B_r [128] more energy is added to the system allowing viscous dissipation to be dominate over molecular conduction. Thus, temperature rises. On the contrary, temperature declines for the case of viscosity parameter as shown in Figure (2.7) because higher values of β, expedites the velocity which reduces the friction force between two adjacent layers of fluid.

2.3.2 Validation

The obtained numerical results for the motion of fluid and particles are presented in Tables 2.1 to 2.3. Table 2.1 describes the difference between particulate flows for the case of Newtonian fluid and Couple stress fluid such that $M = 1.0, C = 0.4$, and the $B_r = 2.0$. Whereas the single and bi-phase flow of Couple stress fluid at various points between the plate is computed in Table 2.2 for the values of $M = 1.0, \gamma = 2.0$ and $B_r = 2.0$. Similarly, thermal variation for B_r, γ and C is listed in Table 2.3 and the computed numerical findings show an excellent adherence with graphical illustrations. This validate the correctness of the obtained solution.

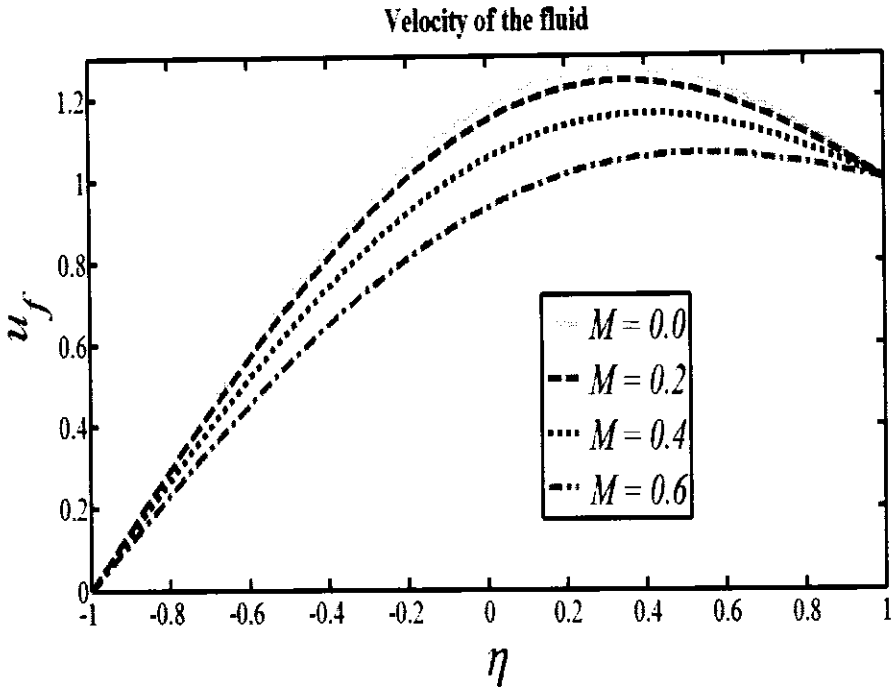

Figure 2.2: Variation of Hartmann number on the flow.

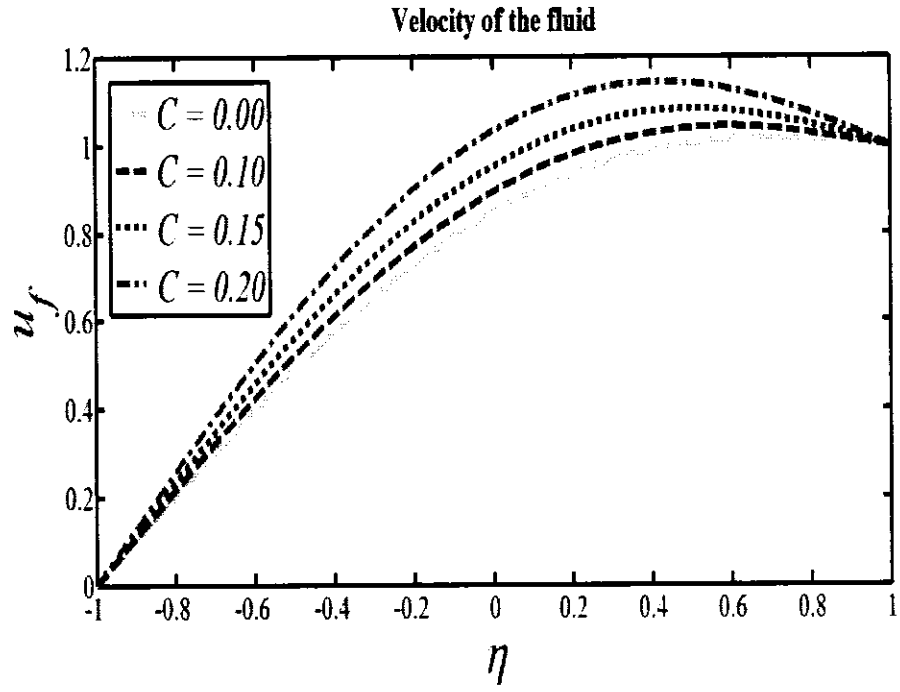

Figure 2.3: Variation of particle concentration on the flow.

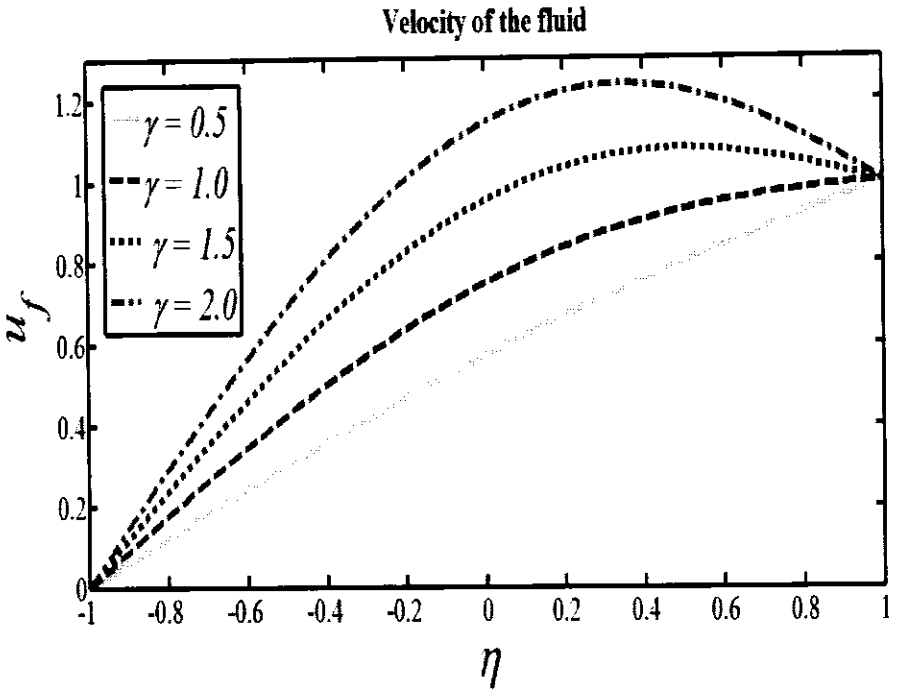

Figure 2.4: Variation of Couples stress parameter on the flow.

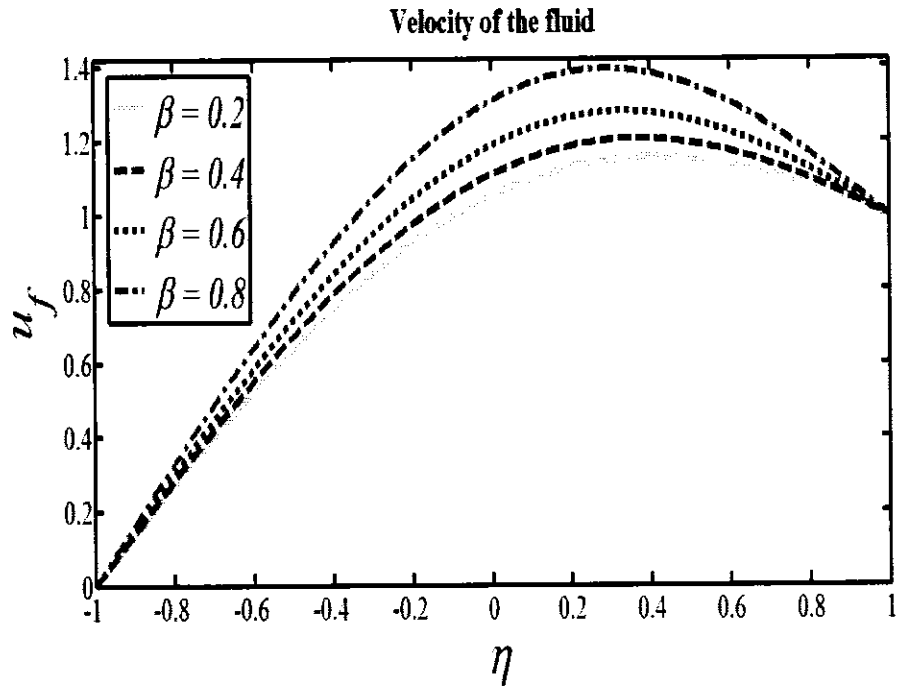

Figure 2.5: Variation of viscous parameter on the flow.

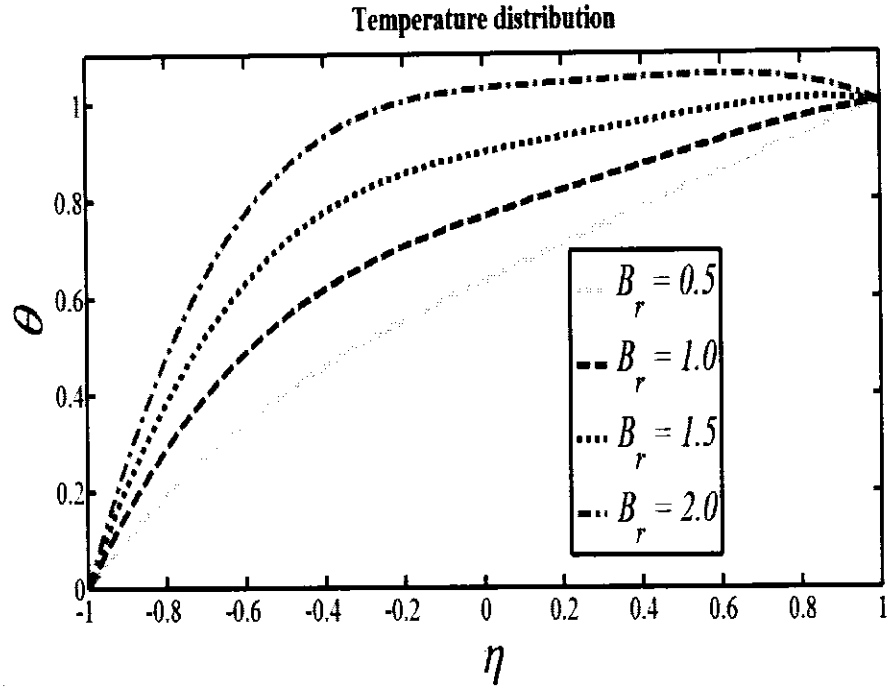

Figure 2.6: Variation of Brinkman number on the temperature.

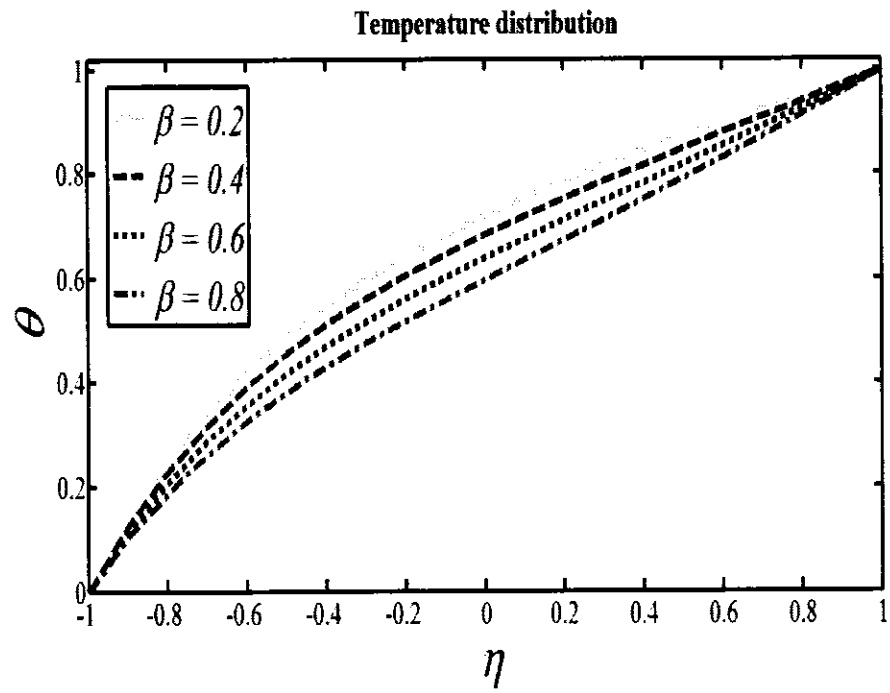

Figure 2.7: Variation of viscous parameter on the temperature.

Table 2.1: Variation in the velocities of both phases for Newtonian case and Couple stress fluid.

η	u_p **Newtonian fluid** For ($\gamma = 0.0$)	u_p **Couple stress fluid** For ($\gamma = 2.0$)	u_f **Newtonian fluid** For ($\gamma = 0.0$)	u_f **Couple stress fluid** For ($\gamma = 2.0$)
-1.0	1.0000	1.0000	0.0000	0.0000
-0.6	1.2000	1.3221	0.2000	0.3221
-0.2	1.4000	1.5826	0.4000	0.5826
0.2	1.6000	1.7698	0.6000	0.7698
0.6	1.8000	1.8998	0.8000	0.8998
1.0	2.0000	2.0000	1.0000	1.0000

Table 2.2: Variation in the velocities for single- and two-phase flows.

η	u_f **Single phase** For ($C = 0.0$)	u_f **Solid-liquid phase** For ($C = 0.4$)	u_p **Solid-liquid phase** For ($C = 0.4$)
-1.0	0.0000	0.0000	1.0000
-0.6	0.2741	0.3221	1.3221
-0.2	0.5117	0.5826	1.5826
0.2	0.7047	0.7698	1.7698
0.6	0.8618	0.8998	1.8998
1.0	1.0000	1.0000	2.0000

Table 2.3: Thermal variation at the different points.

η	θ For ($B_r = 0.0$)	θ For ($B_r = 2.0$)	θ For ($\gamma = 0.0$)	θ For ($C = 0.0$)
-1.0	0.0000	0.0000	0.0000	0.0000
-0.6	0.2000	0.3916	0.3512	0.3578
-0.2	0.4000	0.6066	0.5629	0.5870
0.2	0.6000	0.7528	0.7095	0.7504
0.6	0.8000	0.8785	0.8446	0.8830
1.0	1.0000	1.0000	1.0000	1.0000

2.4 Conclusion

Couple stress fluid a conveying solid particles through horizontal plates is investigated. The viscos dissipation effects have also been reported. Exponentially decreasing viscosity of base fluid is presented by Reynolds model. Transversely acting magnetic fields contributes by hindering the bi-phase flow. The key finding are described as:

- Base fluid is resisted for increasing values of Hartmann number.
- The temperature effectively variate the viscosity of the fluid to cause the shear thinning effects.
- The temperature of the flow mounts in response of higher values of Brinkman number.
- Attenuation of the viscosity results to expedite the flows.
- Higher temperature difference caused by viscosity parameter rises the momentum of the fluid.

Chapter 3

A study of gravitational and magnetic effects on Coupled stress bi-phase liquid suspended with Crystal and Hafnium particles down through an inclined channel

This chapter is related to a bi-phase fluid through an inclined channel. Main carrier is Couple stress fluid which is suspended with two different types of particles i.e., Hafnium particles and crystal particles, respectively. The concerned supercritical flow is affected by externally applied magnetic fields. Two-phase flow is caused by the contribution of gravity due to slanting channel. Routine calculation are followed to seek the solution of modeled flow problem. Physical properties of basaltic flow are also considered as special case for bi-phase flow which display full agreement with the existing literature. The mathematical results have been vetted by parametric study.

3.1 Mathematical formulation

Consider a bi-phase flow through an inclined channel as shown in Figure (3.1). flow is composed of a base liquid and particles. Couple stress fluid serves as the base fluid while two types of particles namely, Hafnium and crystal particles give rise to the

concerned bi-phase fluid. However, it is confirmed that the quantity of particles remains constant.

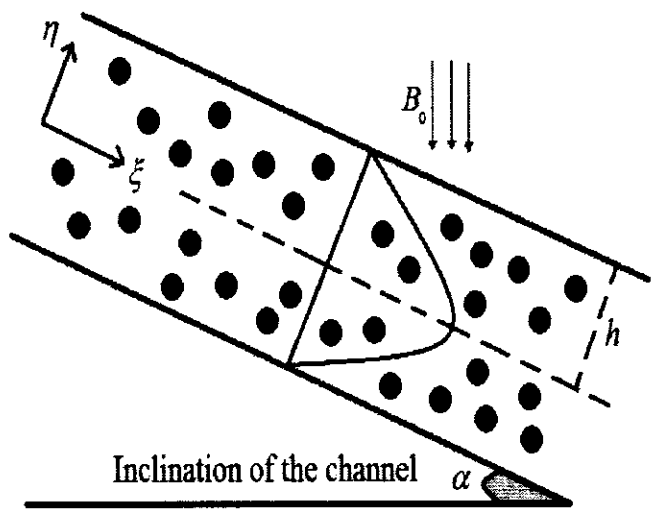

Figure 3.1: Configration of the inclined channel.

If $[u_f(\xi,\eta)\ v_f(\xi,\eta)\ 0]$ and $[u_p(\xi,\eta)\ v_p(\xi,\eta)\ 0]$ denote velocity of base fluid and particles, respectively. Then the governing Eqs. $(1.31) - (1.32)$ of this particulate flow with applied magnetic fields and gravity in components form are given as:

3.1.1 For fluid phase

The fundamental differential equations for conservation of mass and momentum [129] for fluid phase are given as:

$$\frac{\partial u_f}{\partial \xi} + \frac{\partial v_f}{\partial \eta} = 0, \tag{3.1}$$

$$\rho_f(1-C)\left(\frac{\partial u_f}{\partial t}+u_f\frac{\partial u_f}{\partial \xi}+v_f\frac{\partial u_f}{\partial \eta}\right)=\left.\begin{array}{c}-(1-C)\frac{\partial p}{\partial \xi}+SC(u_p-u_f)+\\ \mu_s(1-C)\left(\frac{\partial^2 u_f}{\partial \xi^2}+\frac{\partial^2 u_f}{\partial \eta^2}\right)-\\ \gamma_1(1-C)\left(\frac{\partial^2}{\partial \xi^2}+\frac{\partial^2}{\partial \eta^2}\right)^2 u_f-\\ \sigma B_0^2 u_f+g\rho_f\sin\alpha\end{array}\right\}, \quad (3.2)$$

$$\rho_f(1-C)\left(\frac{\partial v_f}{\partial t}+u_f\frac{\partial v_f}{\partial \xi}+v_f\frac{\partial v_f}{\partial \eta}\right)=\left.\begin{array}{c}-(1-C)\frac{\partial p}{\partial \eta}+SC(v_p-v_f)+\\ \mu_s(1-C)\left(\frac{\partial^2 v_f}{\partial \xi^2}+\frac{\partial^2 v_f}{\partial \eta^2}\right)-\\ \gamma_1(1-C)\left(\frac{\partial^2}{\partial \xi^2}+\frac{\partial^2}{\partial \eta^2}\right)^2 v_f-\\ \sigma B_0^2 v_f-g\rho_f\cos\alpha\end{array}\right\}. \quad (3.3)$$

3.1.2 Particle phase

Conservation of mass and conservation of linear momentum [130] for particle phase are given as:

$$\frac{\partial u_p}{\partial \xi}+\frac{\partial v_p}{\partial \eta}=0. \quad (3.4)$$

$$\rho_p C\left(\frac{\partial u_p}{\partial t}+u_p\frac{\partial u_p}{\partial \xi}+v_p\frac{\partial u_p}{\partial \eta}\right)=-C\frac{\partial p}{\partial \xi}+SC(u_p-u_f), \quad (3.5)$$

$$\rho_p C\left(\frac{\partial v_p}{\partial t}+u_p\frac{\partial v_p}{\partial \xi}+v_p\frac{\partial v_p}{\partial \eta}\right)=-C\frac{\partial p}{\partial \eta}+SC(v_p-v_f). \quad (3.6)$$

Considering the flow to be steady and uni-directional case, Eqs. (3.1) – (3.6) take the following form:

$$\left.\begin{array}{c}\mu_s(1-C)\frac{\partial^2 u_f}{\partial \eta^2}+SC(u_p-u_f)-\gamma_1(1-C)\frac{\partial^4 u_f}{\partial \eta^4}-\sigma B_0^2 u_f+\\ g\rho_f\sin\alpha=(1-C)\frac{\partial p}{\partial \xi}\end{array}\right\}, \quad (3.7)$$

$$\frac{\partial p}{\partial \xi}=S(u_p-u_f). \quad (3.8)$$

3.1.3 Boundary conditions

The relevant boundary conditions at each wall which confines this particulate flow are:

$$(i).u_f(\eta) = 0;\ \text{When}\ \eta = h, \tag{3.9}$$

$$(ii).\frac{\partial^2 u_f}{\partial \eta^2} = 0;\ \text{When}\ \eta = h, \tag{3.10}$$

$$(iii).\ u_f(\eta) = 0;\ \text{When}\ \eta = -h, \tag{3.11}$$

$$(iv).\ \frac{\partial^2 u_f}{\partial \eta^2} = 0;\ \text{When}\ \eta = -h. \tag{3.12}$$

3.2 Solution of the problem

Since Eq. (3.7) is 4[th]-order linear ordinary differential equation coupled with Eq. (3.8) represents the flow dynamics in dimensional form. Therefore, to make it dimensionless, we consider the following.

$$g* = \frac{g}{\bar{g}};\ \rho_{rel} = \frac{\rho_f}{\rho_p};\ Fr = \frac{U_1}{\sqrt{h\bar{g}}};\ k_4 = \frac{\mu_s}{\rho_f h U_1};\ k_5 = \frac{\mu_s}{\rho_p h U_1}. \tag{3.13}$$

In view of dimensionless quantities as described in Eq. (2.10) and Eq. (3.13), the Eqs. (3.7) – (3.12) after neglecting the asterisk, finally give the following look.

$$\frac{d^4 u_f}{d\eta^4} - \gamma^2 \frac{d^2 u_f}{d\eta^2} + \left(\frac{\gamma^2 M^2}{1-C}\right) u_f - \left(\frac{C\,k_4 + k_5}{k_4\,k_5}\right)\left(\frac{\gamma^2 g \sin\alpha}{(1-C)(Fr)^2}\right) + \left(\frac{\gamma^2}{1-C}\right)\frac{dp}{d\xi} = 0, \tag{3.14}$$

$$u_p = u_f - \frac{k_2\,k_5 (Fr)^2 \frac{dp}{d\xi} - g k_2 \sin\alpha}{k_5 (Fr)^2}, \tag{3.15}$$

$$(i).u_f(\eta) = 0;\ \text{When}\ \eta = 1, \tag{3.16}$$

$$(ii).\ \frac{\partial^2 u_f}{\partial \eta^2} = 0;\ \text{When}\ \eta = 1, \tag{3.17}$$

$$(iii).\ u_f(\eta) = 0;\ \text{When}\ \eta = -1, \tag{3.18}$$

$$(iv).\ \frac{\partial^2 u_f}{\partial \eta^2} = 0;\ \text{When}\ \eta = -1. \tag{3.19}$$

Since, the gravitational force is the main contributor to cause the flow through the channel. Nevertheless, significant contribution of pressure gradient is assumed to be uniform at each point of the channel which can be represented as:

$$\frac{dp}{d\xi} = P. \tag{3.20}$$

Substituting Eq. (3.20) in the Eqs. $(3.14) - (3.15)$, then one gets the following expression for liquid and particle phase, respectively.

$$\frac{d^4 u_f}{d\eta^4} - \gamma^2 \frac{d^2 u_f}{d\eta^2} + \frac{\gamma^2 M^2 u_f}{1-C} - \frac{C\,k_4 + k_5}{k_4\,k_5}\left(\frac{\gamma^2 g \sin\alpha}{(1-C)(Fr)^2}\right) + \frac{\gamma^2 P}{1-C} = 0, \tag{3.21}$$

$$u_p = u_f - \frac{k_2\,k_5 (Fr)^2 P - g k_2 \sin\alpha}{k_5 (Fr)^2}. \tag{3.22}$$

The solutions of Eqs. $(3.21) - (3.22)$ subject to the conditions given in Eqs. $(3.16) - (3.19)$, can be obtained as:

$$u_{fluid_C} = \left.\begin{aligned} &A_1\left\{\cosh\left(\sqrt{\frac{\gamma^2 - \sqrt{\gamma^4 - 4A_5}}{2}}\eta\right) + \sinh\left(\sqrt{\frac{\gamma^2 - \sqrt{\gamma^4 - 4A_5}}{2}}\eta\right)\right\} + \\ &A_2\left\{\cosh\left(\sqrt{\frac{\gamma^2 - \sqrt{\gamma^4 - 4A_5}}{2}}\eta\right) - \sinh\left(\sqrt{\frac{\gamma^2 - \sqrt{\gamma^4 - 4A_5}}{2}}\eta\right)\right\} + \\ &A_3\left\{\cosh\left(\sqrt{\frac{\gamma^2 + \sqrt{\gamma^4 - 4A_5}}{2}}\eta\right) + \sinh\left(\sqrt{\frac{\gamma^2 + \sqrt{\gamma^4 - 4A_5}}{2}}\eta\right)\right\} + \\ &A_4\left\{\cosh\left(\sqrt{\frac{\gamma^2 + \sqrt{\gamma^4 - 4A_5}}{2}}\eta\right) - \sinh\left(\sqrt{\frac{\gamma^2 + \sqrt{\gamma^4 - 4A_5}}{2}}\eta\right)\right\} \end{aligned}\right\}. \tag{3.23}$$

The particular integral or solution is obtained as:

$$u_{fluid_P} = \frac{g(\,Ck_4 + \,k_5)\,\mathrm{Sin}(\alpha) - P\;\,k_4\,k_5(Fr)^2}{k_4\,k_5(Fr)^2M^2}. \tag{3.24}$$

Adding Eq. (3.23) and Eq. (3.24) and using the given boundary conditions then main constants of integration are given as:

$$A_1 = \frac{\left\{\begin{matrix}\gamma^2\left(4\,M^2 - \gamma^2 - \sqrt{\gamma^4 - 4\,A_5}\right)(A_7 - A_6\sin\alpha) \\ \mathrm{sech}\left(\sqrt{\dfrac{\gamma^2 - \sqrt{\gamma^4 - 4\,A_5}}{2}}\right)\end{matrix}\right\}}{4\,\gamma^2(4\,M^2 - \gamma^2)A_5}. \tag{3.25}$$

$$A_2 = \frac{\left\{\begin{matrix}\left(\gamma^2 + \sqrt{\gamma^4 - 4\,A_5}\right)(A_7 - A_6\sin\alpha) \\ \mathrm{sech}\left(\sqrt{\dfrac{\gamma^2 - \sqrt{\gamma^4 - 4\,A_5}}{2}}\right)\end{matrix}\right\}}{4\,A_5\sqrt{\gamma^4 - 4\,A_5}}. \tag{3.26}$$

$$A_3 = \frac{(A_6\sin\alpha - A_7)\left\{\left(\gamma^2 - \sqrt{\gamma^4 - 4\,A_5}\right)\mathrm{sech}\left(\sqrt{\dfrac{\gamma^2 + \sqrt{\gamma^4 - 4\,A_5}}{2}}\right)\right\}}{4\,A_5\sqrt{\gamma^4 - 4\,A_5}}. \tag{3.27}$$

$$A_4 = \frac{(A_7 - A_6\sin\alpha)\left\{\left(\sqrt{\gamma^4 - 4\,A_5} - \gamma^2\right)\mathrm{sech}\left(\sqrt{\dfrac{\gamma^2 + \sqrt{\gamma^4 - 4\,A_5}}{2}}\right)\right\}}{4\,A_5\sqrt{\gamma^4 - 4\,A_5}}. \tag{3.28}$$

Thus, one can easily get the velocity of base liquid and Hafnium metal as:

$$u_{fluid} = A_{64}\left(\frac{k_4k_5P(Fr)^2 - g\left(Ck_4 + k_5\right)\sin\alpha}{k_4k_5(1-C)(Fr)^2}\right)\gamma^2\cosh\left(A_{10}\eta\right) -$$
$$A_{60}\left(\frac{k_4k_5P(Fr)^2 - g\left(Ck_4 + k_5\right)\sin\alpha}{k_4k_5(1-C)(Fr)^2}\right)\gamma^2\sinh\left(A_{10}\eta\right) -$$
$$\gamma^2\left(\frac{k_4k_5P(Fr)^2 - g\left(Ck_4 + k_5\right)\sin\alpha}{k_4k_5(1-C)(Fr)^2}\right)\left(\frac{\left(A_{70} + A_{62}(1-C)\right)(1-C)\cosh\left(A_{10}\eta\right)}{A_{77} + A_{74}(1-C)\gamma^4A_5}\right) - \gamma^2$$
$$\left(\frac{k_4k_5P(Fr)^2 - g\left(Ck_4 + k_5\right)\sin\alpha}{k_4k_5(1-C)(Fr)^2}\right)\left(\frac{\left(A_{71} + A_{62}(1-C)\right)(1-C)\sinh\left(A_{10}\eta\right)}{A_{77} + A_{74}(1-C)\gamma^4A_5}\right) - \tag{3.29}$$
$$\gamma^2\left(\frac{A_{61}(1-C)\cosh\left(A_{11}\eta\right)}{2A_{12}}\right)\left(\frac{k_4k_5P(Fr)^2 - g\left(Ck_4 - k_5\right)\sin\alpha}{k_4k_5(1-C)(Fr)^2}\right) +$$
$$\gamma^2\left(\frac{g\left(Ck_4 + k_5\right)\sin\alpha - k_4k_5P(Fr)^2}{k_4k_5A_5(Fr)^2}\right).$$

$$u_{particle} = A_{64}\left(\frac{k_4k_5P(Fr)^2 - g\left(Ck_4 + k_5\right)\sin\alpha}{k_4k_5(1-C)(Fr)^2}\right)\gamma^2\cosh\left(A_{10}\eta\right) - A_{60}$$
$$\left(\frac{k_4k_5P(Fr)^2 - g\left(Ck_4 + k_5\right)\sin\alpha}{k_4k_5(1-C)(Fr)^2}\right)\gamma^2\sinh\left(A_{10}\eta\right) - \gamma^2$$
$$\left(\frac{k_4k_5P(Fr)^2 - g\left(Ck_4 + k_5\right)\sin\alpha}{k_4k_5(1-C)(Fr)^2}\right)\left(\frac{\left(A_{70} + A_{62}(1-C)\right)(1-C)\cosh\left(A_{10}\eta\right)}{A_{77} + A_{74}(1-C)\gamma^4A_5}\right)$$
$$-\gamma^2\left(\frac{k_4k_5P(Fr)^2 - g\left(Ck_4 + k_5\right)\sin\alpha}{k_4k_5(1-C)(Fr)^2}\right)\left(\frac{\left(A_{71} + A_{62}(1-C)\right)(1-C)\sinh\left(A_{10}\eta\right)}{A_{77} + A_{74}(1-C)\gamma^4A_5}\right) \tag{3.30}$$
$$-\gamma^2\left(\frac{A_{61}(1-C)\cosh\left(A_{11}\eta\right)}{2A_{12}}\right)\left(\frac{k_4k_5P(Fr)^2 - g\left(Ck_4 + k_5\right)\sin\alpha}{k_4k_5(1-C)(Fr)^2}\right)$$
$$+\gamma^2\left(\frac{g\left(Ck_4 + k_5\right)\sin\alpha - Pk_4k_5(Fr)^2}{k_4k_5k_4A_5(Fr)^2}\right) + \frac{gk_2\sin\alpha - Pk_2k_5(Fr)^2}{k_5(Fr)^2}.$$

Where, A_5 to A_{77} appear in Eqs. (3.29) and (3.30) can be obtained in routine calculation as given in the appendix.

3.3 Analysis

3.3.1 Graphical illustration

This sections contains facts have been elaborated about the impacts of important parameters such as Froude number Fr, Couple stress parameter γ, inclination of the plane α, concentration of the particles C and Hartmann number M.

In Figures $(3.2) - (3.11)$ offer the flow behavior of two types of multiphase flows suspended with crystals and Hafnium particles, respectively. Figures $(3.2) - (3.3)$ give the variation of Hartmann number on base liquid. It is vivid that both different multiphase flows reduce their rapid motion when Lorentz force becomes dominant.

Opposite trend in the is observed for the case of rise in the number of particle phase in Figures $(3.4) - (3.5)$ as the drag force is effectively strong enough to resist the flow. However, flow of bi-phase fluid suspended with Hafnium is much better than crystal one. Increase in Couple stress parameter also rise the intensity of base fluid velocity due the vanishing couple stresses at the boundary as shown in Figures $(3.6) - (3.7)$. Variation in the position of slanting channel has been spotted in Figures (3.8) and (3.9). It is undeniable fact that higher the inclination of channel, faster is the movement of the flow due to great impact of the gravity.

The Froude number [131] is a dimensionless quantity which used to resistance faced by an object inside the liquid. This is defined as the ratio of inertial forces to gravitational forces and mathematically denoted as:

$$Fr = \frac{V}{\sqrt{g\,h}}. \tag{3.31}$$

Significance of Froude number is to identify flow to be a critical, supercritical and subcritical flow. A *"Supercritical flow"* suspended with two different types of particles through steep channel as Froude number Fr increases infinitely for these type of flows.

The effects of Froude's number which has an effective part in this gravity driven flow are portrayed in Figures (3.10) and (3.11). As a matter of facts, the smooth hunching down curves, consequently, addition rise in the inclination of the flat plate galvanizes the motion of the flow and turning the subcritical flow into supercritical flow down the slope.

Movement of crystal and Hafnium particles are shown in Figures $(3.12) - (3.21)$. One can see that contribution of the pertinent parameters on the movement of particles, remains same as for the case of Couple stress fluid. Moreover, by comparison of fluid phase velocity and particle phase velocity, it is inferred that fluid supports the particles.

3.3.2 Validation

This chapter investigates two different kinds of multiphase flows namely, crystal-Couple stress fluid and Hafnium-Couple stress fluid a symmetric channel. Flow is generated by the gravity while application of uniform magnetic fields is also taken into account. Flow is modeled by using Navier-Stokes equations which are solved exactly subject to the given boundary conditions. The motion of both phases are displayed through graphs clearly indicating the role of each involved parameters. Physical properties of basaltic magma are used a special case of multiphase flow given in Table 3.1. Table 3.2 suggests that owing to higher density of Hafnium particles flow is much faster than flow suspend with crystal particles. Moreover, the results extracted offer great deal of agreement with the present data and adhere to the physical expectation.

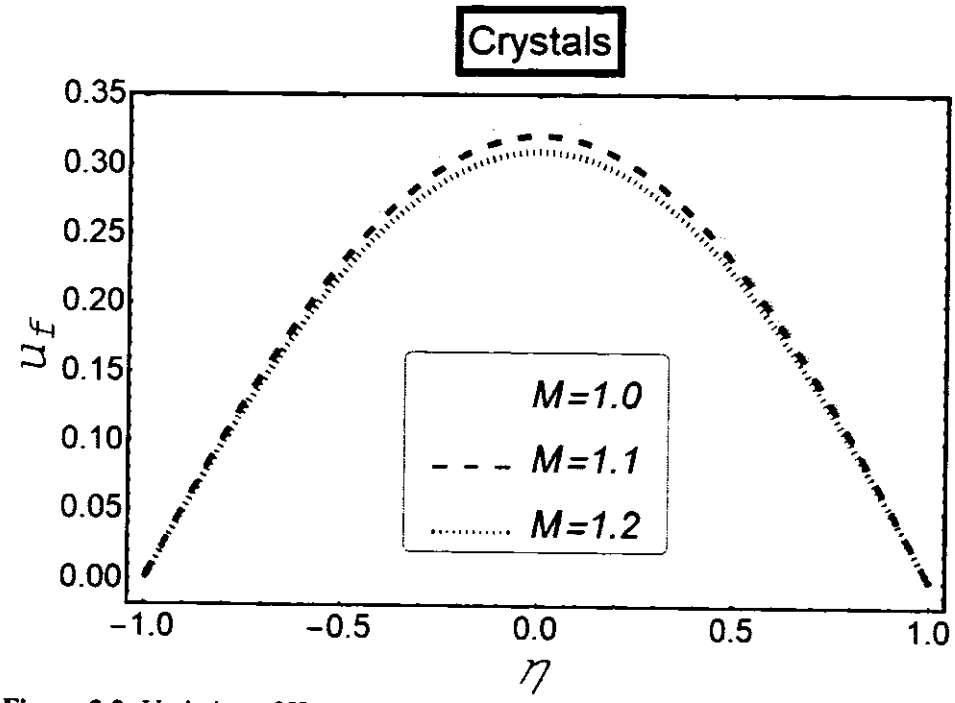

Figure 3.2: Variation of Hartmann number on the fluid.

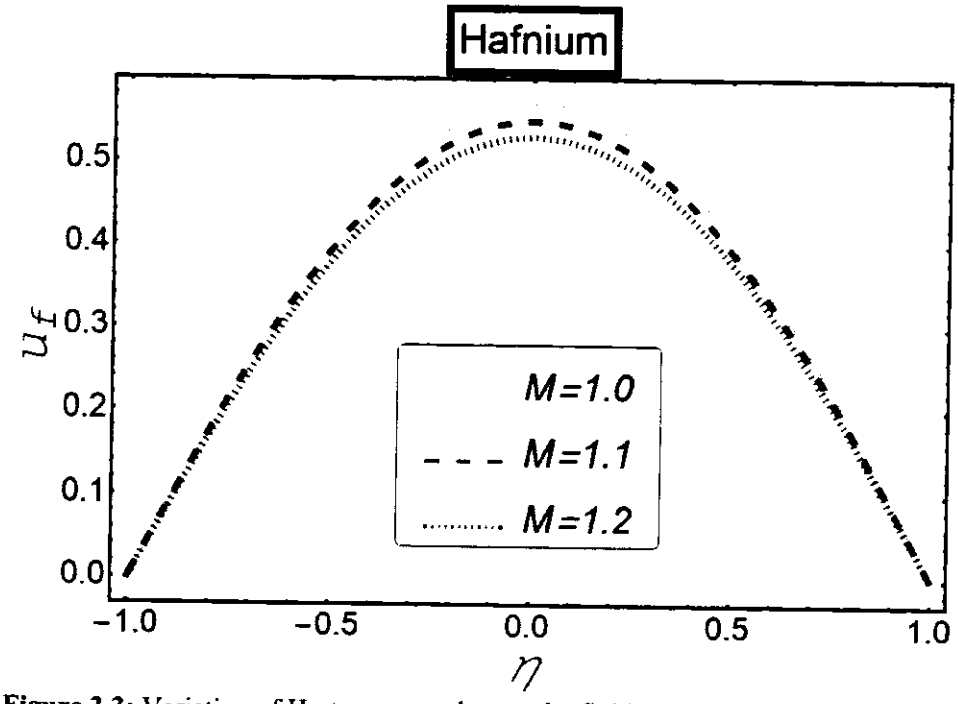

Figure 3.3: Variation of Hartmann number on the fluid.

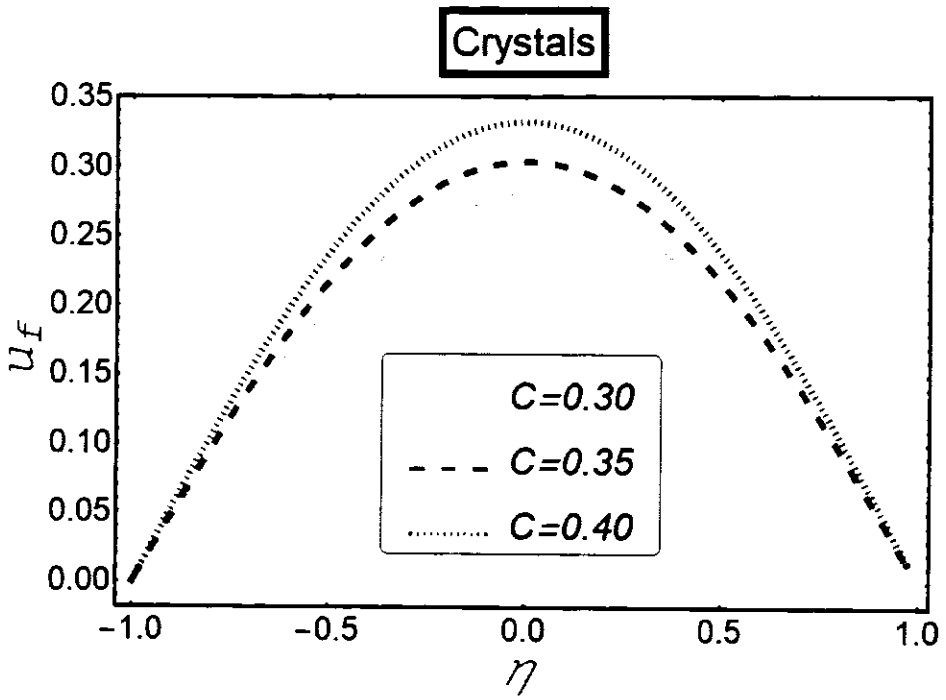

Figure 3.4: Variation of particle concentration on the fluid.

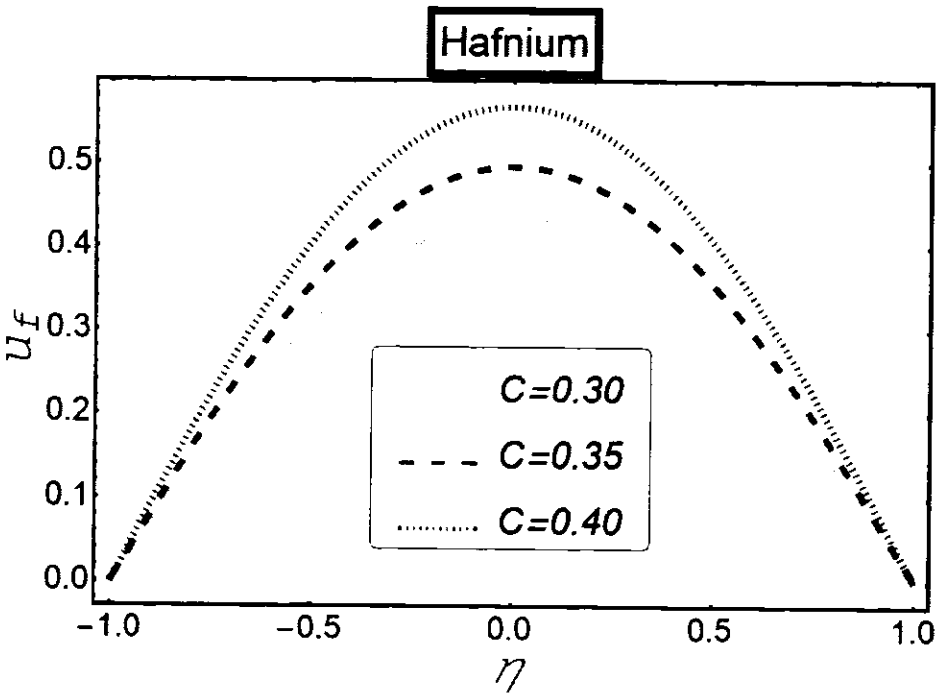

Figure 3.5: Variation of particle concentration on the fluid.

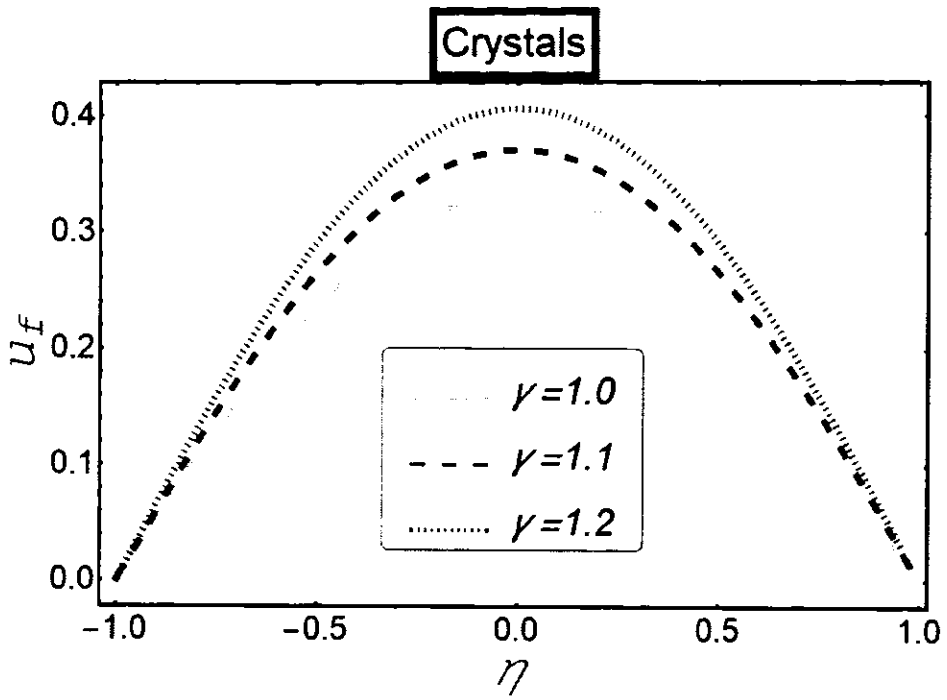

Figure 3.6: Variation of Couple stress parameter on the fluid.

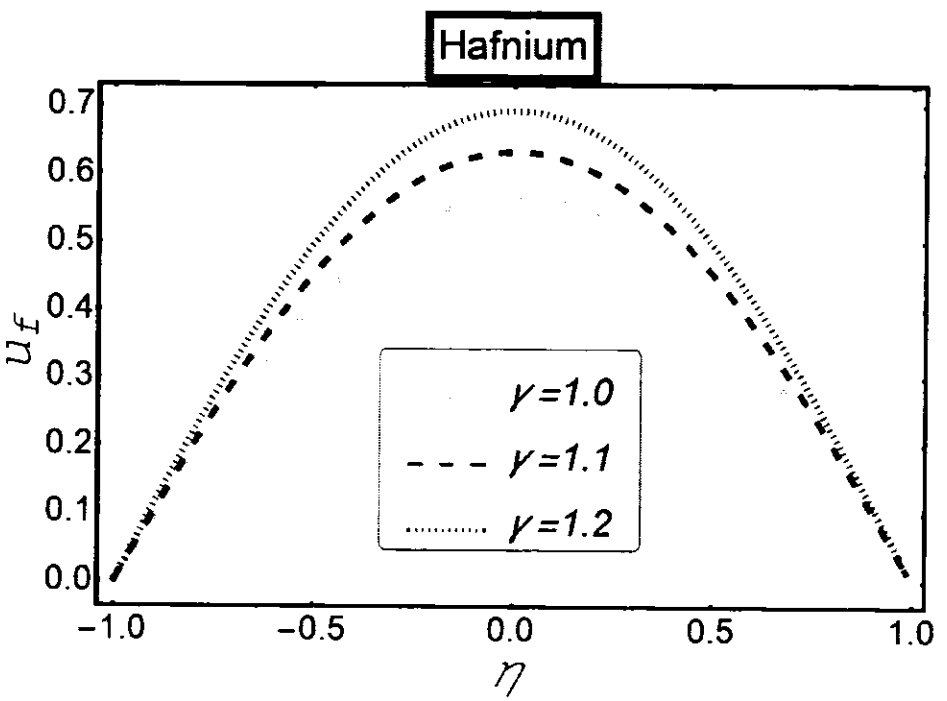

Figure 3.7: Variation of Couple stress parameter on the fluid.

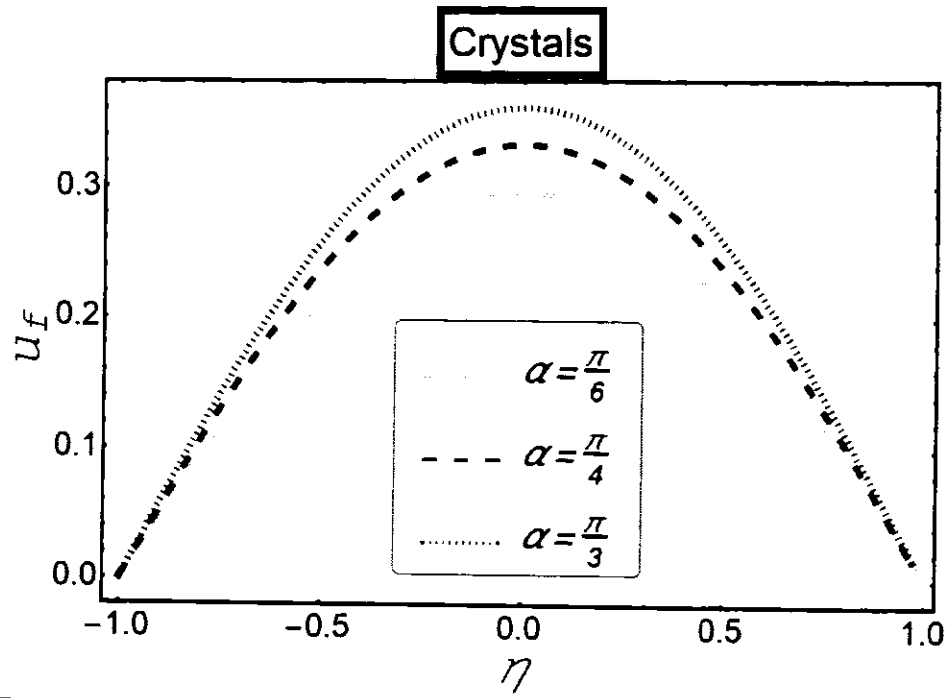

Figure 3.8: Variation of inclination on the fluid.

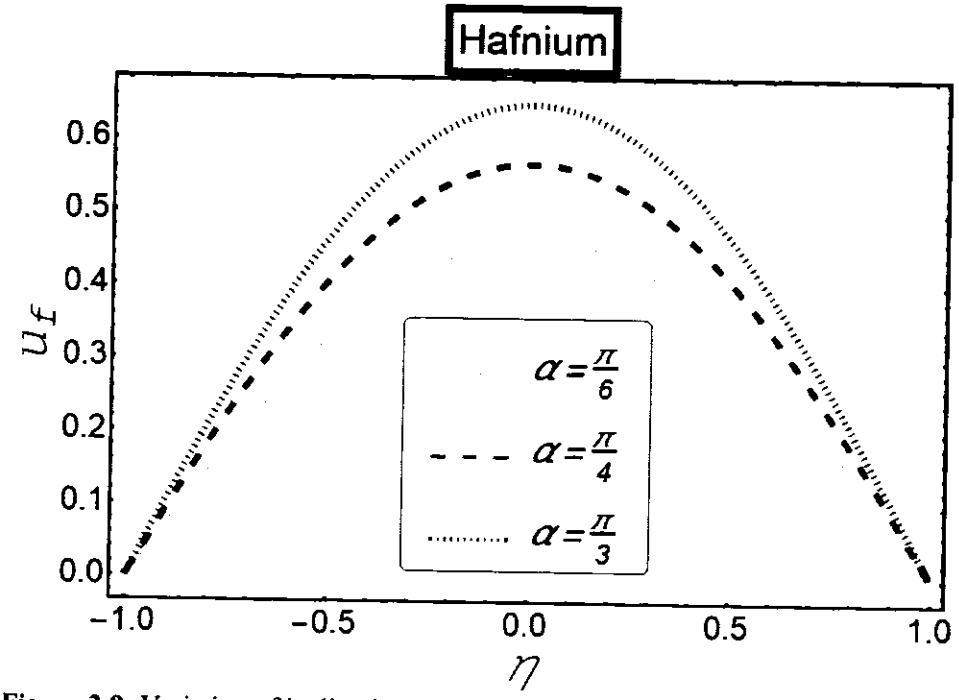

Figure 3.9: Variation of inclination on the fluid.

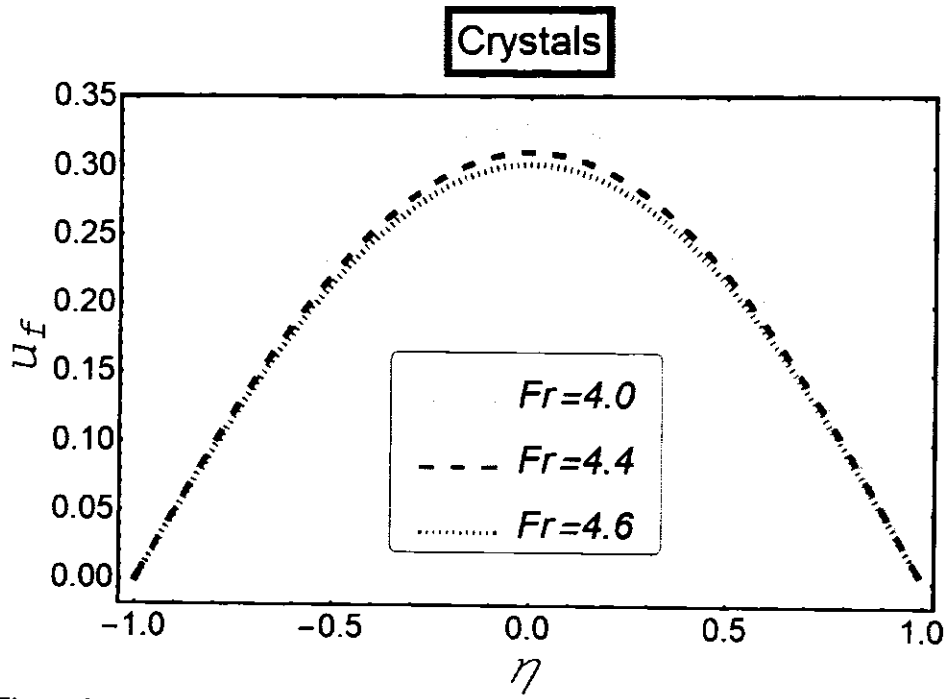

Figure 3.10: Variation of Froude number on the fluid.

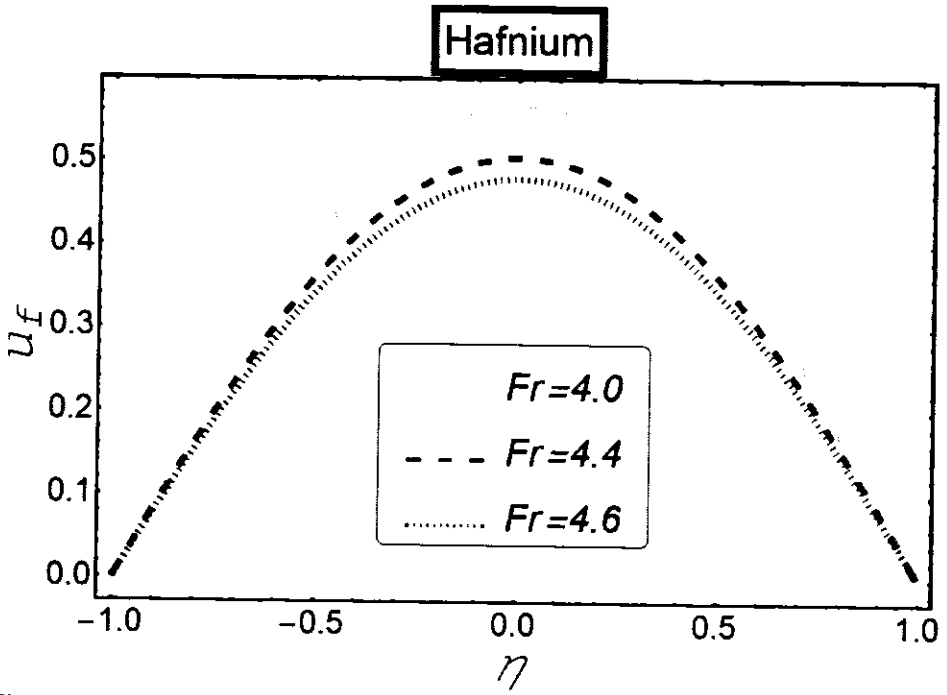

Figure 3.11: Variation of Froude number on the fluid.

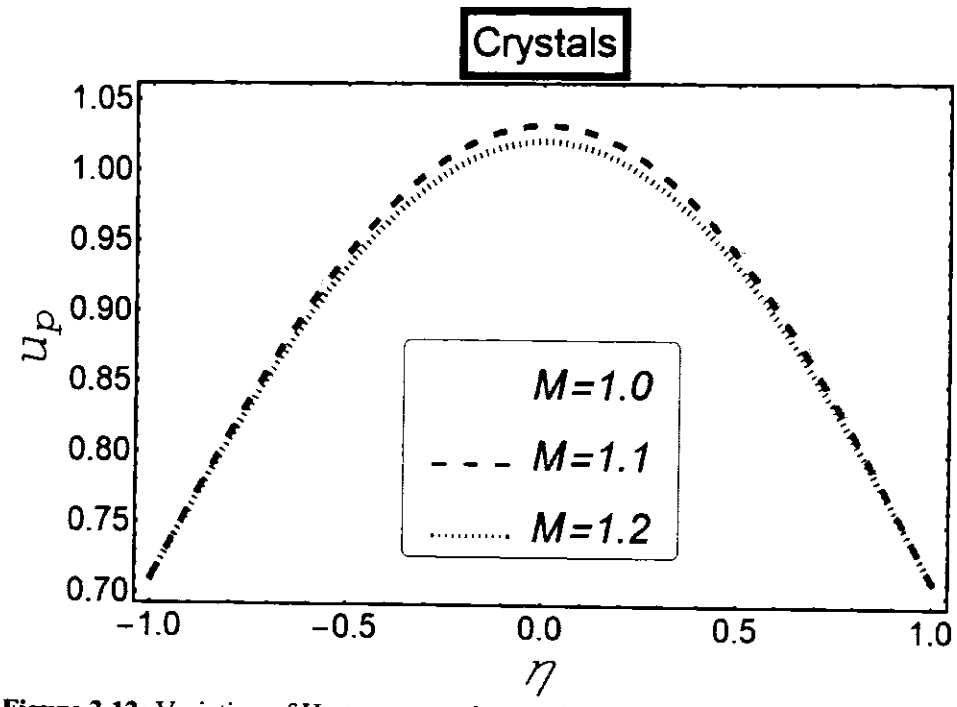

Figure 3.12: Variation of Hartmann number on the particles.

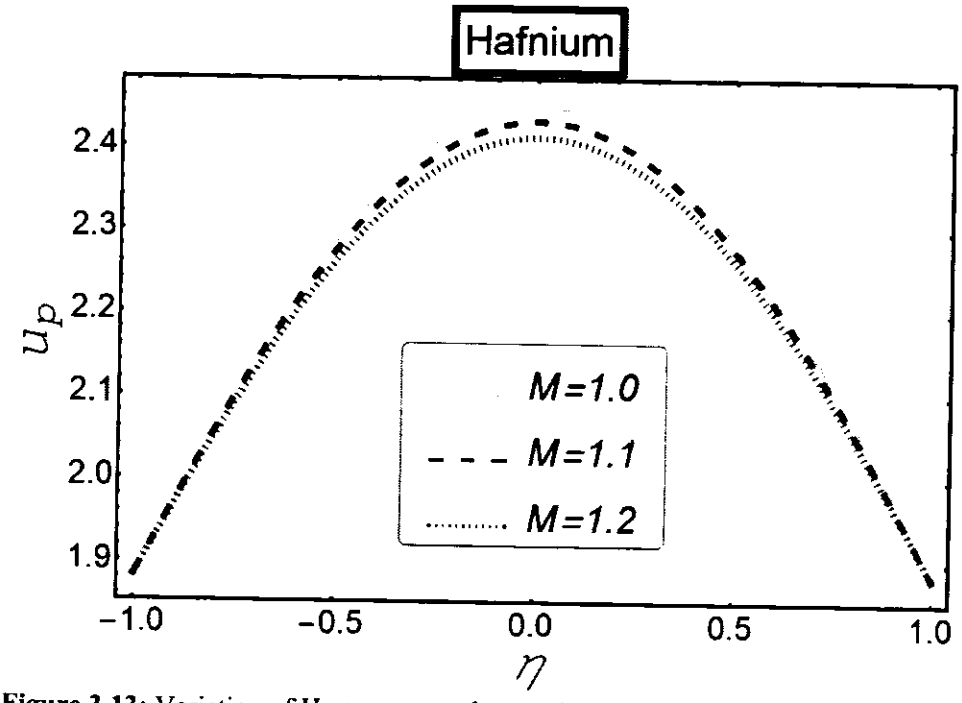

Figure 3.13: Variation of Hartmann number on the particles.

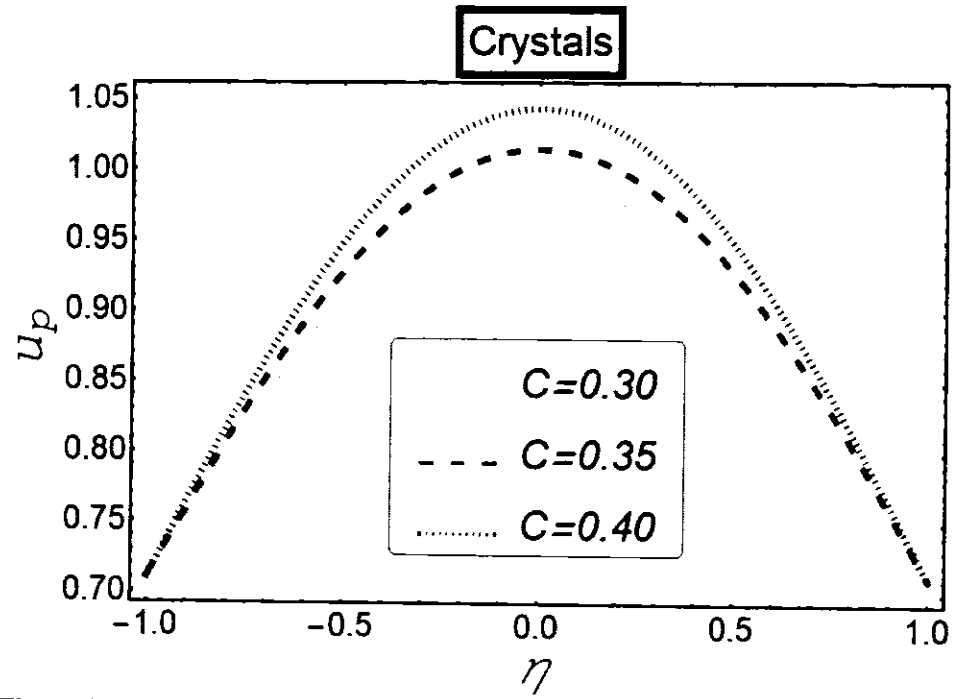

Figure 3.14: Variation of concentration on particles.

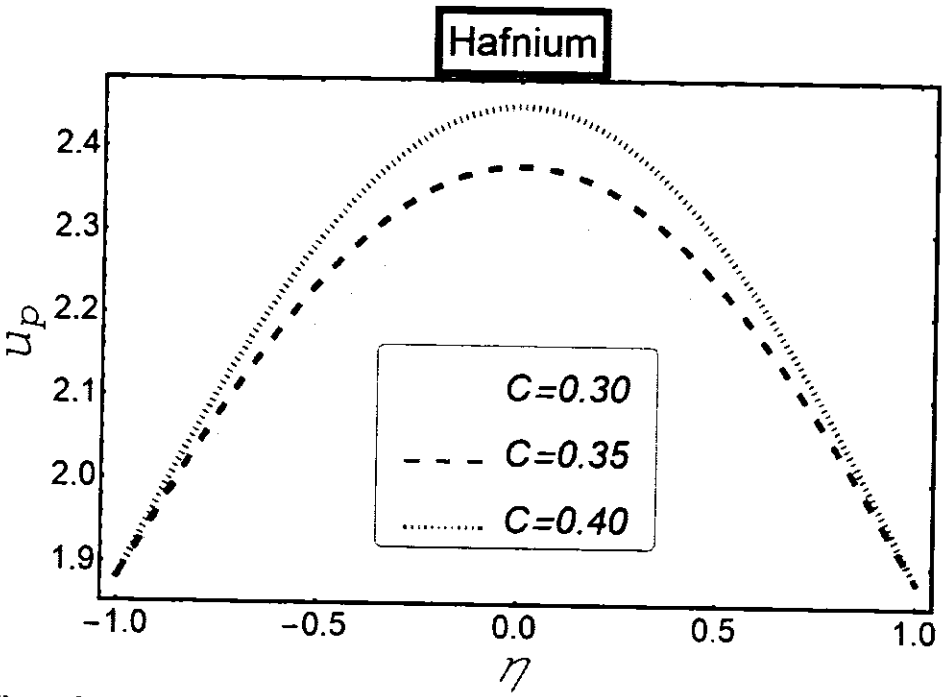

Figure 3.15: Variation of concentration on particles.

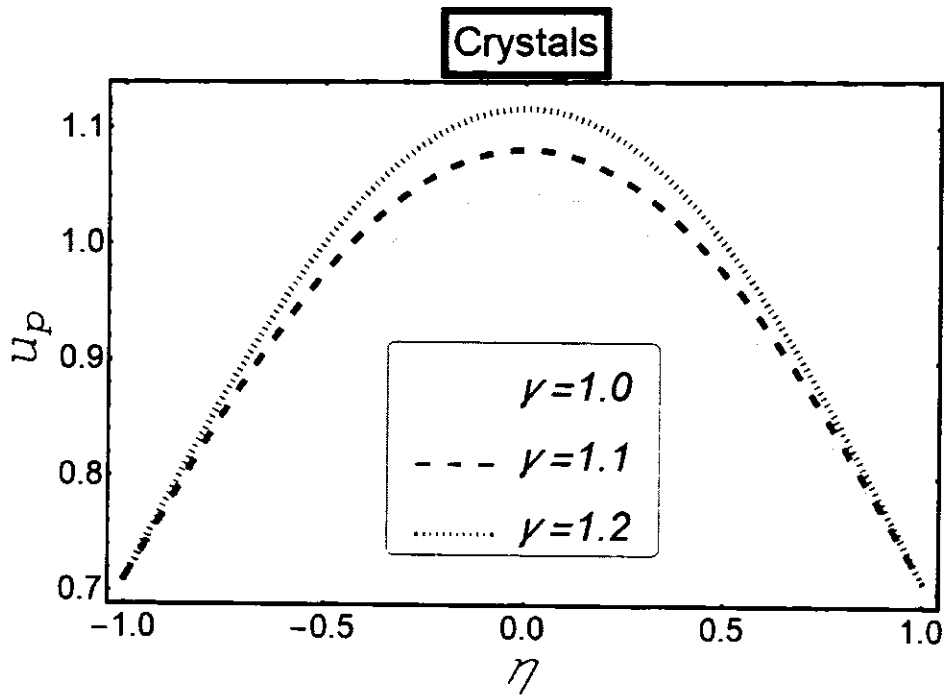

Figure 3.16: Variation of Couple stress parameter on particles.

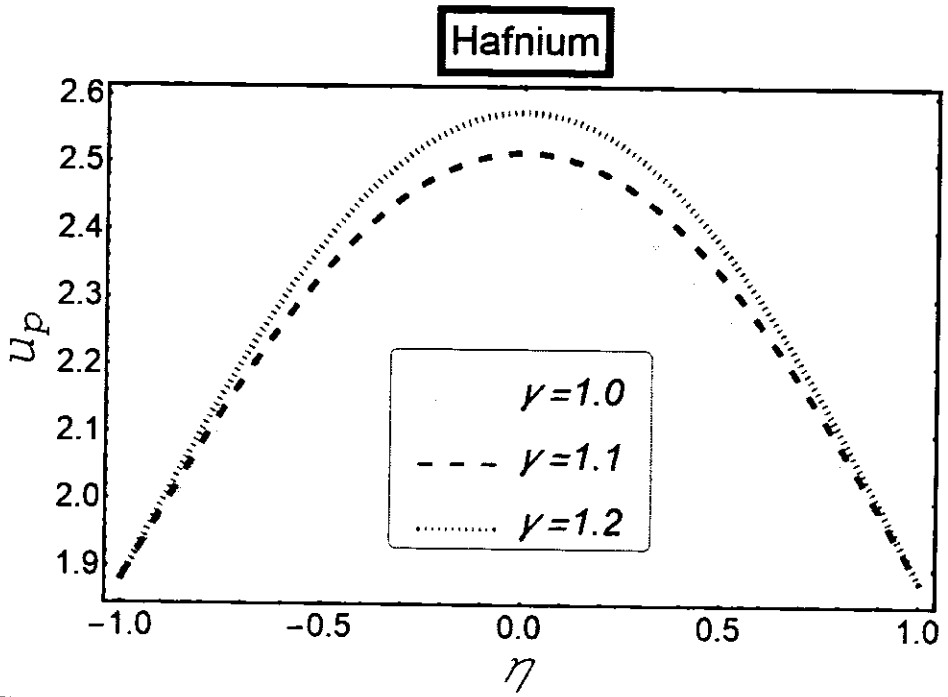

Figure 3.17: Variation of Couple stress parameter on particles.

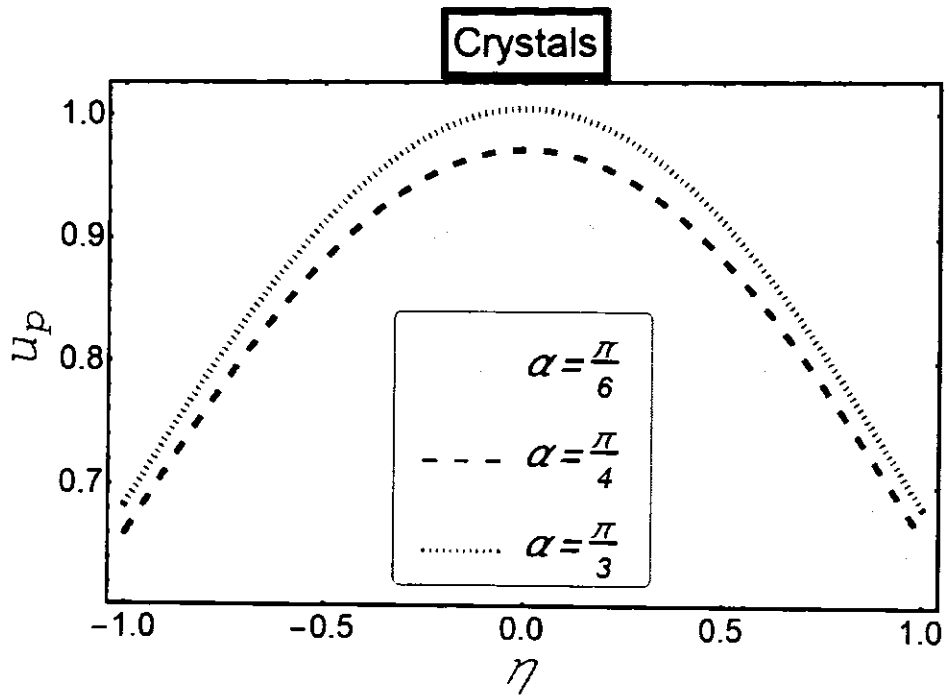

Figure 3.18: Variation of inclination on particles.

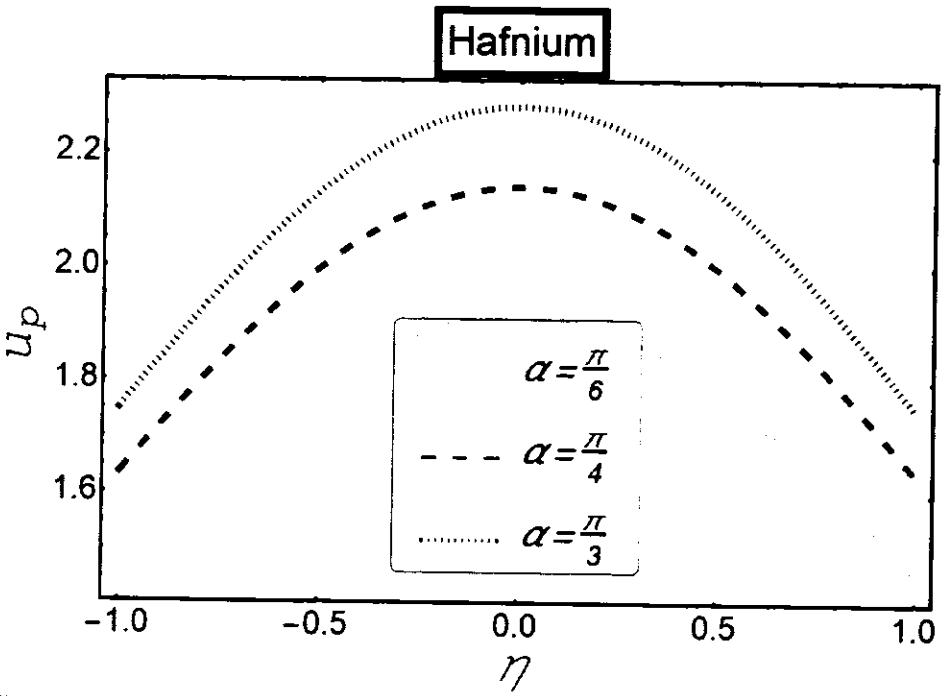

Figure 3.19: Variation of inclination on particles.

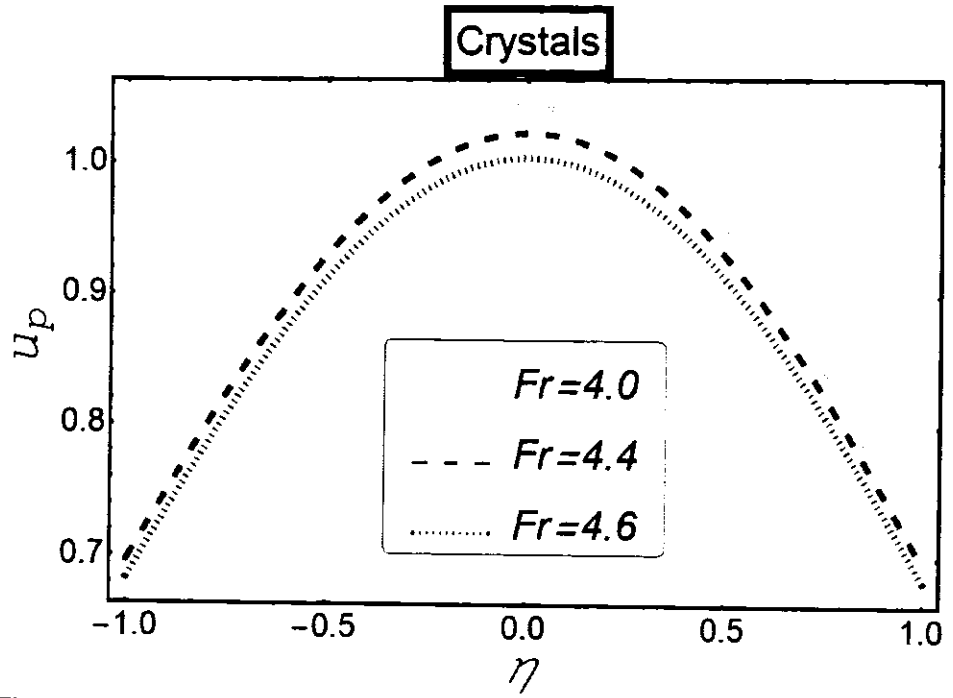

Figure 3.20: Variation of Froude number on particles.

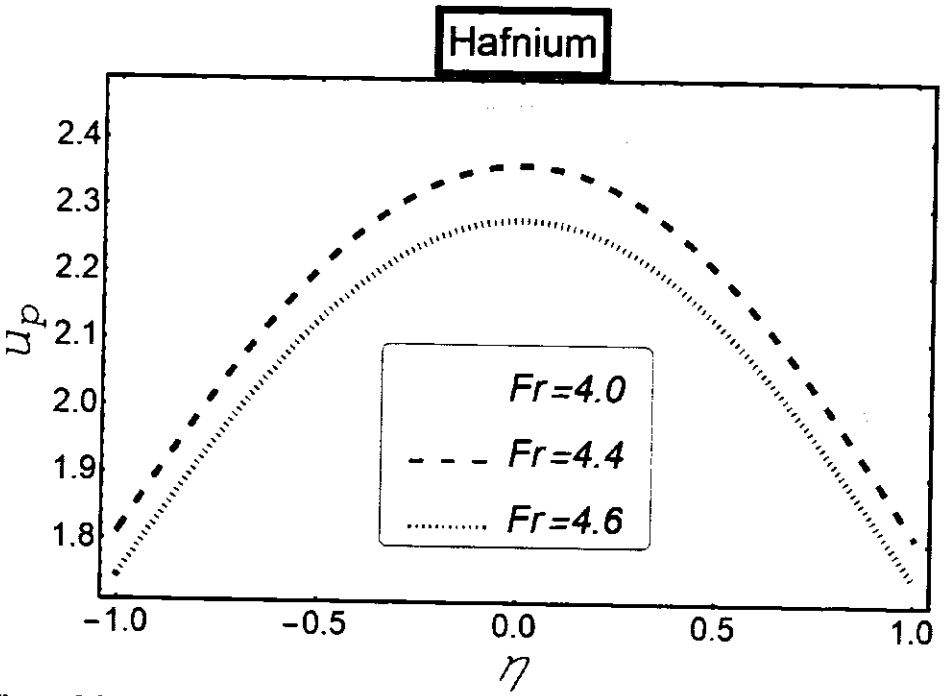

Figure 3.21: Variation of Froude number on particles.

Table 3.1: Physical properties about the composites of the flow.

---	Density (Particle)	Density (Fluid)	Viscosity (Fluid)	Viscosity (Suspension)
Magma	---	$1200\ kgm^{-3}$	$125\ Pa\ s$	$660\ Pa\ s$
Crystals	$2700\ kgm^{-3}$	---	---	---
Hafnium	$13310\ kgm^{-3}$	---	---	---

Table 3.2: Velocity of the base fluid suspended with different particles (up to 5-SF) when $M = 1.0, c = 0.4, \alpha = \frac{\pi}{4}, \gamma = 1.0$ and $Fr = 4.0$.

η	u_f Crystal particles	u_f Hafnium particles
-1.0	0.00000	0.00000
-0.8	0.10531	0.17963
-0.6	0.19859	0.33875
-0.4	0.27103	0.46230
-0.2	0.31672	0.54024
0.0	0.33231	0.56684
0.2	0.31672	0.54024
0.4	0.27103	0.46230
0.6	0.19859	0.33875
0.8	0.10531	0.17963
1.0	0.00000	0.00000

3.4 Conclusion

A comparative analysis is carried out for two different types of multiphase flows through an inclined channel. Crystal-liquid and Hafnium-liquid flows are influenced by the application of transverse magnetic field. Some of key findings are highlighted below:

- Hartmann number and Froude number resist the motion of fluid and particle respectively.
- Both crystal and Hafnium particle are supported by the base fluid.
- Hafnium particles suspends well to form a multiphase flow, as such flow moves faster than crystal-liquid flow.
- Hafnium liquid flow through steep channel is in excellent agreement with the one, as reported for crystal-liquid flow in the existing literature.

Chapter 4

Numerical study on bi-phase Couple stress fluid in the presence of Hafnium and metallic nanoparticles over an inclined plane

This chapter provides a numerical investigation of a particulate flow over an inclined plane. Couple stress fluid serves a base liquid suspended with partially submerged Hafnium particles. Flow is generated due to gravitational effects and free stream flow stretches far from the surface of the slanted plane. Nonlinear flow dynamic is converted in to set of Ordinary Differential Equations (ODEs) employing suitable variables. Runge–Kutta–Fehlberg method is considered to achieve the solution of the flow problem. The contribution of all significant parameters are visualized through graphical results and all findings have been elaborated in complete detail.

4.1 Mathematical formulation

Consider uniform and spherical Hafnium particles submerged in the Couple stress fluid drifting down the slope of an inclined plane as shown in the Figure (4.1). The flow is assumed to be steady and free stream at far away from the flat plane.

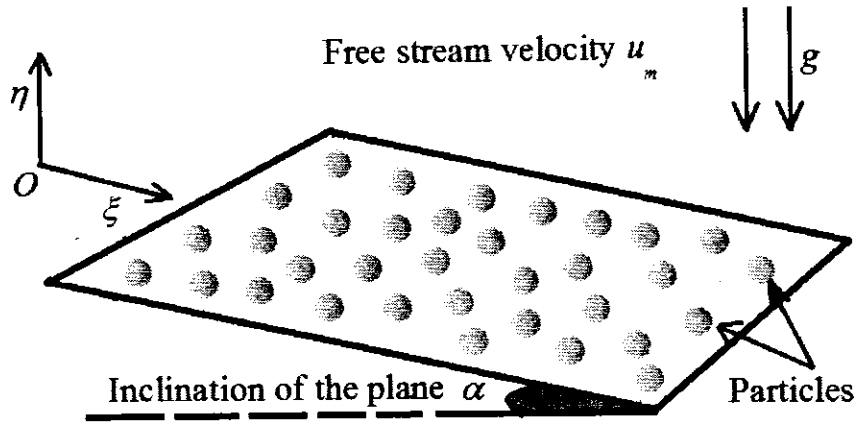

Figure 4.1: Configuration of the semi-infinite plane.

If $[u_f(\xi,\eta), v_f(\xi,\eta), 0]$ and $[u_p(\xi,\eta), v_p(\xi,\eta), 0]$, is the velocity components of base fluid and metallic particles, respectively. Then the governing Eq. (1.31) and Eq. (1.32) in the component form are given as:

4.1.1 For fluid phase

$$\frac{\partial u_f}{\partial \xi} + \frac{\partial v_f}{\partial \eta} = 0, \tag{4.1}$$

$$\rho_f\left(u_f\frac{\partial u_f}{\partial \xi} + v_f\frac{\partial u_f}{\partial \eta}\right) = \left.\begin{matrix}\mu_s\left(\frac{\partial^2 u_f}{\partial \eta^2}\right) - \gamma_1\left(\frac{\partial^4 u_f}{\partial \eta^4}\right) + \frac{CS(u_p - u_f)}{(1-C)} + \\ \frac{g\rho_f}{(1-C)}\sin\alpha - \frac{\partial p}{\partial \xi}\end{matrix}\right\}. \tag{4.2}$$

4.1.2 For particle phase

$$\frac{\partial u_p}{\partial \xi} + \frac{\partial v_p}{\partial \eta} = 0, \tag{4.3}$$

$$\rho_p\left(u_p\frac{\partial u_p}{\partial \xi} + v_p\frac{\partial u_p}{\partial \eta}\right) = CS(u_f - u_p). \tag{4.4}$$

As the given flow phenomenon involves the contribution of the free stream velocity of the fluid i.e., "u_m". Therefore, it is very sensible to consider the following stream functions for both liquid and particles by the following relations:

$$\frac{\partial \bar{\psi}_f}{\partial \eta} = u_f, \text{ and } -\frac{\partial \bar{\psi}_f}{\partial \xi} = v_f, \tag{4.5}$$

$$\frac{\partial \bar{\psi}_p}{\partial \eta} = u_p, \text{ and } -\frac{\partial \bar{\psi}_p}{\partial \xi} = v_p. \tag{4.6}$$

Now, by introducing the following similarity transformations as described by Srinivasacharya and Kaladhar [132] which is an effective tool to convert the above Partial differential equations into ordinary differential equations.

$$\left.\begin{aligned} x = \frac{\eta}{\xi}\sqrt{Re};\ u_f = u_m f'(x);\ v_f = \frac{-1}{2}\sqrt{\frac{u_m \nu}{\xi}}(f - xf') \\ u_p = u_m F'(x);\ v_p = \frac{-1}{2}\sqrt{\frac{u_m \nu}{\xi}}(F - xF') \end{aligned}\right\}. \tag{4.7}$$

In view of Eq. (4.7), after performing mathematical manipulation, Eq. (4.2) takes the following form:

$$\left.\begin{aligned} \rho_f\left(-\frac{\eta {u_m}^2\sqrt{Re}}{\xi^2}f'f'' - \frac{(u_m)^{\frac{3}{2}}\sqrt{\nu Re}}{\xi^{\frac{3}{2}}}(ff'' - xf'f'')\right) = -\frac{x}{\xi}\frac{\partial p}{\partial x} + \\ \frac{\mu u_m Re}{\xi^2}f''' + \frac{CSu_m}{(1-C)}(F' - f') - \frac{\gamma_1 u_m Re^2}{\xi^4}f^v + \frac{g\rho_f}{(1-C)}\sin\alpha \end{aligned}\right\}. \tag{4.8}$$

Using some significant dimensionless constants and parameter that effectively contribute in this particulate flow.

$$\nu = \frac{\mu}{\rho_f};\ Re = \frac{\xi u_m}{\nu};\ F_D = \frac{\xi S}{\rho_f u_m};\ \frac{\partial p}{\partial x} = P;\ \gamma_c = \frac{\gamma_1 Re}{\mu \xi^2};\ Fr = \frac{u_m}{\sqrt{g\xi}} \tag{4.9}$$

In view of Eq. (4.9), one can easily reduce Eq. (4.8) one can easily obtain the Couple stress fluid flow drifting Hafnium particles can be written as follows

$$\gamma_c f'''' = f''' + ff'' + \frac{CF_D}{(1-C)}(F' - f') + \frac{\sin\alpha}{(1-C)(Fr)^2} - P. \tag{4.10}$$

In the same way particle phase reduces to the following non-dimensional expression:

$$F'' = 2F_D \frac{(F' - f')}{(xF' - F)}. \tag{4.11}$$

The boundary conditions which are controlling this particulate the Couple stress fluid flow over and far from the considered flat plane for both phases are respectively defined by:

Case-1: At the inclined flat plane

$$\left.\begin{aligned} (i).\ u_f(\xi,\eta) &= 0, \\ (ii).\ v_f(\xi,\eta) &= 0, \\ (iii).\frac{\partial u_f}{\partial \eta}(\xi,\eta) &= \frac{\partial v_f}{\partial \xi}(\xi,\eta). \end{aligned}\right\};\ \text{at}\ \eta = 0. \tag{4.12}$$

Case-II: Far from the plane

$$\left.\begin{aligned} (iv).\ \frac{\partial u_f}{\partial \eta}(\xi,\eta) &= \frac{\partial v_f}{\partial \xi}(\xi,\eta), \\ (v).\ u_f(\xi,\eta) &= u_m, \\ (vi).u_p(\xi,\eta) &= u_m, \\ (vii).u_p(\xi,\eta) &= v_p(\xi,\eta) \end{aligned}\right\};\ \text{at}\ \eta \to \infty. \tag{4.13}$$

Using Eq. (4.7) in Eqs. (4.12) – (4.13), boundary conditions for both fluid and particle phase in dimensionless form are transformed as:

$$\left.\begin{aligned} (i).\ f(x) &= 0, \\ (ii).\ f'(x) &= 0, \\ (iii).f''(x) &= 0. \end{aligned}\right\};\ \text{at}\ x = 0. \tag{4.14}$$

Similarly, far from the plane

$$\left.\begin{array}{l}(iv).\ f'(x) = 1,\\ (v).\ f''(x) = 0,\\ (vi).\ F'(x) = 1,\\ (vii).F(x) = f(x)\end{array}\right\};\ \text{at } x \to \infty. \tag{4.15}$$

4.2 Solution of the problem

Having a look at the transformed form of mathematical model for fluid and particle phases, it is for sure that neither a closed form nor an analytic solution is possible for such a complex flow problem. There are Couple of reasons that one turns to numerical methods, to seek a formidable solution. First, the transformed ordinary differential equations are nonlinear and coupled with each other. Secondly, the boundary conditions are incomplete for both phases. Therefore, the reduced Eq. (4.10) and Eq. (4.11) are tackled numerically. For this purpose, best suited numerical scheme i.e., Runge–Kutta–Fehlberg method (RKF) is adopted. The requisite of the method is to deal only, with those differential equations which are of first order in nature. The error and mesh size adjustment depend upon the residual of continuation solution. For the solution of any two-point Boundary Value Problem (BVP) method can simply be defined as:

$$y' = g(t, y), \qquad a \le t \le b. \tag{4.16}$$

Corresponding to the boundary conditions:

$$y(a) = 0, \quad \text{and } y(b) = 0. \tag{4.17}$$

An approximated solution $s(t)$ of Eq. (4.17), yields a smooth unflinching curve defined on each subinterval of the mesh which is given below

$$(t_{n^*}, t_{n^*+1}), \text{ Where } n^* = 0,1,2, \ldots N. \tag{4.18}$$

The required subintervals which impart this iterative scheme can be chosen from the following

$$a = t_0 < t_1 < t_2 < t_3 \ldots < t_{n^*-1} < t_{n^*} = b. \tag{4.19}$$

The obtained numerical solution can't be reliable unless $s(t)$ satisfies the boundary conditions besides, the given below differential equations at middle point of each interval and extreme points of each interval, as well.

$$s'(t_{n^*}) = g\left(t_{n^*}, s(t_{n^*})\right) = 0, \tag{4.20}$$

$$s'\left(\frac{t_{n^*} + t_{n^*+1}}{2}\right) = g\left(\left(\frac{t_{n^*} + t_{n^*+1}}{2}\right), s\left(\frac{t_{n^*} + t_{n^*+1}}{2}\right)\right) = 0, \tag{4.21}$$

$$s'(t_{n^*+1}) = g\left(t_{n^*+1}, s(t_{n^*+1})\right) = 0. \tag{4.22}$$

After the introduction of such conditions, one will obtain a nonlinear system of algebraic equations. To tackle nonlinearity these will be linearized before proceeding to the iterative scheme.

For this given problem this numerical technique worked efficiently well and the contribution of different emerging parameters; such as the Couple stress parameter, Froud number, drag force, and density parameters, on $f'(x)$ and $F'(x)$ have been studied through graphs. The effects of the emerging parameters on the $f'(x)$ and $F'(x)$ are studied. The asymptotic boundary conditions are approximated by using a value of 9 for x maximum as follows:

$$x_{max} = 9. \tag{4.23}$$

Therefore, the given conditions defined far from the plane take the form

$$f'(9) = 1, \quad f''(9) = 0, \quad F'(9) = 1, \quad F(9) = f(9). \tag{4.24}$$

4.3 Analysis

The most significant and instructive parametric study of two-phase flow phenomena is carried out in this portion. The main emphasis is given to study the motion of both phases. Consequently, a thorough analysis of each phase velocity is examined for different pertinent parameters, which contribute in various perspectives, namely, local

Couple stress parameter γ_c, drag force coefficient F_D, Froude number Fr, concentration of particles C and inclination of the plane α.

Figures $(4.2) - (4.3)$ describe the role of drag force coefficient on Couple stress fluid and Newtonian fluid case. It is a well-recognized fact that drag force acts like a force of resistance. Therefore, application of drag force on any natural or mechanical flow results to retard the celerity of Couple stress fluid. This can be perceived that due to the instinctive stresses of the Couple stress fluid which further enhance drag force as can be witnessed in Figure (4.2), for the case of Couple stress fluid. Similar type of flow behavior is depicted for Newtonian fluid in Figure (4.3).

The number density of Hafnium particles has been spotted in Figures $(4.4) - (4.5)$, respectively for both types of fluids. Over all behavior of the Couple stress fluid remains the same with an exception that the fluid velocity is further supported by the introduction of additional metallic particles to the flow. With the perception that increase of additional particles will hamper the flow by further strengthening the drag. But, one must not ignore the role of an inclined plane due to gravity which contributes a lot by increasing the momentum of the particles. This galvanizes the velocity of both types of fluids.

The Froude number has a significance usage. It arises in such flow phenomenon where a free surface of the fluid is involved. For a common approach this dimensionless number describes as how gravity affects a moving liquid. This number has many applications in naval and aerospace engineering. In such dynamics, Froude number helps engineers to analyze the resistance of a moving body which is partially submerged in the fluid. This claim is approved in the Figures $(4.6) - (4.7)$. Here, velocity of the fluid is drastically reducing due to Froude number. By increasing inertial forces or

minimizing the effects of external fields, metallic particles exerts some extra force of repulsion on the fluid and hampered both flows. One must not have any confusion to infer the results by looking at Figures (4.8) – (4.9), corresponding to the variation in the inclination of the flat plane. It is convincing reality about any flow over a flat plane that higher the inclination of the plane, faster the movement of the objects lying on its surface.

Figures (4.10) – (4.14) are dedicated to study that how the movement of Hafnium particles is influenced by the concerned key parameters. It is seen that the particles find hard to move freely in both types of base fluid, subject to increase in drag force coefficient which is evident in the relevant figures.

It is obvious that drag force increases the resistance between any two adjacent metallic particles. Henceforth, the free movement of the particles gradually declines. Figure (4.12) identifies the role of Froude number on the metallic particles. One can see that as motion of the particles is resisted by the higher values of Froude number. On the other hand, in Figure (4.13) elevation of the slanted plane. It is observed that higher slope of the plane allows the particles to drift down quickly. Finally, in Figure (4.14) the concentration of the particles is varied. As quantity of particles is increased then their movement is also increased. Finally, the comparison between Newtonian fluid and Couple stress fluid is made in Figure (4.15). Here, one can clearly see that Newtonian fluid moves faster as compared to Couple stress fluid. This can be termed as the effects of viscous forces in Couple stress fluid are greater than Newtonian fluid. However, the fluid velocity for both cases increase against the increase in particle concentration.

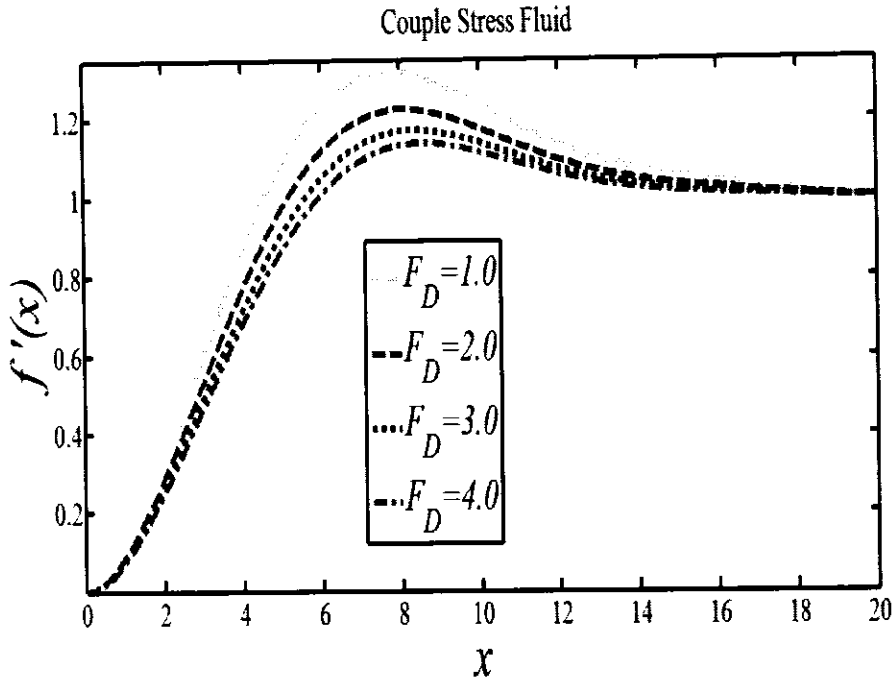

Figure 4.2: Variation of drag force coefficient on the fluid velocity.

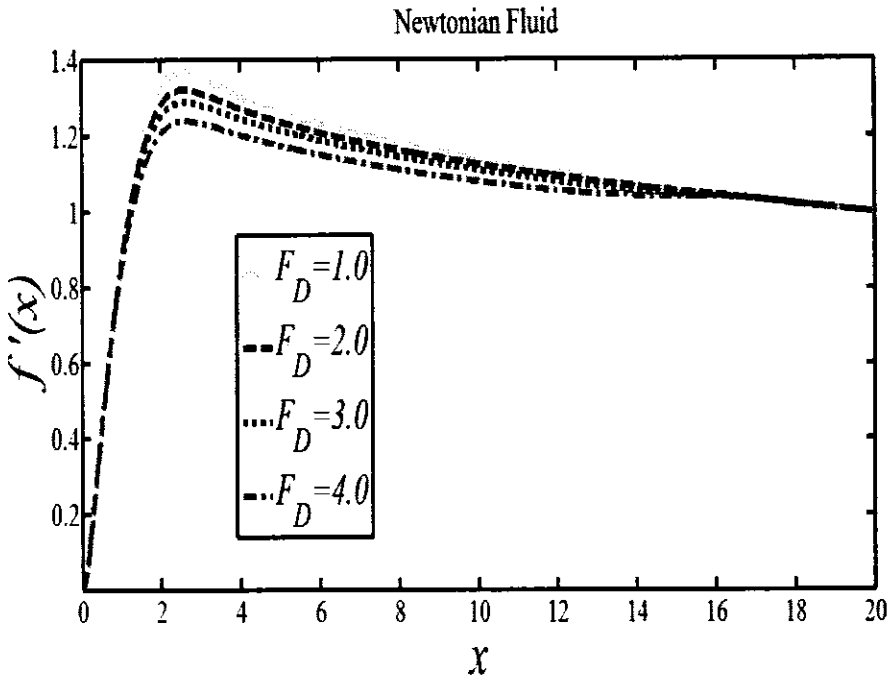

Figure 4.3: Variation of drag force coefficient on the fluid velocity.

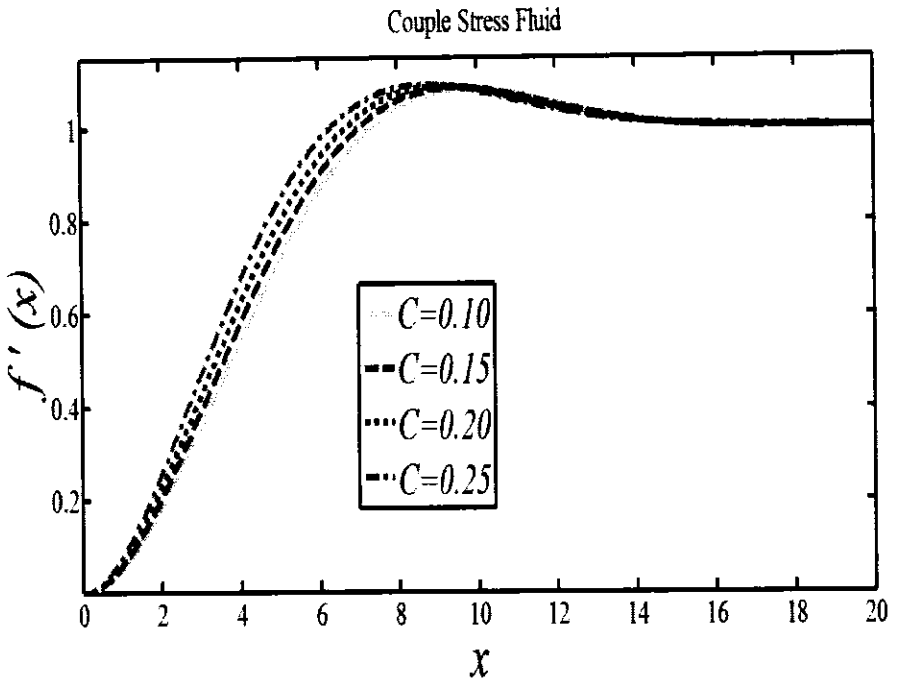

Figure 4.4: Variation of particle concentration on the fluid velocity.

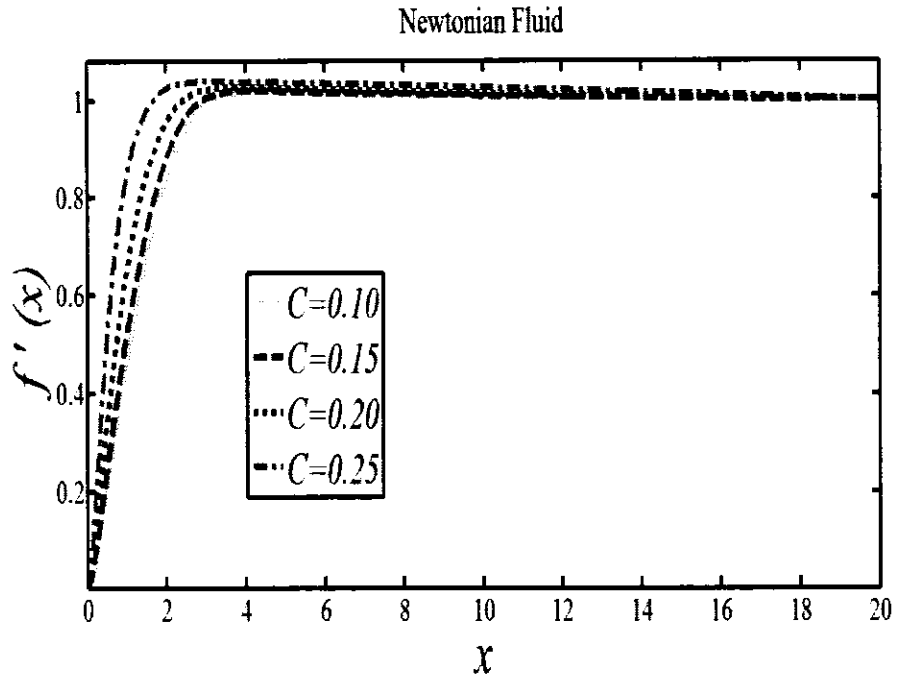

Figure 4.5: Variation of particle concentration on the fluid velocity.

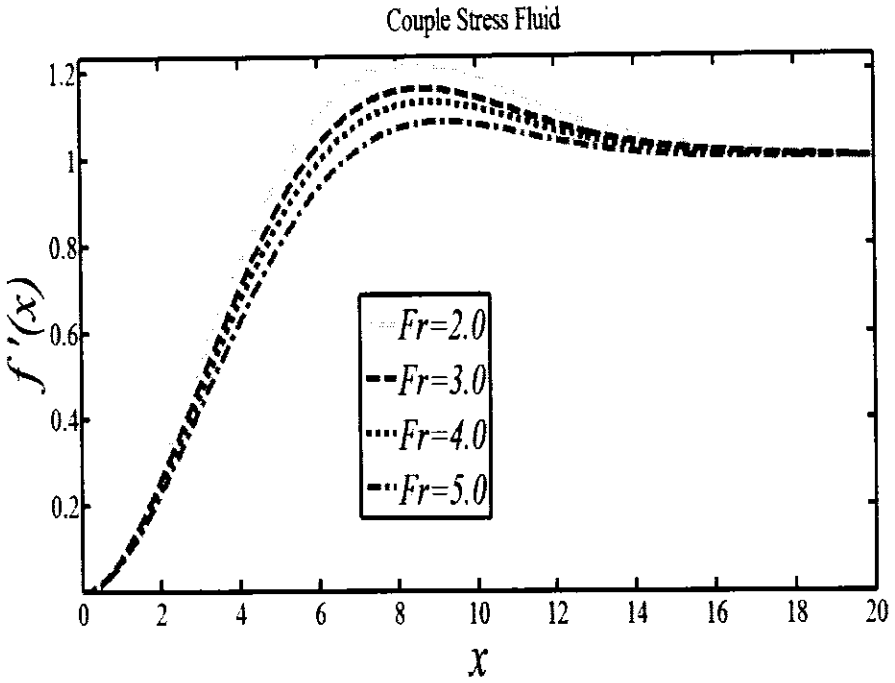

Figure 4.6: Variation of Froude number on the fluid velocity.

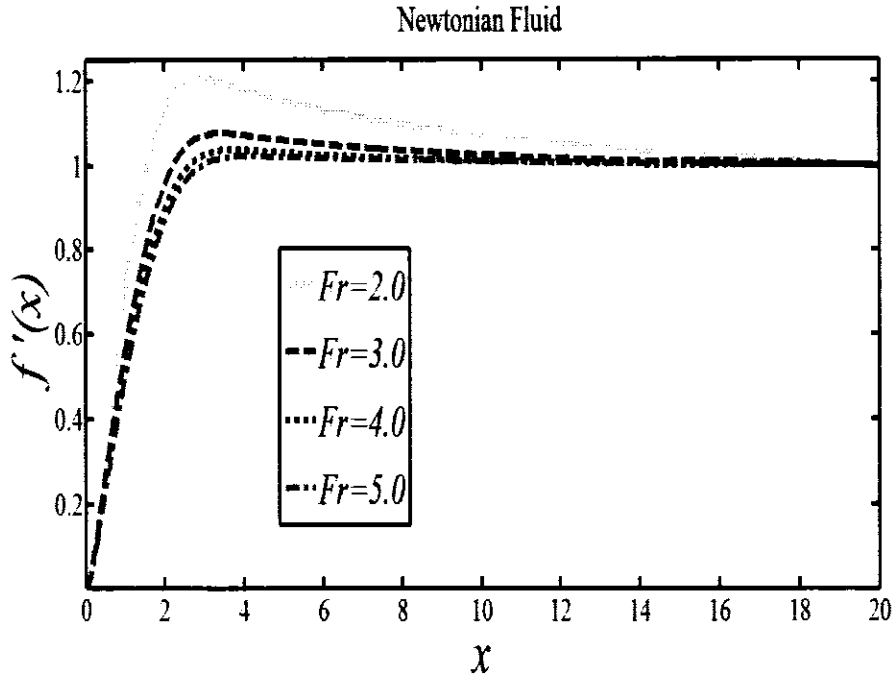

Figure 4.7: Variation of Froude number on the fluid velocity.

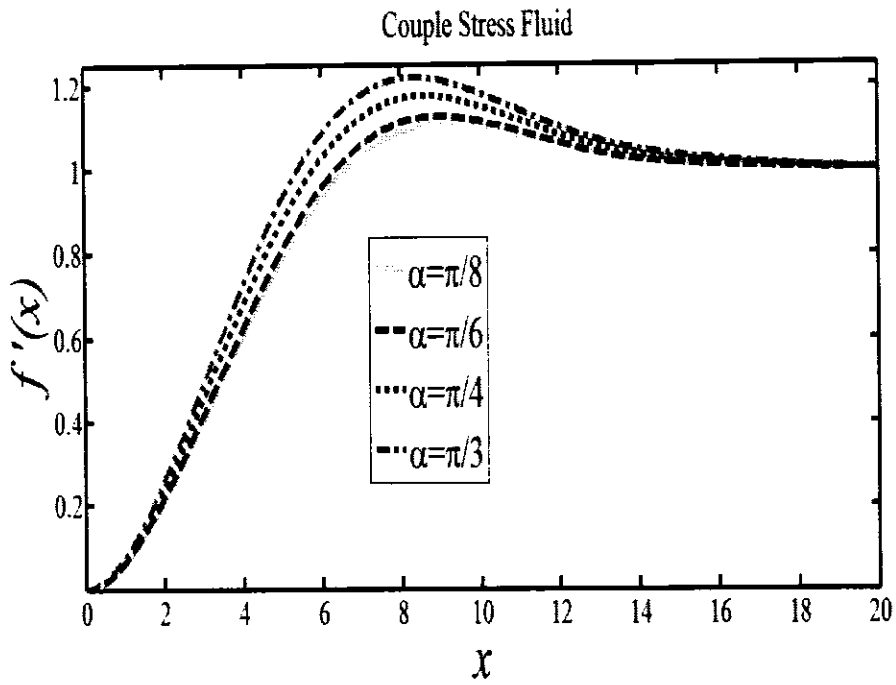

Figure 4.8: Variation of inclination of the plane on the fluid velocity.

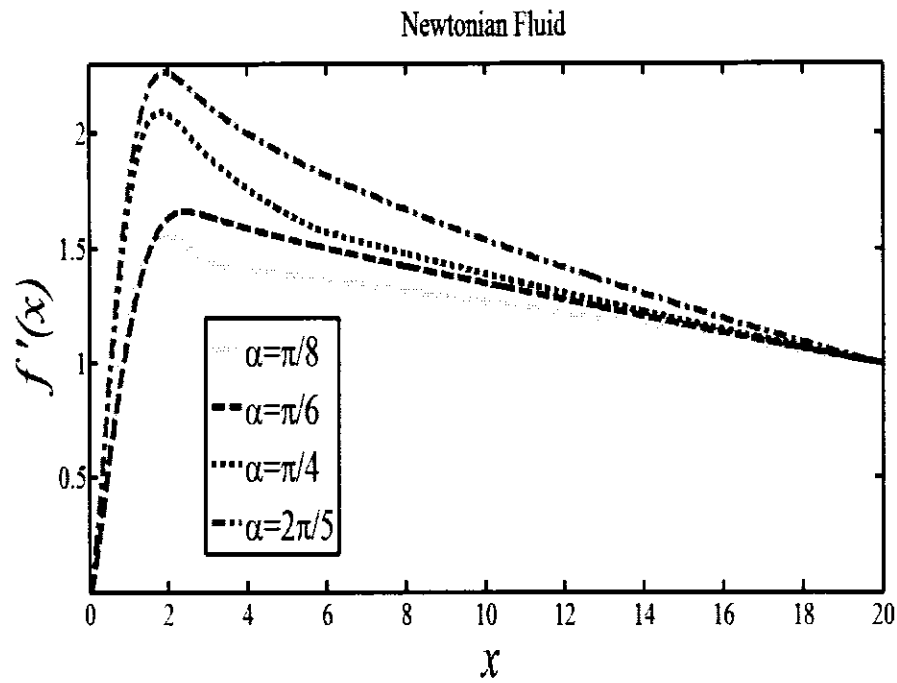

Figure 4.9: Variation of inclination of the plane on the fluid velocity.

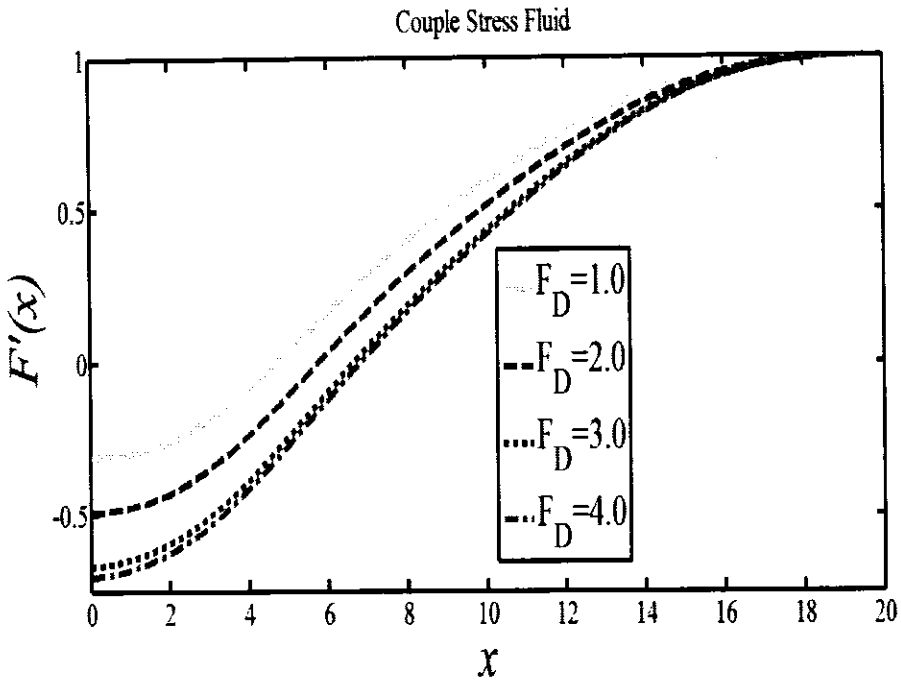

Figure 4.10: Variation of drag force coefficient on velocity of particle.

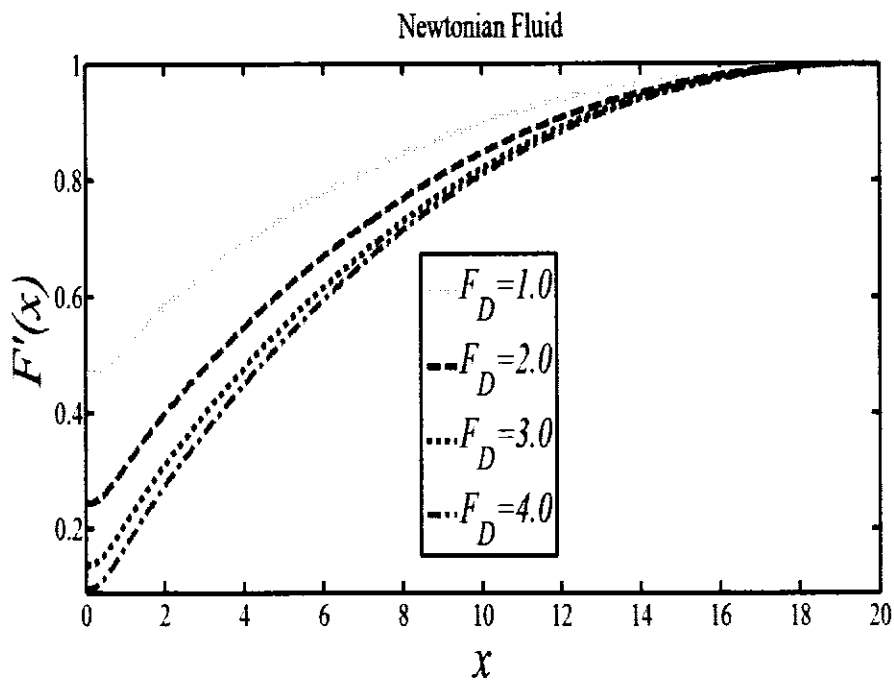

Figure 4.11: Variation of drag force coefficient on velocity of particle.

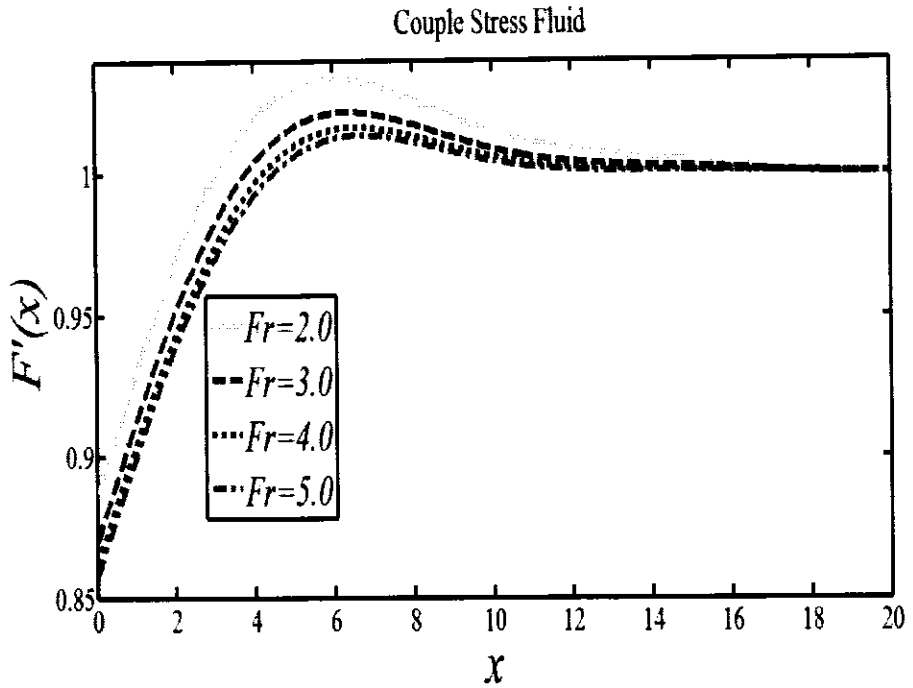

Figure 4.12: Variation of Froude number on velocity of particle.

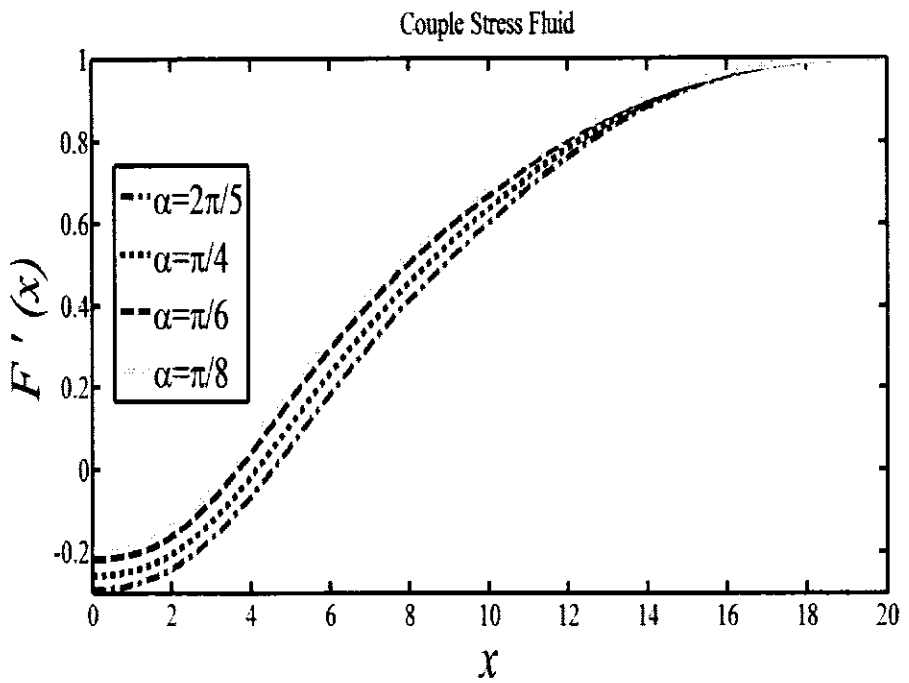

Figure 4.13: Variation of inclination of the plane on velocity of particle.

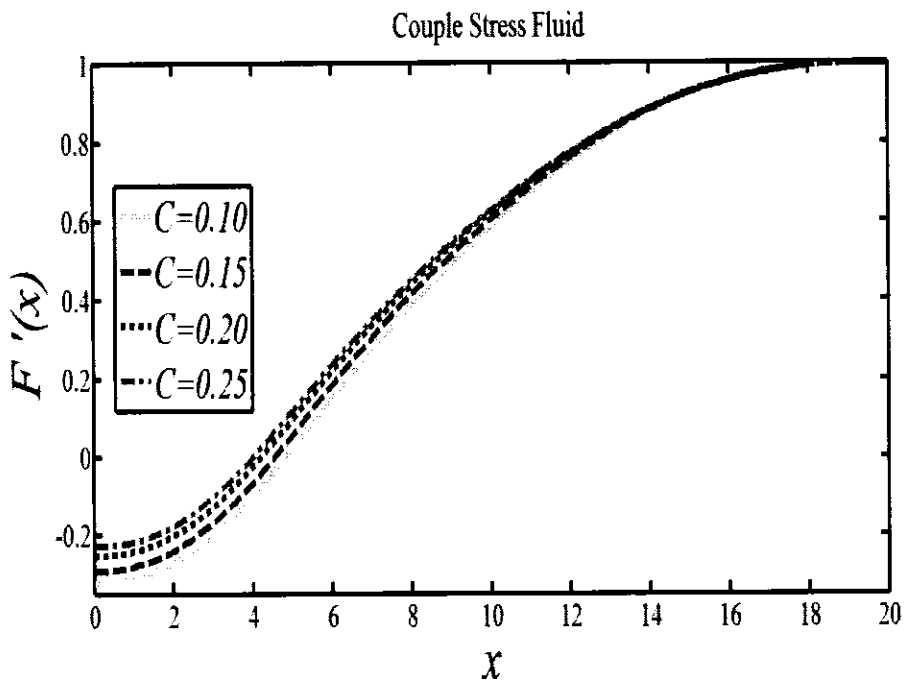

Figure 4.14: Variation of particle concentration on velocity of particle.

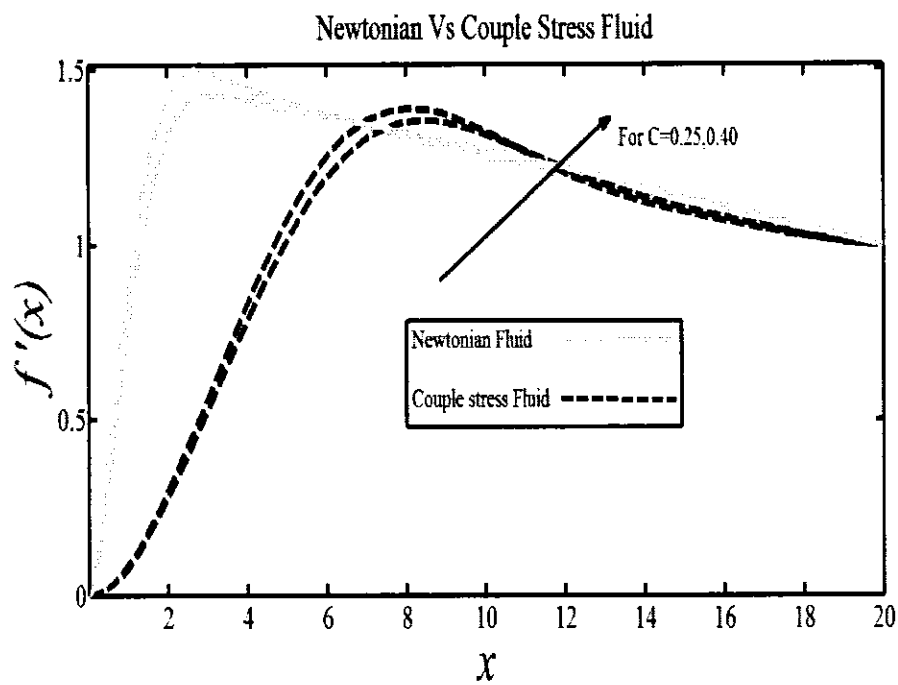

Figure 4.15: Variation of particle concentration on both types of fluids.

4.4 Conclusion

A granular flow of Hafnium particles is studied moving down the surface of a plane in this study. The Couple stress fluid serves to represent a slanting non-Newtonian flow that stretches boundless from the flat surface of the plan. The flow is modeled with a great skill by taking Navier-Stokes' equations into account. Having applied a suitable transformation, Runge–Kutta–Fehlberg technique is preferred to seek a compatible numerical solution for such nonlinear flow problem. Flow pattern of both phases are examined through graphs to make sure that flow has complete agreement with the mathematical formulation. In addition to this, some new findings have also been inferred which are enlisted below:

- The drag force resists the Couple stress fluid while the Newtonian flow is supported by increasing the velocity.
- For both types of flows, movement of the particle is retarded gradually against the drag force coefficient.
- An increase in the plane rapidly increases the velocity of both phases.
- The addition of new metallic particles act differently on the velocity of each phase.
- The movement of each particle and fluid (both the Couple stress and Newtonian) is retarded due the variation in Froud number.
- The coefficient of drag force and the inclination of the plane cause different on skin friction coefficient.
- The fluid model reduces back to Newtonian one by removing or eliminating the parameter of Couple stress parameter as shown in each figures that provides clear evidence for the validation of reported results.

Chapter 5

Modelling study on heated Couple stress fluid peristaltically conveying gold nanoparticles through coaxial tubes

This chapter i relevant to the peristaltic transport of Couple stress fluid through the space between coaxial cylinders. The inner tube is rigid in composition while outer cylinder has elastic walls. The investigation suggests a remedy for swollen or disorder in the human tissues and organs by means of nano size particles. The higher thermal conductivity and large atomic number of gold can effectively easily malign tissues, as the rapid Brownian diffusion of the particle, rapidly convey medicine to the effected organs. The nano fluid flow is modeled with the momentum and energy equation are taken into account along with the mass transfer equation for the diffusion of the concentration of particle.

5.1 Mathematical formulation

If $\vec{V} = [U(R,Z,t)\ \ 0\ \ W(R,Z,t)]$ represents the flow of nanofluid through concentric tubes as shown in the Figure below. Blood is considered as the flow of Couple stress fluid which suspends with the nano-size gold particles to form a nanofluid. For

Brownian and thermophoresis diffusion of golden particles from higher region of concentration to the lower region Buongiorno model is considered.

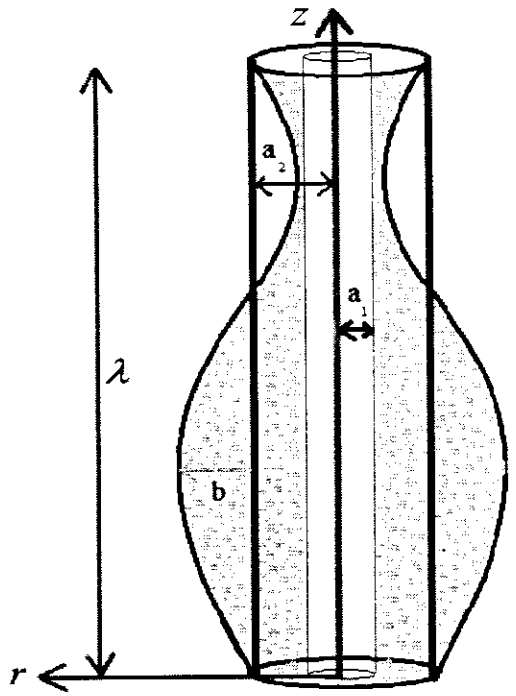

Figure 5.1: Configuration of coaxial tubes.

The component form of Eqs. (1.31) – (1.34) that describe the momentum convection, thermal convection and mass/particle convection after employing Oberbeck-Boussinesq approximation are given as:

$$\frac{U}{R}+\frac{\partial U}{\partial R}+\frac{\partial W}{\partial Z}=0, \tag{5.1}$$

$$\rho_{nf}\left(\frac{\partial U}{\partial t}+U\frac{\partial U}{\partial R}+W\frac{\partial U}{\partial Z}\right)=\left.\begin{aligned}&-\frac{\partial p}{\partial R}+\mu_{nf}\left(\frac{\partial^2 U}{\partial R^2}+\frac{1}{R}\frac{\partial U}{\partial R}+\frac{\partial^2 U}{\partial Z^2}\right)-\\&\gamma_1\left[\begin{aligned}&\frac{\partial^4 U}{\partial R^4}+\frac{2\partial^3 U}{R\partial R^3}+\frac{\partial^2 U}{R^2\partial R^2}+\\&\frac{\partial^4 U}{\partial R^2\partial Z^2}+\frac{\partial U}{R^3\partial R}+\frac{\partial^3 U}{R\partial R\partial Z^2}+\\&\frac{\partial^4 U}{\partial Z^2\partial R^2}+\frac{\partial^3 U}{R\partial Z^2\partial R}+\frac{\partial^4 U}{\partial Z^4}\end{aligned}\right]\end{aligned}\right\}, \tag{5.2}$$

$$\rho_{nf}\left(\frac{\partial W}{\partial t}+U\frac{\partial W}{\partial R}+W\frac{\partial W}{\partial Z}\right)=\left.\begin{array}{l}-\frac{\partial p}{\partial Z}+\mu_{nf}\left(\frac{\partial^2 W}{\partial R^2}+\frac{1}{R}\frac{\partial W}{\partial R}+\frac{\partial^2 W}{\partial Z^2}\right)-\\ \gamma_1\left[\begin{array}{l}\frac{\partial^4 W}{\partial R^4}+\frac{2\partial^3 W}{R\partial R^3}+\frac{\partial^2 W}{R^2\partial R^2}+\\ \frac{\partial^4 W}{\partial R^2\partial Z^2}+\frac{\partial W}{R^3\partial R}+\frac{\partial^3 W}{R\partial R\partial Z^2}+\\ \frac{\partial^4 W}{\partial Z^2\partial R^2}+\frac{\partial^3 W}{R\partial Z^2\partial R}+\frac{\partial^4 U}{\partial Z^4}\end{array}\right]+\\ [\varphi\rho_p+(1-\varphi)\{\rho_f(1-\beta_T(T-\theta_w))\}]g\end{array}\right\}, \quad (5.3)$$

$$(\rho c)_{nf}\left(\frac{\partial T}{\partial t}+U\frac{\partial T}{\partial R}+W\frac{\partial T}{\partial Z}\right)=\left.\begin{array}{l}k_1\left(\frac{\partial^2 T}{\partial R^2}+\frac{1}{R}\frac{\partial T}{\partial R}+\frac{\partial^2 T}{\partial R^2}\right)+\\ (\rho c)_{np}\left[\begin{array}{l}D_b\left(\frac{\partial\varphi}{\partial R}\frac{\partial T}{\partial R}+\frac{\partial\varphi}{\partial Z}\frac{\partial T}{\partial Z}\right)+\\ \frac{D_T}{\theta_w}\left\{\left(\frac{\partial T}{\partial R}\right)^2+\left(\frac{\partial\varphi}{\partial Z}\right)^2\right\}\end{array}\right]\end{array}\right\}, \quad (5.4)$$

$$\left(\frac{\partial\varphi}{\partial t}+U\frac{\partial\varphi}{\partial R}+W\frac{\partial\varphi}{\partial Z}\right)=\left.\begin{array}{l}D_b\left(\frac{\partial^2\varphi}{\partial R^2}+\frac{1}{R}\frac{\partial\varphi}{\partial R}+\frac{\partial^2\varphi}{\partial Z^2}\right)+\\ \frac{D_T}{\theta_w}\left(\frac{\partial^2 T}{\partial R^2}+\frac{1}{R}\frac{\partial T}{\partial R}+\frac{\partial^2 T}{\partial R^2}\right)\end{array}\right\}. \quad (5.5)$$

The corresponding boundary at the extreme walls:

Case 1. At the rigid wall:

$$\left.\begin{array}{l}(i).W(R)=0,\\ (ii).\ T(R)=\theta_1,\\ (iii).\varphi(R)=\phi_1.\end{array}\right\};\ \text{When}\quad R=a_1. \quad (5.6)$$

Case 2. At the flexible wall:

$$\left.\begin{array}{l}(iv).W(R)=0,\\ (v).\ T(R)=\theta_2,\\ (vi).\varphi(R)=\phi_2.\end{array}\right\};\ \text{When}\ R=\tilde{r}_3=a_2+b\cos\frac{2\pi}{\lambda}(Z-\tilde{c}\tilde{t}). \quad (5.7)$$

Eqs. (5.1) – (5.7) is the peristaltic transport of nanofluid in a laboratory frame which requires to be shifted into a wave frame. This can be achieved by the introduction of the given below transformation in the above equations.

$$\left.\begin{array}{c} \tilde{r} = R;\ \ \tilde{z} = Z - \tilde{c}\tilde{t}\ ;\ \tilde{u}(\tilde{r},\tilde{z}) = U(R,Z,\tilde{t})\ ;\ \tilde{w}(\tilde{r},\tilde{z}) = W(R,Z,\tilde{t}) - \tilde{c}; \\ \tilde{\phi}(\tilde{r},\tilde{z}) = \varphi(R,Z,\tilde{t})\ ;\ \tilde{\theta}(\tilde{r},\tilde{z}) = T(R,Z,\tilde{t}) \end{array}\right\}. \tag{5.8}$$

Having use the above wave transformation in Eqs. (5.1) – (5.7), the obtained equation can be non-dimensionalised with following variables and parameter.

$$\left.\begin{array}{c} \frac{\tilde{r}}{a_2} = r;\ \ \frac{\tilde{z}}{\lambda} = z\ ;\ \frac{\tilde{u}\lambda}{\tilde{c}a_2} = u\ ;\ \frac{\tilde{w}}{\tilde{c}} = w\ \ ;\ \frac{a_2^2 p}{\tilde{c}\lambda\mu_{nf}} = \tilde{p}\ ;\ \frac{\tilde{\theta} - \theta_2}{\theta_1 - \theta_2} = \theta\ ; \\ \frac{b}{a_2} = \epsilon_1;\ 1 + \epsilon_1\cos(2\pi z) = r_3\ ;\ \sqrt{\frac{\mu_{nf}}{\gamma_1}}a_2 = \gamma\ ;\ \frac{k_1}{(\rho c)_{nf}} = \epsilon_3\ ; \\ \frac{(\rho c)_{np}}{(\rho c)_{nf}} = \epsilon_2;\ \frac{a_2}{\lambda} = \delta;\ \frac{{a_2}^2(\phi_1 - \phi_2)(\rho_{np} - \rho_{nf})g}{\tilde{c}\mu_{nf}} = B_d; \\ \frac{D_t(\theta_1 - \theta_2)}{\theta_2} = N_t;\ \frac{{a_2}^2(\theta_1 - \theta_2)\,(1 - \phi_2)\rho_{nf}\beta_T g}{\tilde{c}\mu_{nf}} = G_r; \\ \frac{\tilde{r}_3}{a_2} = r_3; \frac{a_1}{a_2} = r_2;\ D_b(\phi_1 - \phi_2) = N_b;\ \frac{\tilde{c}\,\tilde{t}}{\lambda} = t;\ \frac{\tilde{\phi} - \phi_2}{\phi_1 - \phi_2} = \phi; \\ E_1 = \frac{\tilde{c}m_1^* a_2^3}{\lambda^3\mu_{nf}};\ E_2 = \frac{-m_2^* a_2^3}{\lambda^2\mu_{nf}};\ E_3 = \frac{-m_3^* a_2^3}{\tilde{c}\lambda^3\mu_{nf}}. \end{array}\right\}. \tag{5.9}$$

The assumption of long wave length gives the final form of nanofluid flow:

$$\frac{\partial}{\partial r}(ru) + \frac{\partial w}{\partial z} = 0, \tag{5.10}$$

$$\frac{d\tilde{p}}{dr} = 0, \tag{5.11}$$

$$\frac{d^2w}{dr^2} + \frac{1}{r}\frac{dw}{dr} - \frac{1}{\gamma^2}\left(\frac{d^4w}{\partial r^4} + \frac{2}{r}\frac{d^3w}{dr^3} - \frac{1}{r^2}\frac{d^2w}{dr^2} + \frac{1}{r^3}\frac{dw}{dr}\right) + B_d\phi + G_r\theta = \frac{d\tilde{p}}{dz}, \tag{5.12}$$

$$\epsilon_3\left(\frac{d^2\theta}{dr^2} + \frac{1}{r}\frac{d\theta}{dr}\right) + \epsilon_2\left(N_b\left(\frac{d\theta}{dr}\right)\left(\frac{d\phi}{dr}\right) + N_t\left(\frac{d\theta}{dr}\right)^2\right) = 0, \tag{5.13}$$

$$N_b\left(\frac{d^2\phi}{dr^2} + \frac{1}{r}\frac{d\phi}{dr}\right) + N_t\left(\frac{d^2\theta}{dr^2} + \frac{1}{r}\frac{d\theta}{dr}\right) = 0. \tag{5.14}$$

The boundary conditions at different walls are listed as:

$$\left.\begin{array}{l}(i).w(r)=-1,\\(ii).\frac{d^2w}{dr^2}(r)=0,\\(iii).\theta(r)=1,\\(iv).\phi(r)=1.\end{array}\right\};\ \text{When } r=r_2. \tag{5.15}$$

$$\left.\begin{array}{l}(v).\ w(r)=-1,\\(vi).\frac{d^2w}{dr^2}(r)=0,\\(vii).\theta(r)=0,\\(viii).\phi(r)=0,\\(xi).\frac{d^2w}{dr^2}-\frac{1}{\gamma^2}\left(\frac{d^4w}{\partial r^4}+\frac{2}{r}\frac{d^3w}{dr^3}-\frac{1}{r^2}\frac{d^2w}{dr^2}+\frac{1}{r^3}\frac{dw}{dr}\right)+\\\frac{1}{r}\frac{dw}{dr}+B_d\phi+G_r\theta=(E_1+E_3)\frac{d^3r_3}{dr^3}+E_2\frac{d^2r_3}{dr^2}\end{array}\right\};\ \text{When } r=r_3. \tag{5.16}$$

5.2 Solution of problem

If $w_0(r)$, $\theta_0(r)$, $\phi_0(r)$ denote the initial guess and $\mathcal{L}_w$, $\mathcal{L}_\theta$, $\mathcal{L}_\phi$ represent the linear operator for momentum, thermal and mass flux density, respectively as defined of higher order differential mapping [133] as:

$$w_0(r)=-1, \tag{5.17}$$

$$\theta_0(r)=\frac{r-r_2}{r_1-r_2}, \tag{5.18}$$

$$\phi_0(r)=\frac{r-r_2}{r_1-r_2}. \tag{5.19}$$

In view of main governing equations, the linear operators may easily be selected as:

$$\mathcal{L}_w=w''(r), \tag{5.20}$$

$$\mathcal{L}_\theta=\theta''(r), \tag{5.21}$$

$$\mathcal{L}_{\phi} = \phi''(r). \tag{5.22}$$

Deformation problems at zeroth-order can be expressed as:

$$(1-\epsilon)\mathcal{L}_w\{w(r,\epsilon) - w_0(r)\} = \epsilon\hbar_w N_w\{w(r,\epsilon),\ \theta(r,\epsilon),\ \phi(r,\epsilon)\}, \tag{5.23}$$

$$(1-\epsilon)\mathcal{L}_\theta\{\theta(r,\epsilon) - \theta_0(r)\} = \epsilon\hbar_\theta N_\theta\{w(r,\epsilon),\ \theta(r,\epsilon),\ \phi(r,\epsilon)\}, \tag{5.24}$$

$$(1-\epsilon)\mathcal{L}_\phi\{\phi(r,\epsilon) - \phi_0(r)\} = \epsilon\hbar_\phi N_\phi\{w(r,\epsilon),\ \theta(r,\epsilon),\ \phi(r,\epsilon)\}. \tag{5.25}$$

The analytic solution can be obtained by defining the following sets of boundary conditions:

$$\left.\begin{array}{l}(i).\, w(r,\epsilon) = -1\\ (ii).\ \frac{d^2w}{dr^2}(r,\epsilon) = 0\\ (iii).\ \theta(r,\epsilon) = 1\\ (iv).\ \phi(r,\epsilon) = 1\end{array}\right\};\ \text{When } r = r_2. \tag{5.26}$$

$$\left.\begin{array}{l}(v).\, w(r,\epsilon) = -1\\ (vi).\ \frac{d^2w}{dr^2}(r,\epsilon) = 0\\ (vii).\ \theta(r,\epsilon) = 0\\ (viii).\ \phi(r,\epsilon) = 0\end{array}\right\};\ \text{When } r = r_3. \tag{5.27}$$

Since, the convergence of analytic solutions [134] heavily depends upon the best optimum value of some non-zero auxiliary parameters. One can easily identify those given in Eqs. $(5.23) - (5.25)$, such as h_w, h_θ and h_φ. However, the presence of nonlinear operators N_w, N_θ and N_ϕ along with the embedding parameter "ϵ" lies in the interval $0 \leq \epsilon \leq 1$ defines the given criteria:

$$\left.\begin{array}{lll}For & \epsilon = 0 & \epsilon = 1\\ w(r,\epsilon) & w_0(r) & w(r)\\ \theta(r,\epsilon) & \theta_0(r) & \theta(r)\\ \phi(r,\epsilon) & \phi_0(r) & \phi(r)\end{array}\right\}. \tag{5.28}$$

$$N_w[w(r,\epsilon),\ \theta(r,\epsilon),\ \phi(r,\epsilon)] = \left.\begin{aligned}\frac{d^2w}{dr^2}+\frac{1}{r}\frac{dw}{dr}-P+B_d\phi+G_r\theta-\\ \frac{1}{\gamma^2}\left(\frac{d^4w}{\partial r^4}+\frac{2}{r}\frac{d^3w}{dr^3}-\frac{1}{r^2}\frac{d^2w}{dr^2}+\frac{1}{r^3}\frac{dw}{dr}\right)\end{aligned}\right\}, \tag{5.29}$$

$$N_\theta[w(r,\epsilon),\ \theta(r,\epsilon),\ \phi(r,\epsilon)] = \left.\begin{aligned}\alpha\left(\frac{d^2\theta}{dr^2}+\frac{1}{r}\frac{d\theta}{dr}\right)+\\ \tau\left(N_b\left(\frac{d\theta}{dr}\right)\left(\frac{d\phi}{dr}\right)+N_t\left(\frac{d\theta}{dr}\right)^2\right)\end{aligned}\right\}, \tag{5.30}$$

$$N_\phi[w(r,\epsilon),\ \theta(r,\epsilon),\ \phi(r,\epsilon)] = N_b\left(\frac{d^2\phi}{dr^2}+\frac{1}{r}\frac{d\phi}{dr}\right)+N_t\left(\frac{d^2\theta}{dr^2}+\frac{1}{r}\frac{d\theta}{dr}\right). \tag{5.31}$$

Variation of the embedding parameter ϵ in the suggested domain causes $w(r,\epsilon), \theta(r,\epsilon)$ and $\phi(r,\epsilon)$ to vary form initial guess $w_0(r)$, $\theta_0(r)$ and $\phi_0(r)$ to desired $w(r,\epsilon)$, $\theta(r,\epsilon)$ and $\phi(r,\epsilon)$ solution.

Let us expand $w(r,\epsilon), \theta(r,\epsilon)$ and $\phi(r,\epsilon)$ in Taylor's series as:

$$w(r,\epsilon) = w_0(r)+\sum_{q=1}^{\infty} w_q(r)\epsilon^q, \tag{5.32}$$

$$\theta(r,\epsilon) = \theta_0(r)+\sum_{q=1}^{\infty} \theta_q(r)\epsilon^q, \tag{5.33}$$

$$\phi(r,\epsilon) = \phi_0(r)+\sum_{q=1}^{\infty} \phi_q(r)\epsilon^q. \tag{5.34}$$

Here, $w_q(r)$, $\theta_0(r)$ and $\phi_0(r)$ are respectively defined as:

$$w_q(r) = \frac{1}{q!}\left.\frac{\partial^q w(r,\epsilon)}{\partial\epsilon^q}\right|_{\epsilon=0}, \tag{5.35}$$

$$\theta_0(r) = \frac{1}{q!}\frac{\partial^q \theta(r,\epsilon)}{\partial \epsilon^q}\bigg|_{\epsilon=0}, \tag{5.36}$$

$$\phi_0(r) = \frac{1}{q!}\frac{\partial^q \phi(r,\epsilon)}{\partial \epsilon^q}\bigg|_{\epsilon=0}. \tag{5.37}$$

The expression of q^{th}- order deformation for Eqs. (5.23) – (5.25) are laid down in the following equations.

$$\mathcal{L}_w\left[w_q(r) - \chi_q w_{q-1}(r)\right] = h_w \Re_q{}^w(r), \tag{5.38}$$

$$\mathcal{L}_\theta\left[\theta_q(r) - \chi_q \theta_{q-1}(r)\right] = h_\theta \Re_q{}^\theta(r), \tag{5.39}$$

$$\mathcal{L}_\phi\left[\phi_q(r) - \chi_q \phi_{q-1}(r)\right] = h_\phi \Re_q{}^\phi(r). \tag{5.40}$$

The relevant boundary conditions at rigid and elastic wall can be represented as:

$$\left.\begin{array}{l}(i).\, w_q(r,\epsilon) = -1\\ (i).\frac{d^2 w_q}{dr^2}(r,\epsilon) = 0\\ (ii).\ \theta_q(r,\epsilon) = 1\\ (iii).\ \phi_q(r,\epsilon) = 1\end{array}\right\};\ \text{When } r = r_2. \tag{5.41}$$

$$\left.\begin{array}{l}(v).\, w_q(r,\epsilon) = -1\\ (vi)\frac{d^2 w_q}{dr^2}(r,\epsilon) = 0\\ (vii).\ \theta_q(r,\epsilon) = 0\\ (viii).\ \phi_q(r,\epsilon) = 0\end{array}\right\};\ \text{When } r = r_3, \tag{5.42}$$

$$\chi_q = \begin{cases} 0, & Whenever\ q < 0,\\ 1, & when\ ever\ q > 1.\end{cases} \tag{5.43}$$

$$\Re_q^w(r) = w''_q + \frac{1}{r}w'_q - \frac{1}{\gamma^2}\left(w''''_q + \frac{2}{r}w'''_q - \frac{1}{r^2}w''_q + \frac{1}{r^3}w'_q\right) - P + \left.\begin{array}{l} \\ B_d\phi_q + G_r\theta_q\end{array}\right\}, \tag{5.44}$$

$$\Re_q^{\theta}(r) = \alpha\left(\theta''_q + \frac{1}{r}\theta'_q\right) + \tau\left[N_b \sum_{k_1=0}^{q} \theta'_k \phi'_{k-q} + N_t\left(\theta'_q\right)^2\right], \tag{5.45}$$

$$\Re_q^{\phi}(r) = N_b\left(\phi''_q + \frac{1}{r}\phi'_q\right) + N_t\left(\theta''_q + \frac{1}{r}\theta'_q\right). \tag{5.46}$$

The q^{th}-order approximation for solution can be stated as:

$$w(r) = w_0(r) + \sum_{n^*=1}^{q} w_{n^*}(r), \tag{5.47}$$

$$\theta(r) = \theta_0(r) + \sum_{n^*=1}^{q} \theta_{n^*}(r), \tag{5.48}$$

$$\phi(r) = \phi_0(r) + \sum_{n^*=1}^{q} \phi_{n^*}(r). \tag{5.49}$$

Solution of the problem is obtained with the help of Mathematica package BVPh 2.0 method [135] correct up-to second iteration. And, the separate analytical expressions, respectively for momentum, thermal and mass convection are given as

$$w(r)=-1-\frac{\gamma^2 h_w}{47}\left\{G_r\left[\begin{array}{l}-\frac{220}{7}r^9+\frac{2178}{35}r^8-\frac{10943}{2500}r^3+\frac{4498}{1000}r^2-\frac{2627}{2000}r-\frac{67931}{25000}+h_\theta\\ \left\{\begin{array}{l}-\frac{33}{7}r^{10}+\frac{66}{7}r^9-\frac{1089}{700}r^8-\frac{6624}{1000}r^3+\frac{3476}{500}r^2-\frac{1987}{1000}r-\frac{2689}{6250}+\\ N_b\left(r^{11}-\frac{209}{60}r^9+\frac{1089}{1750}r^8+\frac{1079}{250}r^3+\frac{4557}{1000}r^2+\frac{259}{200}r-\frac{283}{1000}\right)+N_t\end{array}\right\}\\ \left(\frac{6079}{100}r^{11}-\frac{209}{60}r^9+\frac{1089}{1750}r^8+\frac{26983}{625}r^3-\frac{11393}{25000}r^2+\frac{64759}{5000}r+\frac{1769}{6250}\right)\end{array}\right]+\right.$$

$$\left.\left[B_r\left[\begin{array}{l}\frac{220}{7}r^9+\frac{2178}{35}r^8-\frac{10943}{2500}r^3+\frac{4468}{1000}r^2-\frac{2627}{2000}r-\frac{2717}{1000}+h_\phi\\ \left(-\frac{66}{7}r^{10}+\frac{132}{7}r^9-\frac{1089}{350}r^8-\frac{6624}{5000}r^3+\frac{3476}{250}r^2-\frac{1987}{5000}r-\frac{4302}{5000}\right)\end{array}\right]+\right.\right.$$

$$\left.\left.\begin{array}{l}\frac{396}{7}r^8+\frac{14698}{1000}r^3+\frac{4890}{3125}r^2-\frac{110241}{2500}r-\frac{4884}{5000}\end{array}\right]\right\}-$$

$$\frac{\gamma^2 h_w^2}{11007}\left\{\begin{array}{l}\left[\begin{array}{l}\frac{6988}{55}r^{12}+\frac{18239}{1000}r^7-\frac{42559}{1000}r^5-\frac{1783}{200}r^3+10075r^2-\frac{1672}{625}r-\frac{65087}{100}+\\ \gamma^2\left(\frac{24}{11}r^{14}+\frac{2111}{1250}r^9-\frac{43151}{200}r^8+r^7-\frac{3017}{625}r^3+\frac{5977}{1000}r^2-\frac{7241}{500}r-\frac{1011}{2500}\right)+B_d\end{array}\right.\\ \left[\begin{array}{l}\gamma^2\left(-\frac{12}{5}r^{14}-\frac{15723}{3125}r^9-\frac{24646}{4000}r^8-\frac{11263}{1000}\right)-\frac{9261}{11}r^{13}-\frac{3494}{25}r^{12}-\frac{253}{200}r^5-\\ \frac{53043}{400}-r^3\left(\frac{1367}{1000}\gamma^2+\frac{2137}{125}\right)-r\left(\frac{4101}{1000}\gamma^2+\frac{2781}{500}\right)+r^2\left(\frac{8361}{5000}\gamma^2+\frac{413}{500}\right)+\\ r^7\left(\frac{4101}{1000}\gamma^2+\frac{2781}{200}\right)\end{array}\right]+G_r\\ \left[\begin{array}{l}\gamma^2\left(-\frac{12}{5}r^{14}-\frac{15723}{31250}r^9-\frac{24646}{4000}r^8-\frac{1407}{125}\right)-\frac{9261}{11}r^{13}-\frac{3494}{25}r^{12}-\frac{1267}{1000}r^5-\\ \frac{132607}{1000}+r^7\left(\frac{1132}{625}\gamma^2-\frac{13589}{2500}\right)-r^3\left(\frac{1367}{1000}\gamma^2+\frac{2137}{125}\right)+r^2\left(\frac{33464}{20000}\gamma^2+\frac{41353}{2000}\right)-\\ r\left(\frac{4101}{1000}\gamma^2+\frac{55621}{1000}\right)\end{array}\right]\end{array}\right\}. \tag{5.50}$$

In the same way, one can determine an explicit expression for temperature profile as given below.

$$\theta(r)=\frac{11}{10}-r+h_\theta\left\{\begin{array}{l}-r^2+\frac{6r}{5}-\frac{11}{10}+N_t\left(\frac{r^3}{3}-\frac{133r}{300}+\frac{11}{250}\right)+N_b\\ \left(\frac{r^3}{3}-\frac{133r}{300}+\frac{11}{250}+h_\phi\left(\frac{r^4}{6}-\frac{r^3}{5}+\frac{11r}{500}-\frac{121}{60000}\right)\right)\end{array}\right\}$$
$$+h_\theta^2\left\{\begin{array}{l}N_t\left(\frac{7r^4}{24}+\frac{r^3}{5}-\frac{133r^2}{120}+\frac{7r}{250}+\frac{979}{24000}\right)-\frac{r^3}{3}+\frac{3r^2}{10}\\ +\frac{r}{12}-\frac{11}{1000}+N_t^2\left(-\frac{r^5}{20}+\frac{133r^3}{1800}-\frac{6389r^2}{3600}+\frac{319}{1875}\right)+\\ \frac{5r^4}{24}-\frac{r^3}{10}+\frac{39r}{1000}+N_b^2\left(-\frac{r^5}{40}+\frac{133r^3}{3600}-\frac{6389r^2}{72000}+\frac{319}{37500}\right)\\ +N_t\left(-\frac{3r^5}{40}+\frac{133r^3}{1200}+\frac{6389r}{24000}+\frac{319}{12500}\right)-\frac{133r^2}{1200}+\frac{407}{8000}\end{array}\right\}. \quad (5.51)$$

$$\phi(r)=h_\phi^2\left\{\begin{array}{l}N_t h_\theta\left[N_t\left(\frac{r^4}{12}-\frac{61r}{500}+\frac{1463}{1200}\right)-\frac{r^3}{6}-\frac{133r}{600}+\frac{9r}{125}-\frac{11}{500}\right]+h_\theta N_b^2\\ \left(\frac{r^4}{24}-\frac{133r^2}{1200}+\frac{9r}{125}-\frac{1463}{2400}\right)+N_t\\ \left[\begin{array}{l}h_\theta\left\{N_t\left(\frac{r^4}{8}-\frac{133r^2}{1200}-\frac{r}{20}+\frac{1463}{2400}\right)\right\}\\ -\frac{r^3}{6}+\frac{3r^2}{10}-\frac{83r}{600}-\frac{11}{1000}-2r^2+\\ \frac{12r}{5}-\frac{11}{50}\end{array}\right]\end{array}\right\}\times$$
$$\left(\frac{3r^2}{5}-\frac{2r^3}{3}+\frac{r}{6}-\frac{11}{500}\right)-r+\frac{h_\phi}{N_b}+\frac{11}{10}. \quad (5.52)$$

The analytical expressions given in Eqs. (5.47) – (5.49) contain auxiliary parameters h_w, h_θ and h_ϕ which help to converge the solution with their best selection. Figure (5.2)

shows the h −curves of velocity, temperature and concentration, respectively. The estimated values of such parameters range in the interval $-0.8 < h_w < -0.2$, $-0.7 < h_\theta < 0.3$ and $-0.6 < h_\phi < 0.2$. It is observed that HAM solution converges for $h_w = -0.5$, $h_\theta = -0.2$ and $h_\phi = -0.3$.

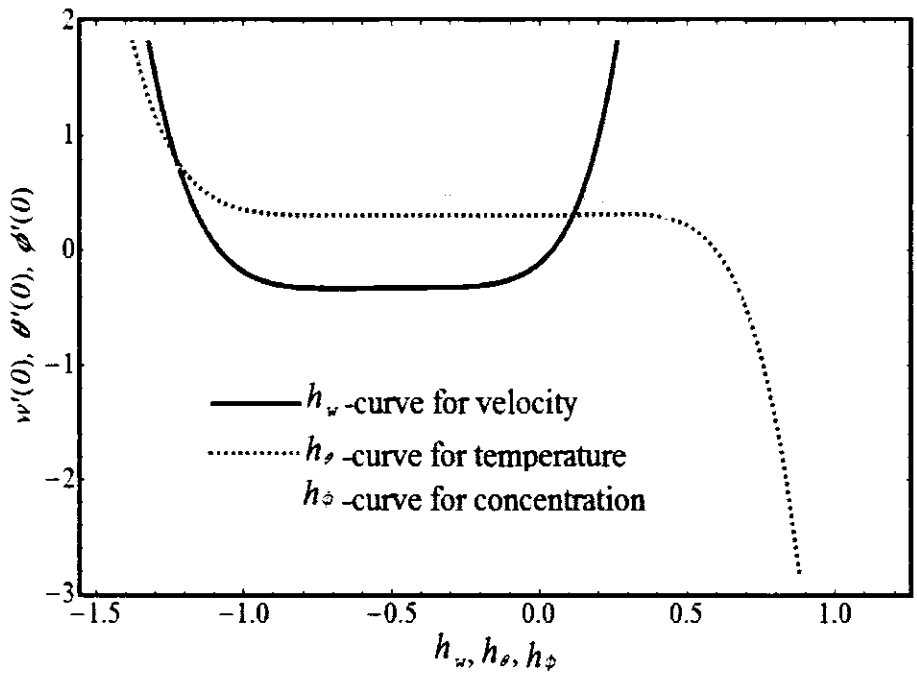

Figure 5.2: $\hbar$ curves.

5.3 Analysis

This section is relevant to the graphical survey about the changing behaviors of axial velocity, thermal convection and diffusion of the particles. The displayed graphs have also been elaborated in detail which describe the altering trend caused by change in different parameters and variable. The most important of such variables are Brownian motion parameter N_b, Grashof number G_r, Brownian diffusion constant B_d, thermophoresis parameter N_t and Couple stress parameter γ as shown in Figures (5.3) – (5.11).

Velocity of nanofluid is plotted in Figures (5.3) – (5.7). One sees that the nanofluid moves faster subject to rise in the value of G_r by looking at Figure (5.3). Heating effects attenuates fluid thickness and allowing the buoyance force to become strong. This results to bring rise in fluid and fluid velocity increases by increasing G_r. Same trend in the motion of nanofluid is observed in Figure (5.4). In which B_d rises the velocity due to temperature difference in the fluid. For density of fluid depends on temperature. By varying N_b the random motion of gold particles gets intense and due to inter-particle collision momentum of the rises as shown in Figure (5.5). The contribution of γ shows that velocity rises by changing its numerical value. This can be inferred that due to vanishing couple stresses as given Figure (5.6). On contrary, fluid declines its speed for the case of N_t, when thermophoretic forces become strong and start resisting the flow in Figure (5.7).

Figure (5.8) – (5.9) show the significance of nano-particles. As such particles are famous for enhancing heat therefore, temperature of nanofluid rises. For higher values of N_b, the random motion of golden particle intense and more energy is added to the system by their collision in Figure (5.8). However, in Figure (5.9) thermophoretic forces expedite the heat convection by transporting heat form higher region to lower, and hence the temperature rises due to N_t. A similar trend in the concentration of golden particles is witnessed in Figures (5.10)-(5.11) respectively. An increase in N_t results to shift golden particles for higher region of concentration to lower region with in the space of coaxial tubes. Therefore, the concentration declines in Figure (5.10). However, for the case of N_b rapid flow of causes the reduction of concentration in Figure (5.11).

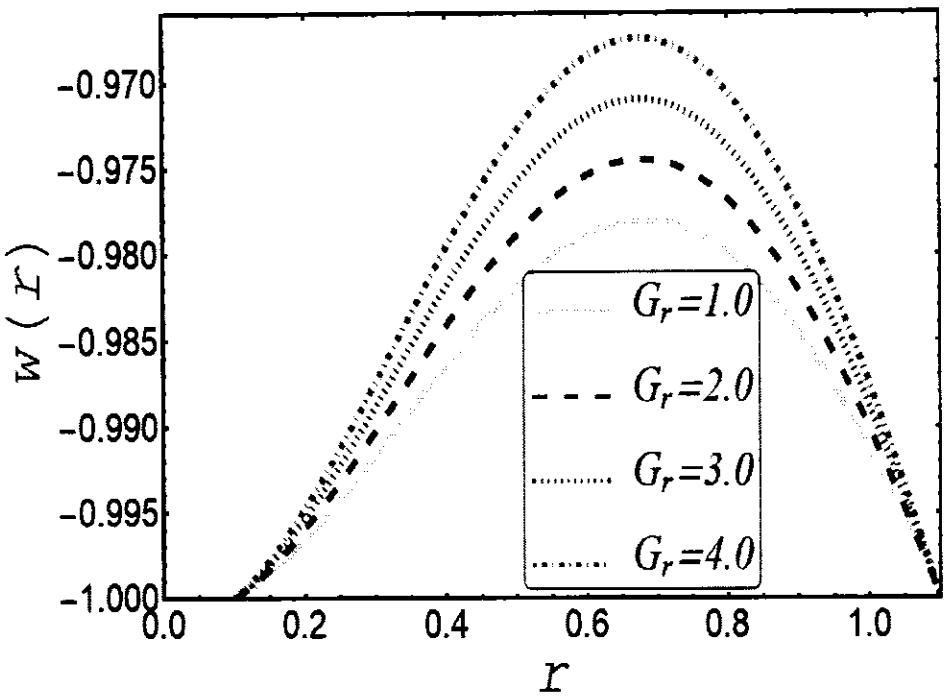

Figure 5.3: Variation of Grashof number on velocity.

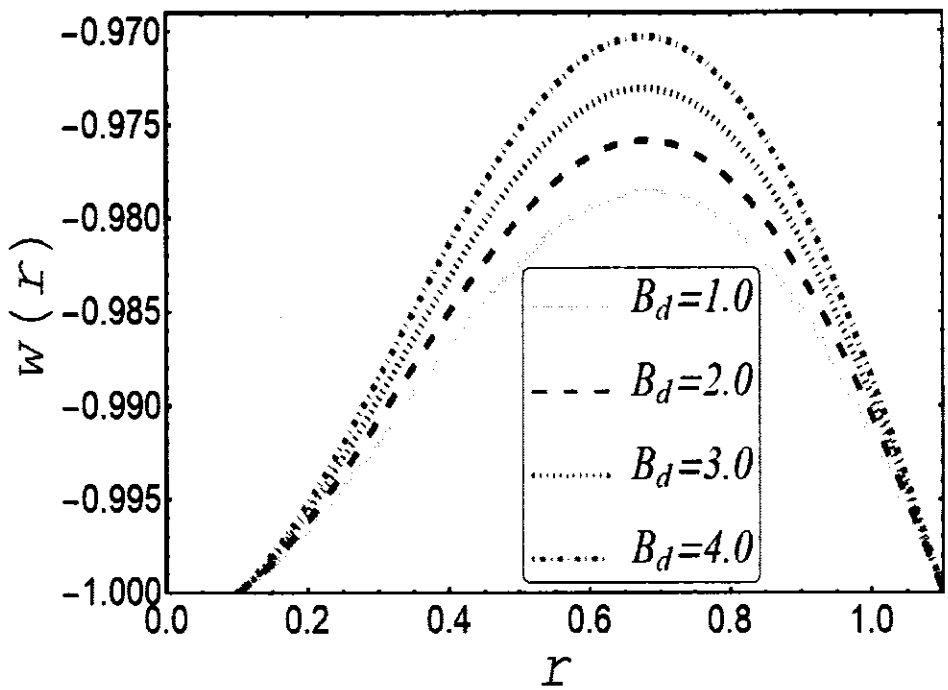

Figure 5. 4: Variation of Brownian diffusion constant on velocity.

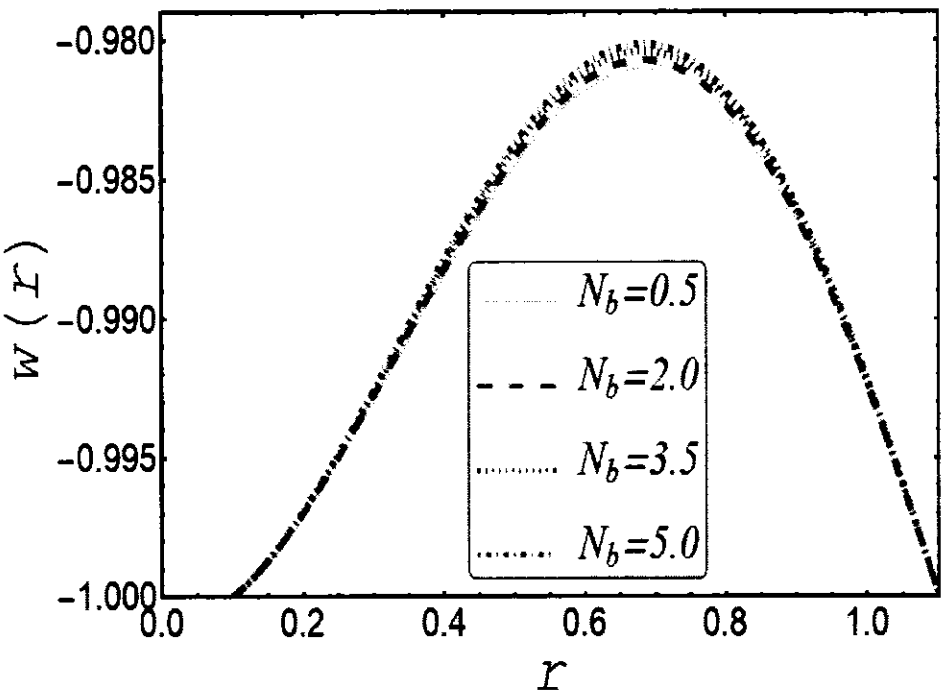

Figure 5.5: Variation of Brownian motion parameter on velocity.

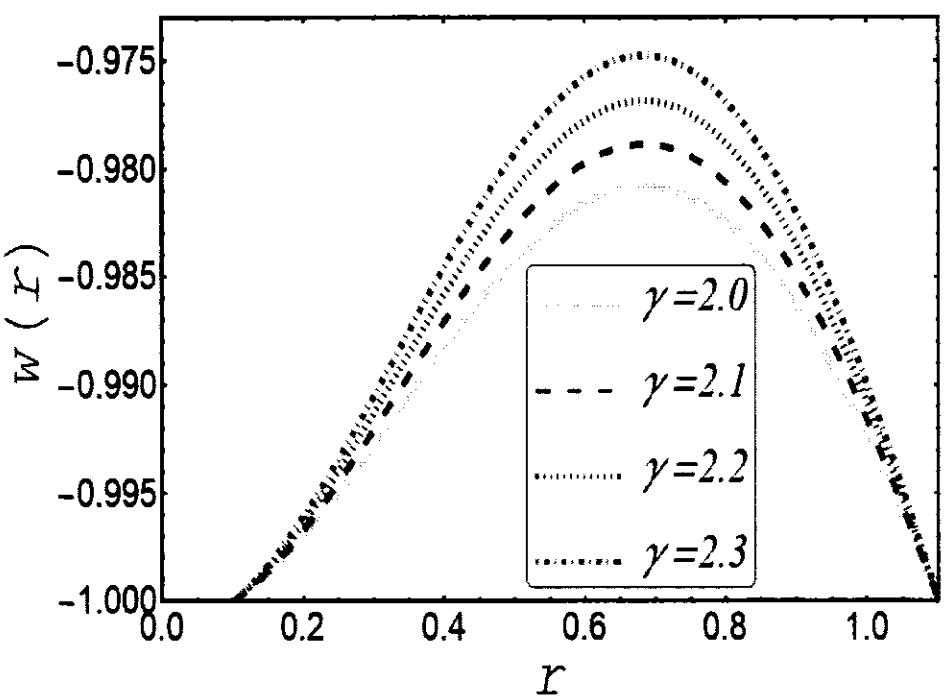

Figure 5.6: Variation of Couple stress parameter on velocity.

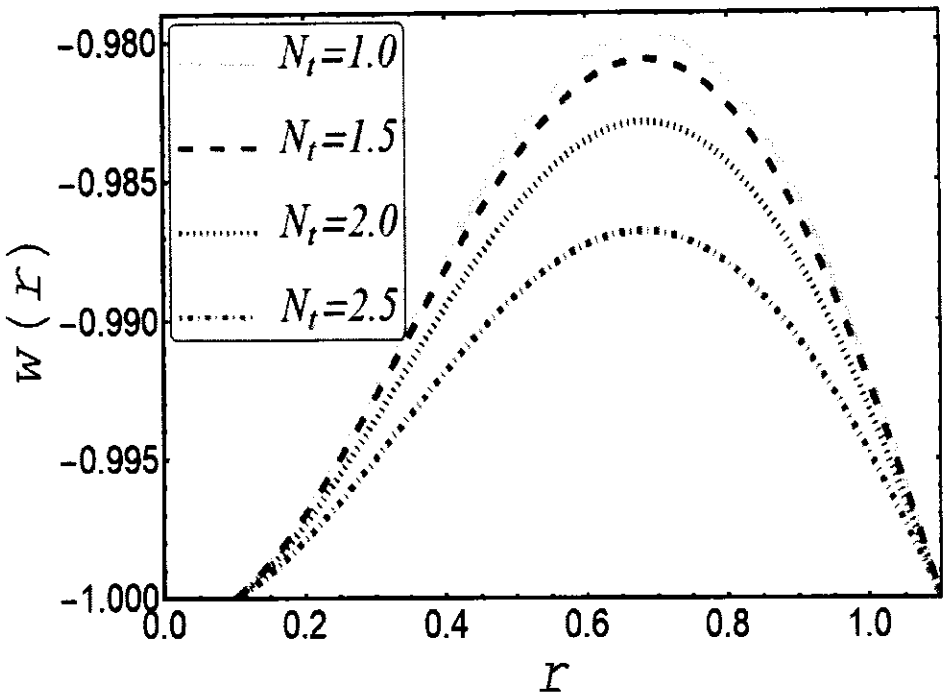

Figure 5.7: Variation of thermophoresis parameter on velocity.

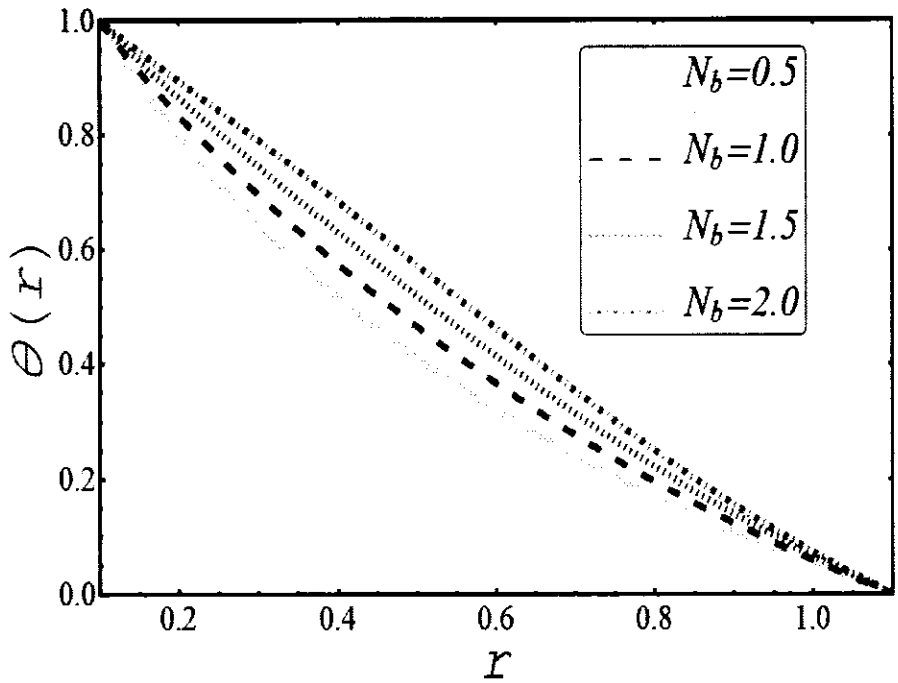

Figure 5.8: Variation of Brownian motion parameter on temperature.

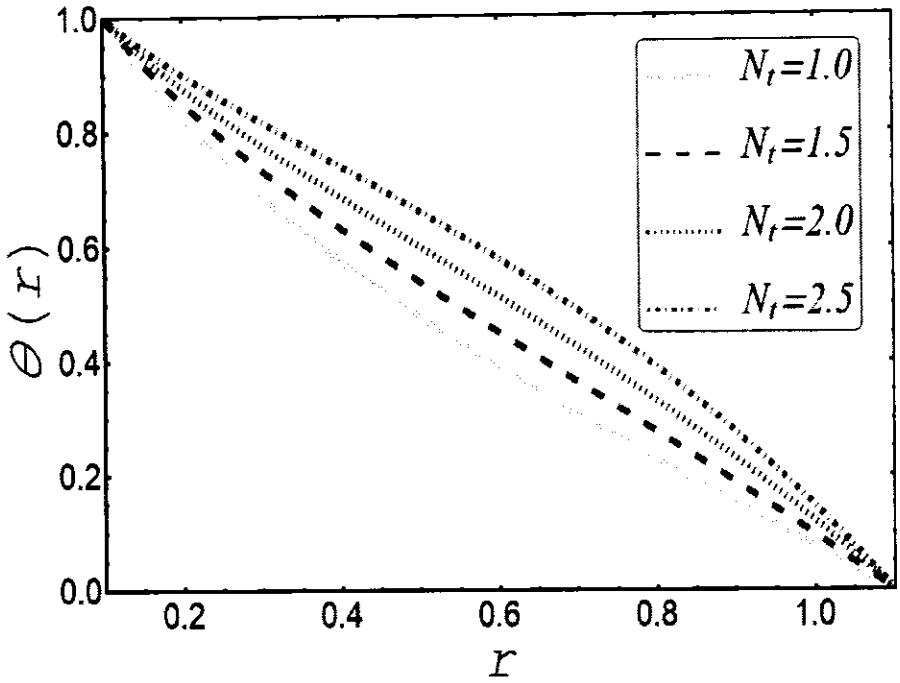

Figure 5.9: Variation of thermophoresis parameter on temperature.

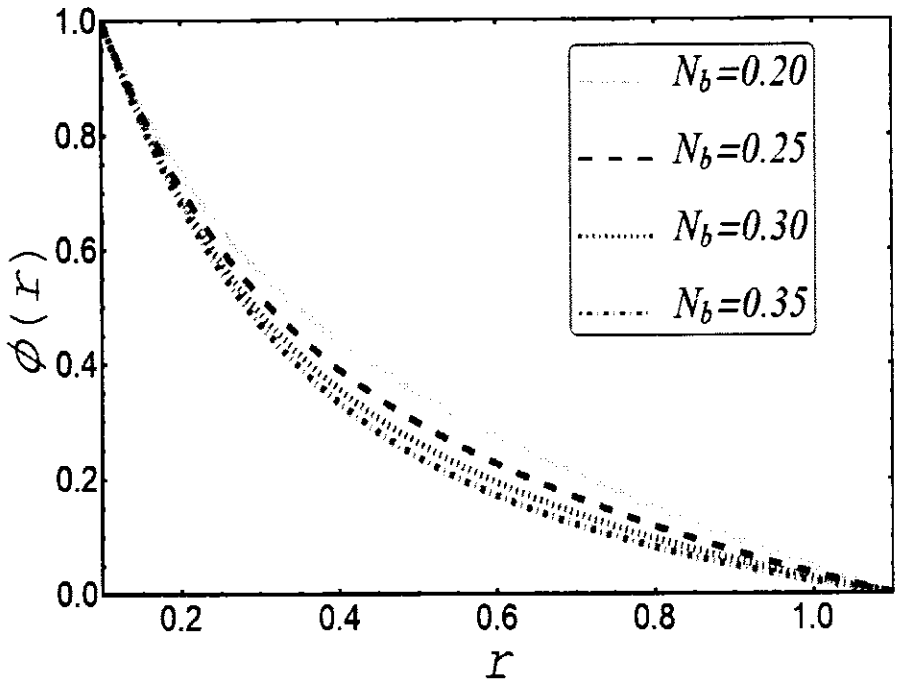

Figure 5.10: Variation of Brownian motion parameter on nanoparticle concentration.

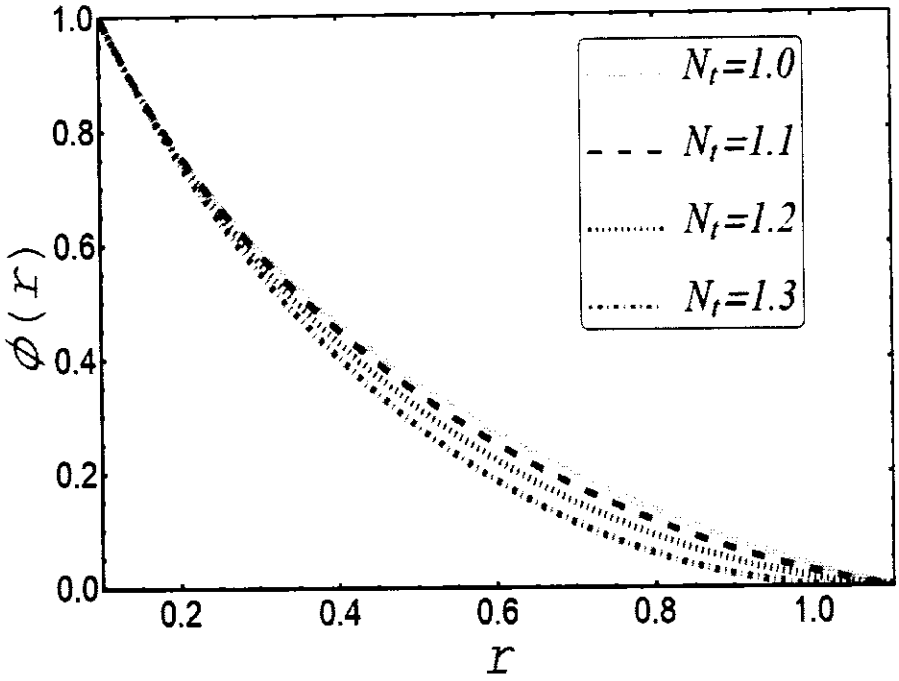

Figure 5.11: Variation of thermophoresis parameter on nanoparticle concentration.

5.4 Conclusion

Tiny size of golden particles are used as a remedy for arthritis and cancer. Couple stress fluid is treated as blood with transport the heated particles by means of peristalsis. Inner tube which is injected through veins carries the required drug to cure damaged tissues. The nanoflow is modeled with the help of means of momentum, thermal and mass transfer equations. The nonlinear flow problem is solved analytically by considering HAM. The analytical results are confirmed by making parametric study and found them in complete agreement. Some of the key findings are highlighted as:

- Higher thermal conductivity of gold particles enhances the temperature which are suitable for therapy .
- Due to Grashof number buoyancy force becomes strong and increases the motion of the fluid.

- Thermophoretic force resists the flow thorough coaxial tubes.
- Couple stress increases the peristaltic motion of nanofluid.
- The study reduces to merely Newtonian case by eliminating the Couple stress parameter.

Chapter 6

Peristaltic flow of Couple stress fluid suspended with nanoparticles under the influence of chemical reaction and activation energy

The current chapter basically, is an extension of previous chapter. The additional contribution of chemical reaction and activation energy are incorporated to expedite the performance of golden particles. Modified Arrhenius law activates golden particles to convey medicine effectively. Similarly, for Brownian and thermophoresis diffusion, Buongiorno model is used.

6.1 Mathematical formulation

The sinusoidal waves travel with a constant speed through its walls, due to the stress caused by an unsteady movement of heated nanofluid between the gap of coaxial tubes, as shown in Figure 5.1. Again, the Couple stress fluid transports the gold nanoparticles (GNPs) affected by chemical reaction, as well as activation energy through vacant space of coaxial tubes. Then the flow dynamics as governed by the Eqs. $(1.31) - (1.34)$ in components form are expressed as:

$$\frac{U}{R} + \frac{\partial U}{\partial R} + \frac{\partial W}{\partial Z} = 0, \tag{6.1}$$

$$\rho_{nf}\left(\frac{\partial U}{\partial t}+U\frac{\partial U}{\partial R}+W\frac{\partial U}{\partial Z}\right)=\left.\begin{aligned}&-\frac{\partial p}{\partial R}+\mu_{nf}\left(\frac{\partial^2 U}{\partial R^2}+\frac{1}{R}\frac{\partial U}{\partial R}+\frac{\partial^2 U}{\partial Z^2}\right)-\\&\gamma_1\left[\begin{array}{c}\frac{\partial^4 U}{\partial R^4}+\frac{2\partial^3 U}{R\partial R^3}+\frac{\partial^2 U}{R^2\partial R^2}+\\ \frac{\partial^4 U}{\partial R^2\partial Z^2}+\frac{\partial U}{R^3\partial R}+\frac{\partial^3 U}{R\partial R\partial Z^2}+\\ \frac{\partial^4 U}{\partial Z^2\partial R^2}+\frac{\partial^3 U}{R\partial Z^2\partial R}+\frac{\partial^4 U}{\partial Z^4}\end{array}\right]\end{aligned}\right\}, \tag{6.2}$$

$$\rho_{nf}\left(\frac{\partial W}{\partial t}+U\frac{\partial W}{\partial R}+W\frac{\partial W}{\partial Z}\right)=\left.\begin{aligned}&-\frac{\partial p}{\partial Z}+\mu_{nf}\left(\frac{\partial^2 W}{\partial R^2}+\frac{1}{R}\frac{\partial W}{\partial R}+\frac{\partial^2 W}{\partial Z^2}\right)-\\&\gamma_1\left[\begin{array}{c}\frac{\partial^4 W}{\partial R^4}+\frac{2\partial^3 W}{R\partial R^3}+\frac{\partial^2 W}{R^2\partial R^2}+\\ \frac{\partial^4 W}{\partial R^2\partial Z^2}+\frac{\partial W}{R^3\partial R}+\frac{\partial^3 W}{R\partial R\partial Z^2}+\\ \frac{\partial^4 W}{\partial Z^2\partial R^2}+\frac{\partial^3 W}{R\partial Z^2\partial R}+\frac{\partial^4 U}{\partial Z^4}\end{array}\right]+\\&[\varphi\rho_p+(1-\varphi)\{\rho_f(1-\beta_T(T-\theta_w))\}]g\end{aligned}\right\} \tag{6.3}$$

$$(\rho c)_{nf}\left(\frac{\partial T}{\partial t}+U\frac{\partial T}{\partial R}+W\frac{\partial T}{\partial Z}\right)=\left.\begin{aligned}&k_1\left(\frac{\partial^2 T}{\partial R^2}+\frac{1}{R}\frac{\partial T}{\partial R}+\frac{\partial^2 T}{\partial R^2}\right)+\\&(\rho c)_{np}\left[\begin{array}{c}D_b\left(\frac{\partial\varphi}{\partial R}\frac{\partial T}{\partial R}+\frac{\partial\varphi}{\partial Z}\frac{\partial T}{\partial Z}\right)+\\ \frac{D_T}{\theta_w}\left\{\left(\frac{\partial T}{\partial R}\right)^2+\left(\frac{\partial\varphi}{\partial Z}\right)^2\right\}\end{array}\right]\end{aligned}\right\}, \tag{6.4}$$

$$\left(\frac{\partial\varphi}{\partial t}+U\frac{\partial\varphi}{\partial R}+W\frac{\partial\varphi}{\partial Z}\right)=\left.\begin{aligned}&D_b\left(\frac{\partial^2\varphi}{\partial R^2}+\frac{1}{R}\frac{\partial\varphi}{\partial R}+\frac{\partial^2\varphi}{\partial Z^2}\right)+\\&\frac{D_T}{\theta_w}\left(\frac{\partial^2 T}{\partial R^2}+\frac{1}{R}\frac{\partial T}{\partial R}+\frac{\partial^2 T}{\partial R^2}\right)-\\&k_r^2\left(\frac{T}{\theta_w}\right)^n(\varphi-\varphi_w)exp\left(\frac{-E_a}{k^*T}\right)\end{aligned}\right\}. \tag{6.5}$$

Transformations which are used in previous chapter again play vital role to shift the flow dynamics from laboratory frame to wave frame as described by the Eq. (5.6) and further applying dimensionless quantities as given in Eq. (5.7), respectively. Then the above governing Eqs. (6.2) – (6.5), in view of Oberbeck-Boussinesq approximation and long wave length assumption can be presented in dimensionless form as:

$$\frac{d^2w}{dr^2}+\frac{dw}{rdr}-\frac{1}{\gamma^2}\left(\frac{d^4w}{dr^4}+\frac{2}{r}\frac{d^3w}{dr^3}+\frac{d^2w}{r^2dr^2}+\frac{dw}{r^3dr}\right)+B_d\phi+G_r\theta=\frac{dp}{dz}, \quad (6.6)$$

$$\epsilon_3\left(\frac{d^2\theta}{dr^2}+\frac{1}{r}\frac{d\theta}{dr}\right)+\epsilon_2\left\{N_b\left(\frac{d\phi}{dr}\right)\left(\frac{d\theta}{dr}\right)+N_t\left(\frac{d\theta}{dr}\right)^2\right\}=0, \quad (6.7)$$

$$\left.\begin{aligned} N_b\left(\frac{d^2\phi}{dr^2}+\frac{1}{r}\frac{d\phi}{dr}\right)+N_t\left(\frac{d^2\theta}{dr^2}+\frac{1}{r}\frac{d\theta}{dr}\right)-\phi\{\ A^*(\ \beta^*\theta+1)^n N_b\}\\ \exp\left(\frac{-E^*}{\beta^*\theta+1}\right)=0 \end{aligned}\right\}. \quad (6.8)$$

In concentration equation chemical reaction and activation energy are responsible for the emergence of some new nondimensional quantities, which are defined as:

$$E^*=\frac{E_a}{k\theta_w};\quad A^*=\frac{k_r^2}{D_b};\ \beta^*=\frac{(\theta_m-\theta_w)}{\theta_w}. \quad (6.9)$$

6.2 Solution of the problem

The governing Eqs. (6.6) – (6.8) involve nonlinearity and are coupled with each others. Therefore, an exact solution of this peristaltic nanofluid flow problem is not easy. This constraint of choice restricts, to seek a numerical solution with the help of some suitable numerical technique, such as Keller-box method [136]. The reason for choosing Keller-box numerical scheme is that this method is much faster and more flexible to use as compared to other methods. In addition, this has been extensively used and tested on boundary layer flows. By means of said method, the solution can be attained by using four steps: (i) First reduce the system of equations to a first order system; (ii) then write the difference equations by means of central differences; (iii) now linearize the resulting nonlinear equation by Newton's method, if needed; and (iv) finally the block-tridiagonal-elimination technique is used to solve the linear system.

6.3 Analysis

This graphical section is relevant to the effectively contributing parameters, which influence axial velocity of Couple stress fluid, temperature of nanofluid, and concentration of nano sized Hafnium particles, respectively. The involved parameters have a greater impression on the flow, namely, Couple stress parameter γ, Brownian motion N_b and thermophoresis parameters N_t, Grashof number G_r, and Brownian diffusion constant B_d emerging due to the presence of heat and metallic particles. Moreover, a modified Arrhenius mathematical term yields some additional parameters, such as reaction rate A^*, activation energy E^*, temperature difference parameter β^*, and the fitted rate constant n, assuming the contribution of peristaltic pressure to be constant. To make this more systematic, the main portion is further divided into four subsections.

6.3.1 Axial velocity

Axial velocity is spotted in Figures (6.1) – (6.3) for Couple stress parameter, Brownian diffusion constant, and Grashof number. Axial velocity, as shown in Figure (6.1), accelerates in response to an increases in Couple stress parameter. This is mainly due to the decrease in friction, which arises from the particle (i.e., base-fluid particles) additives, which constitute a size-dependent effect in Couple stress fluids. In addition to the preceding remark, the rotational field of fluid particles is minimal as well. The peristaltic motion of outer walls of the tube also contributes by rapidly pushing the fluid in the axial direction, as B_d gets numerically variated in Figure (6.2). Figure (6.3) displays a different picture of the velocity of the fluid for the case of thermophoresis diffusion constant. The diagram basically describes the influence of buoyancy in terms of Grashof number G_r. As one can see from Eq. (6.17), the buoyancy effects are mainly due to gravity and temperature difference. Therefore, increase in G_r attenuates the

fluid's momentum by aggravating buoyant force. This brings a vivid decline in the velocity of the fluid. Furthermore, the relation defining Gr suggests that if $Gr > 0$, then this physically describes the heating of the nanofluid, while a reverse case can be expected for $Gr < 0$.

6.3.2 Thermal distribution

The temperature distribution of the nanofluid in the presence of additional chemical reaction and activation energy are portrayed in Figure (6.4) and Figure (6.5). The variation of the Brownian motion parameter has noticeable effects on the nanofluid temperature, as the Brownian motion is generated due the collision of nanoparticles, driving the particles to a random motion. The collision of the particles, whether mutual or with the fluid molecules, is enhanced by the inward contraction of the flexible walls. Due to this factor Brownian motion parameter, N_b accumulates some additional thermal energy in the fluid, as shown in Figure (6.4). The nanoparticles were further thermally charged by the increase in N_t. It is important to keep in mind that the thermophoresis forces become stronger in the response of larger values of N_t, which finally result in higher temperature, as seen in Figure (6.5). Sometimes, such variations are credited to the thermal boundary layer thickness as well. Obviously, this increase in fluid temperature is due to increase in the random motion of nanoparticles when the above-mentioned parameters are increased.

6.3.3 Nanoparticle concentration profile

The concentration of golden particles is observed in Figures (6.6) – (6.7), when the N_b and N_t, respectively, are given higher numeric values. The random motion of the nanoparticles is seen to be faster in response to increase in the values of said parameters, which makes diffusion of nanoparticles rapid and fast. Therefore, rising curves show an increase in the concentration of nanoparticles. Moreover, this contribution of

Brownian motion identifies the quick movement of hotter gold particle, from the region of higher temperature to lower temperature. The thermophoresis forces also bring positive effects on the golden particles by making the concentration strong against the higher numerical variation in N_t, as is noticeable in Figure (6.7). With the same trend of influence, an onward surge of activation energy again gives a rise to the golden solution. One can see in Figure (6.8) that the boundary layer thickness of the particles gets depreciated when E_a is further motivated to transport the required drug or medicine to the desired target. The Arrhenius equation, which gives the mathematical description of the introduction of activation energy into any system, clearly reveals that the reduction in heat and acceleration of E_a returns a low reaction rate constant. In the process, this slows down the chemical reaction and results in higher concentration of the particles, which confirms the accumulation of gold nanoparticles at the location of the malign tissue or organ to cured. Finally, the surge in concentration of gold particles is evidenced by the decline in Figures $(6.9) - (6.11)$. The temperature difference ratio brings a remarkable decline in concentration of the heated nanoparticles. As the difference between the ambient fluid temperature and wall temperature widens, the concentration boundary layer thickness expands. This thickness resists the increase in particle concentration displayed in Figure (6.9). Similarly, retardation can be witnessed for reaction rate and fitted rate constant. It can be conceived that the rise in these parameters and constants sharpens the chemical reaction, which motivates the concentration gradient at the wall of the inner tube. Hence, a vivid reduction in the concentration of the particles occurs, as is seen in Figures $(6.10) - (6.11)$.

6.3.4 Trapping phenomenon / streamline configuration

Finally, the most significant phenomena relevant to any peristaltic motion in a living organism is known as "Trapping". Essentially, this is the appearance of a round closed

bolus, which is identified as the hallow cavity, transporting the required medication to the desired tissues or organs, as shown in Figures (6.12) – (6.18). In Figures (6.12) and (6.13), one can easily notice that the fluids face less resistance when traveling through the coaxial space, as the contours reduce in size and configuration. In contrast, the Couple stress fluid results in shrinking the streamlines and generates the circulating boluses, as depicted in Figure (6.14). Isotherms of the Brownian motion parameter keep binding closer together, which allows the bolus to expand, as established in Figures (6.15) and (6.16), whereas the thermophoresis parameter provides extra potential for isotherms to compress the bolus inwards. Hence, the bolus keeps getting smaller. In the last two graphs, contours are sketched in order to see how concentration is influenced by the reaction rate constant and thermophoresis parameter. One can see in Figure (6.17) that the bolus bulges out as the reaction rate constant gets stronger, whereas a reverse trend is observed for the thermophoresis parameter in Figure (6.18).

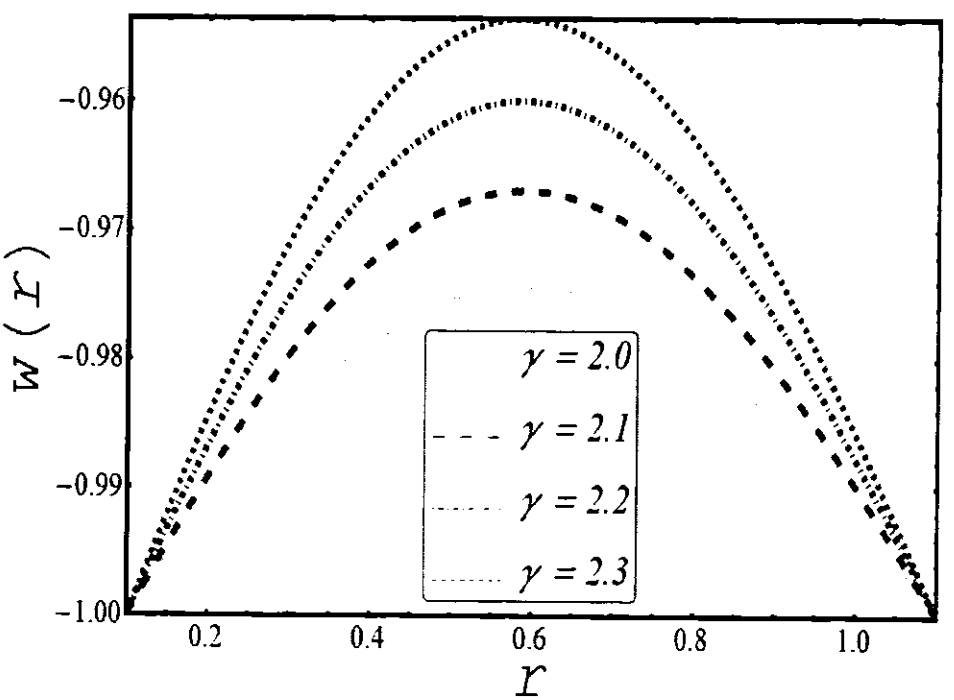

Figure 6.1: Variation of Couple stress parameter on velocity.

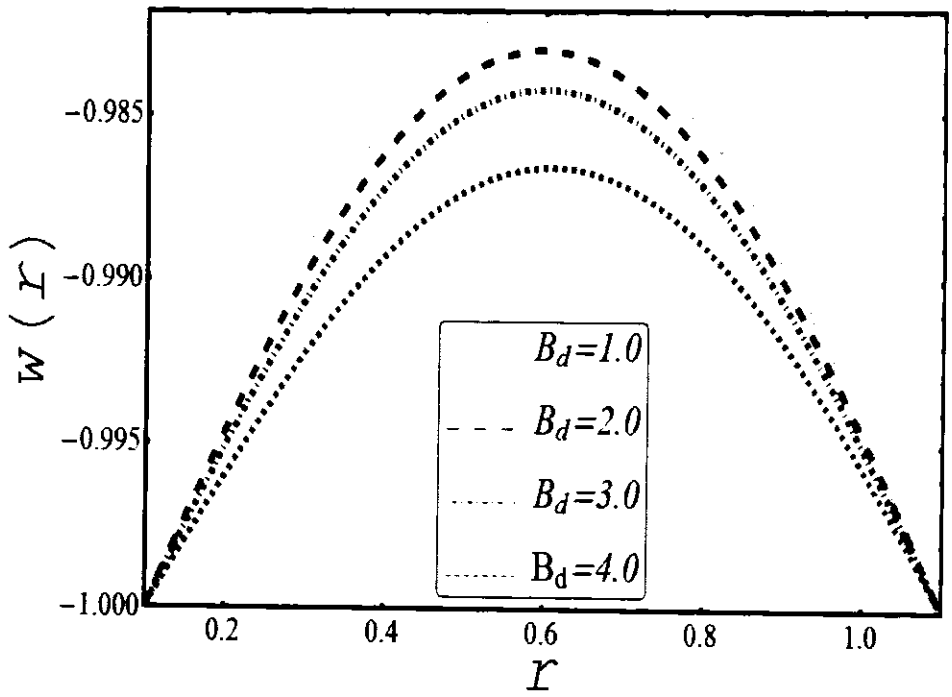

Figure 6.2: Variation of Brownian diffusion constant on velocity.

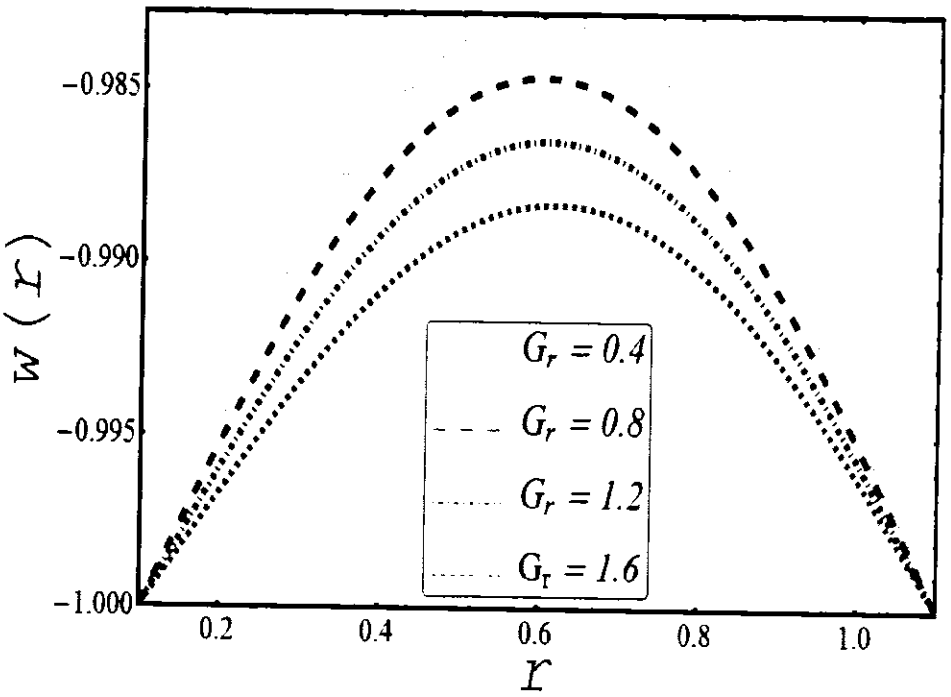

Figure 6.3: Variation of Grashof number on velocity.

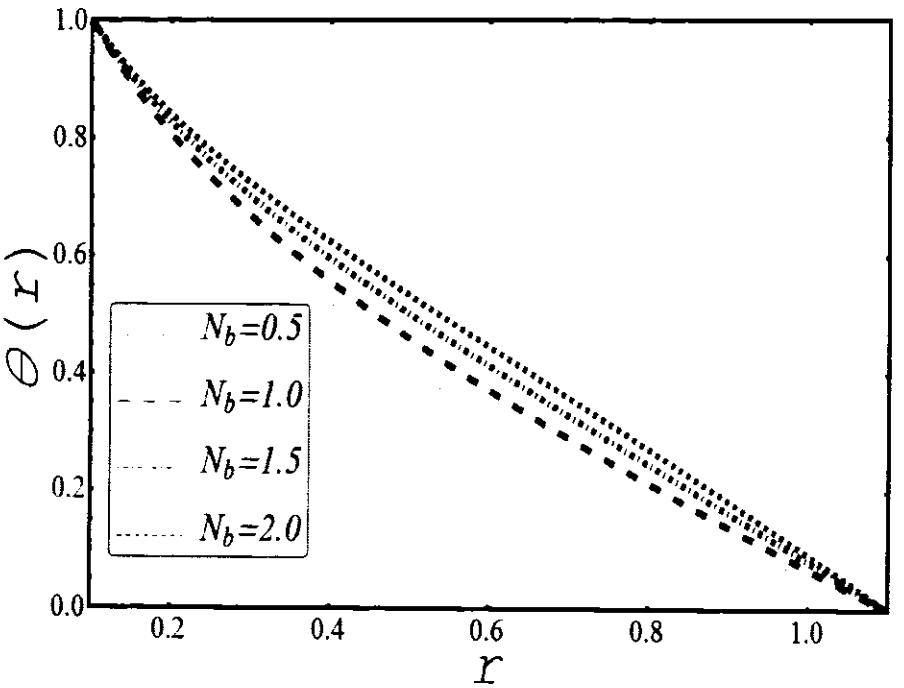

Figure 6.4: Variation of Brownian motion parameter on temperature.

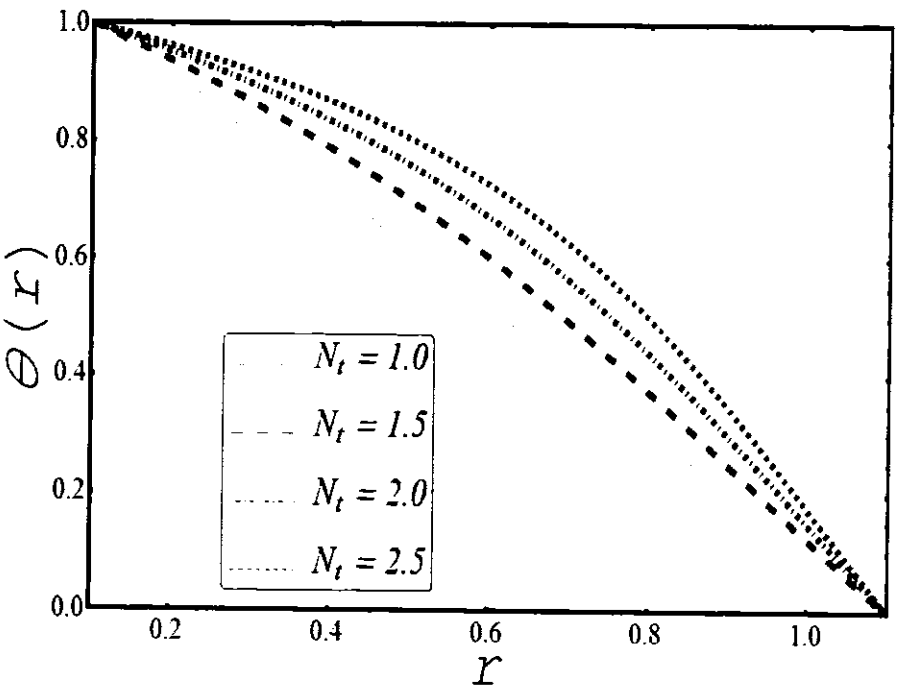

Figure 6.5: Variation of thermophoresis parameter on temperature.

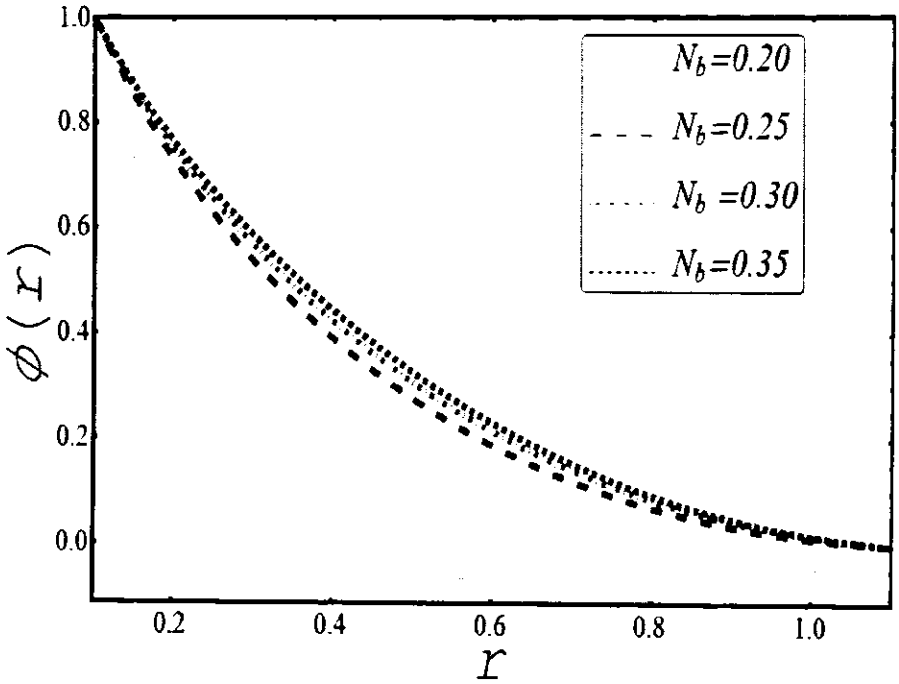

Figure 6.6: Variation of Brownian motion parameter on nanoparticle concentration.

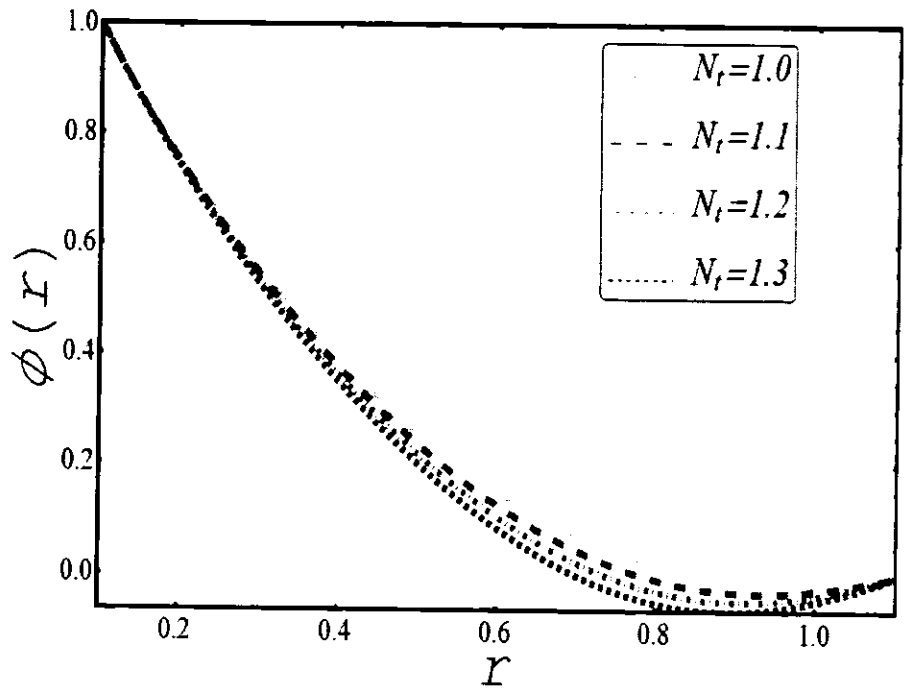

Figure 6.7: Variation of thermophoresis parameter on nanoparticle concentration.

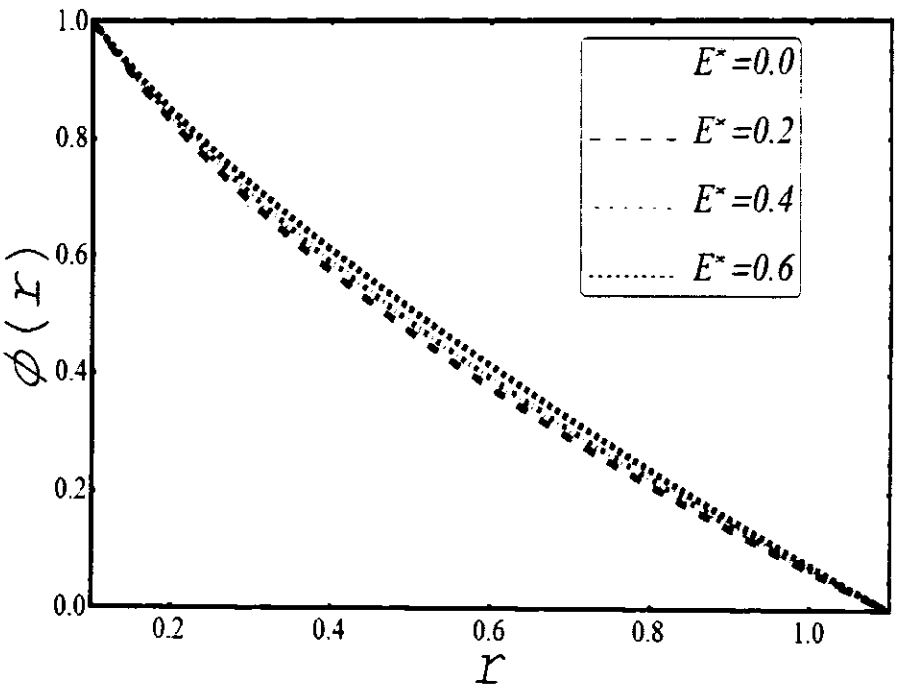

Figure 6.8: Variation of activation energy on nanoparticle concentration.

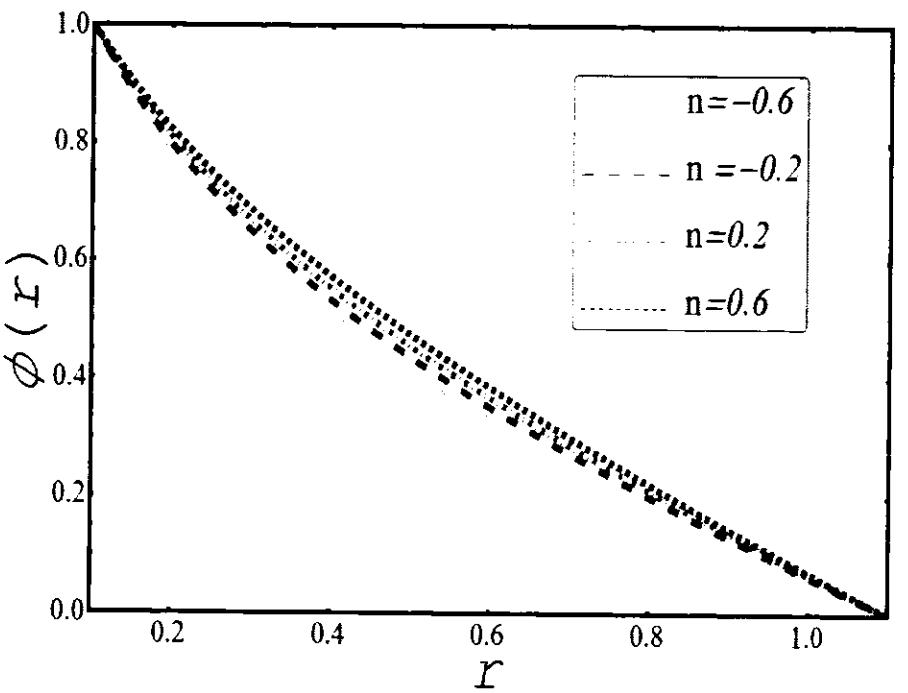

Figure 6.9: Variation of fitted rate constant on nanoparticle concentration.

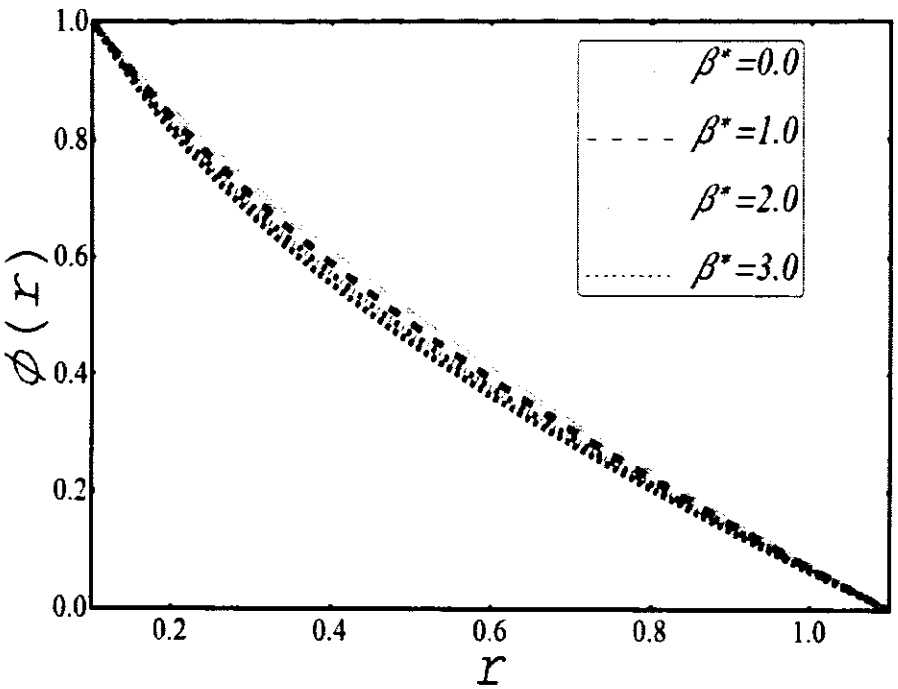

Figure 6.10: Variation of temperature ratio on nanoparticle concentration.

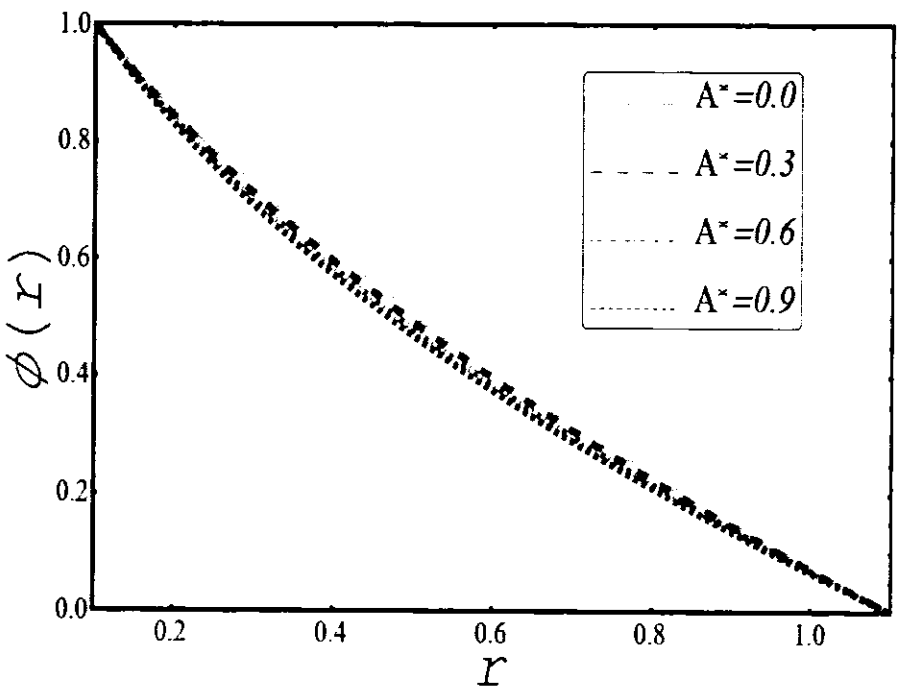

Figure 6.11: Variation of reaction rate constant on nanoparticle concentration.

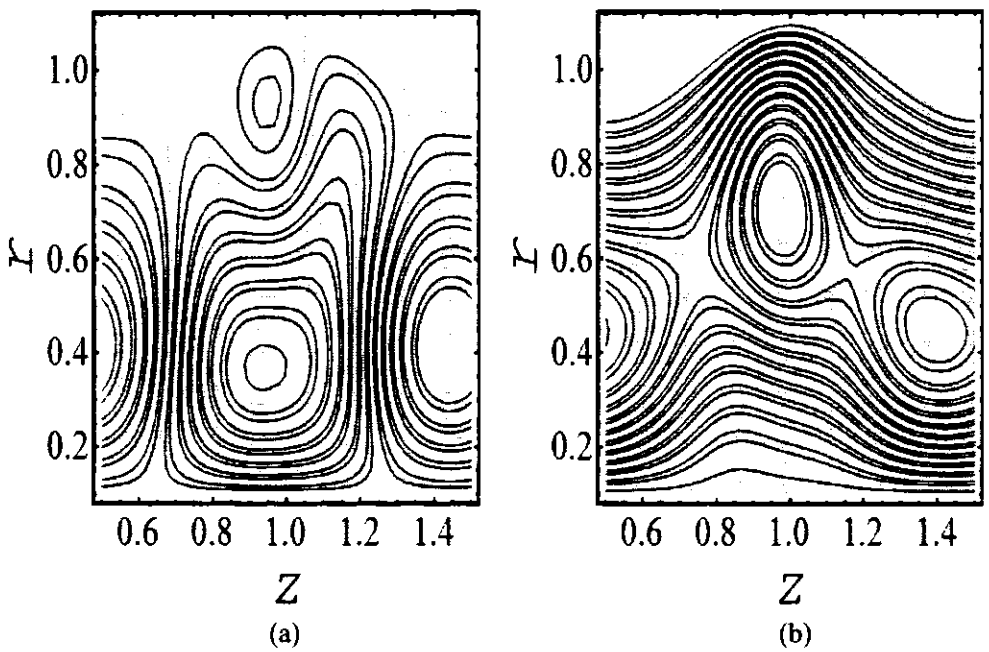

Figure 6.12: Streamlines for Brownian diffusion constant. (a). $B_d = 1.0$;
(b). $B_d = 2.0$

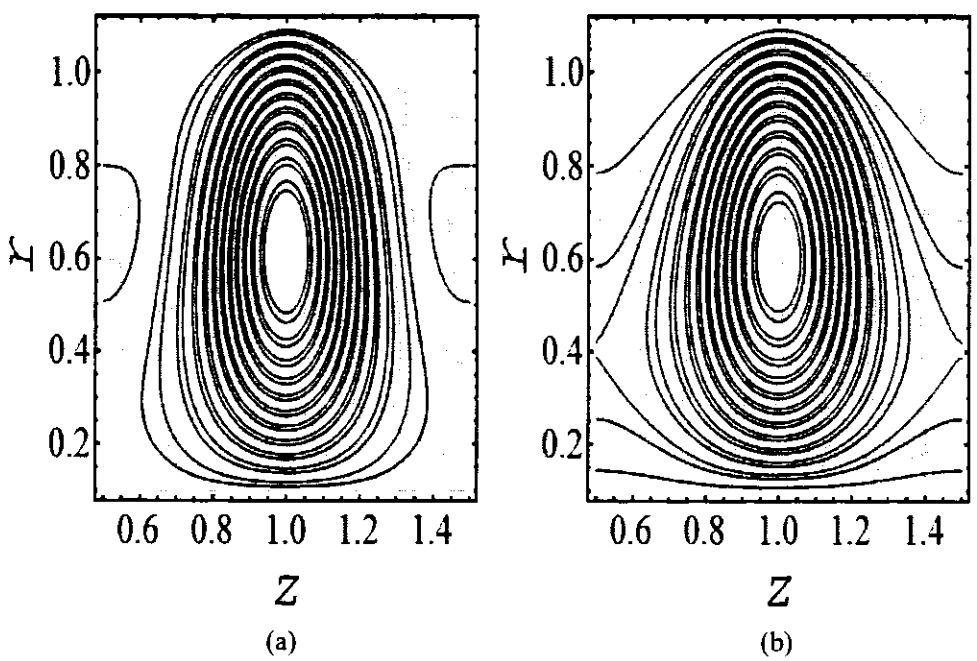

Figure 6.13: Stream lines for Grashof number. (**a**): For $G_r = 1.5$;
(**b**): For $G_r = 4.0$.

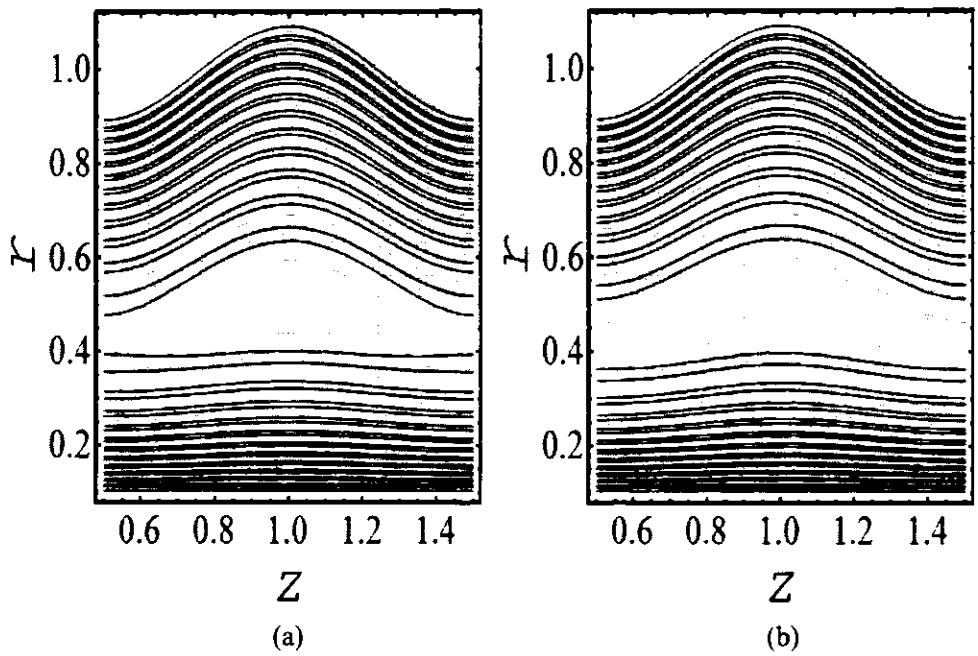

Figure 6.14: Contour plot for reaction rate constant. (**a**). For $A^* = 0.5$;

(**b**). For $A^* = 1.0$.

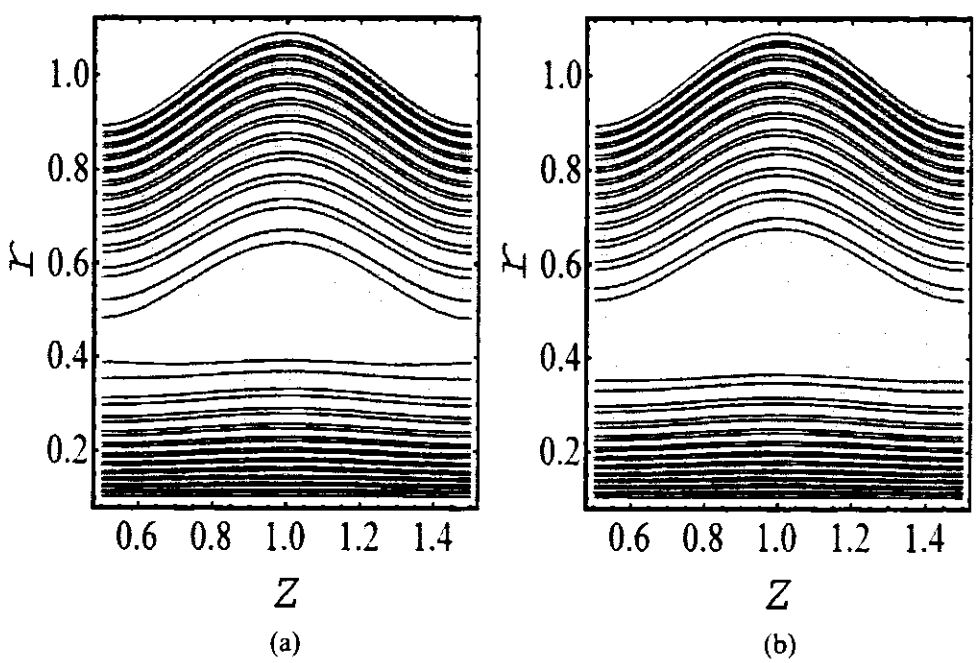

Figure 6.15: Contour plot for thermophoresis parameter. (**a**). For $N_t = 1.0$;

(**b**). For $N_t = 1.5$.

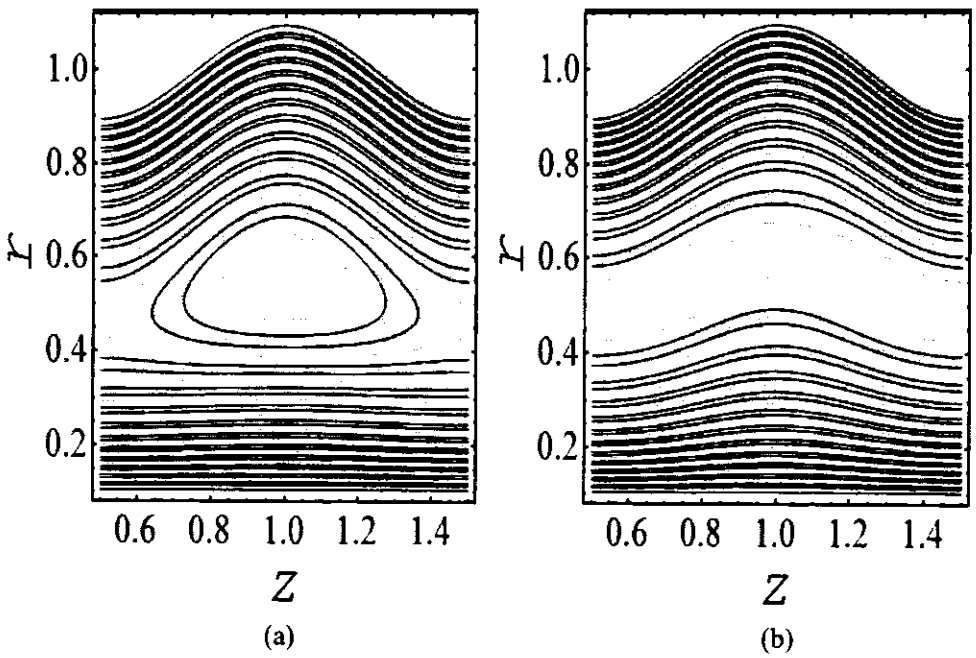

Figure 6.16: Isotherms for Brownian motion parameter. (**a**). For $N_b = 0.5$; (**b**). For $N_b = 4.0$

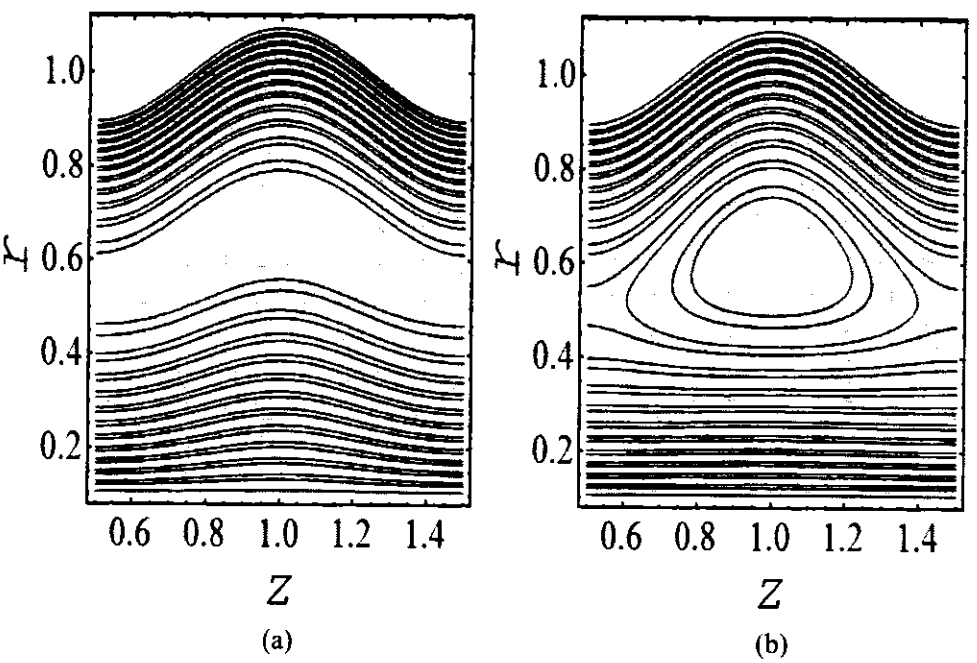

Figure 6.17: Isotherms for thermophoresis parameter. (**a**). For $N_t = 0.75$; (**b**). For $N_t = 3.0$.

6.4 Conclusion

A numerical investigation is carried out for the peristaltic flow of nanofluids between the gap of two coaxial tubes with different configurations and structures. The nanofluid is composed of gold particles, while the Couple stress fluid serves as the solvent. To enhance the mutual interaction of gold particles, or the interaction of molecules with the base fluid, additional effects of chemical reaction and activation energy have also been taken into consideration. The performed study reveals very informative results. Such results include that axial velocity is fully supported by the Couple stress parameter and Brownian diffusion constant, in contrast to the Grashof number. The temperature of the nanofluid remains high for both involved parameters, which are thermophoresis and Brownian motion parameter. Looking at the graphs of concentrations of the metallic particles, it is inferred that activation energy, thermophoresis, and Brownian motion parameters cause an increase in the concentration of particles, whereas temperature ratio, reaction rate, and fitted rate constants do not support the increase. In the final portion of the graphical study, the number and size of the circulating boluses are depicted. One can easily notice that boluses get enlarged in response to the Brownian motion parameter, Couples stress parameter, and reaction rate constant. However, a reverse trend is observed for the Grashof number, thermophoresis parameter, and Brownian diffusion constant. The key finding can be summarized as:

- Strong buoyant force results in retarded axial velocity for the thermophoresis parameter.
- Peristaltic movement of the outer tube enhances the Brownian motion and raises the temperature of the nanofluid.
- Activation energy entering the process enlarges the thickness of concentration.

- The reaction rate constant increases concentration at the catheter, which decreases the concentration of nanoparticles.
- N_b shrinks the bolus in size by strengthening isotherms and closed paths of concentration lines.
- The Couple stress parameter and reaction rate constant give freedom to the bolus to swell by binding the stream lines closer to each another.

Appendix

$$A_5 = M^2\gamma^2;$$

$$A_6 = \frac{4\,A_5}{1-C};$$

$$A_7 = \gamma^4 - A_6;$$

$$A_8 = \gamma^2 - \sqrt{A_7};$$

$$A_9 = \gamma^2 + \sqrt{A_7};$$

$$A_{10} = \sqrt{\frac{A_8}{2}};$$

$$A_{11} = \sqrt{\frac{A_9}{2}};$$

$$A_{12} = A_5\sqrt{A_7};$$

$$A_{13} = \cosh(A_{10})\cosh(A_{11});$$

$$A_{14} = \cosh(A_{11})\sinh(A_{10});$$

$$A_{15} = \cosh(A_{10})\sinh(A_{11})$$

$$A_{16} = \sinh(A_{10})\sinh(A_{11});$$

$$A_{17} = \cosh(A_{11}) - \sinh(A_{11});$$

$$A_{18} = \cosh(A_{11}) + \sinh(A_{11});$$

$$A_{19} = \sinh(A_{11}) - \cosh(A_{11});$$

$$A_{20} = \cosh(A_{10}) + \sinh(A_{10});$$

$$A_{21} = \cosh(A_{11})\,(1-C)\sinh(A_{11});$$

$$A_{22} = A_{13} + A_{14} + A_{15} + A_{16};$$

$$A_{23} = A_{17}\,A_{11}^2;$$

$$A_{24} = \frac{A_{17}\,(1-C)}{A_5};$$

$$A_{25} = \frac{A_{18}\,(1-C)}{A_5};$$

$$A_{26} = A_{24} - A_{25};$$

$$A_{27} = \sinh(A_{10})\sinh^3(A_{11});$$

$$A_{28} = A_{11}^2\cosh(A_{11});$$

$$A_{35} = \cosh(A_{10})\cosh^2(A_{11});$$

$$A_{36} = \sinh(A_{10})\sinh^2(A_{11});$$

$$A_{37} = A_{20}\,A_{30};$$

$$A_{38} = A_{35}\,A_{36};$$

$$A_{39} = A_{13}\,A_{27};$$

$$A_{40} = A_5\,A_{39};$$

$$A_{41} = A_{31} + A_{32};$$

$$A_{42} = A_{34}\cosh(A_{10});$$

$$A_{43} = A_5\,A_{38};$$

$$A_{44} = A_8\sinh(A_{10});$$

$$A_{45} = A_8\cosh(A_{10});$$

$$A_{46} = \frac{A_{45}}{2} - \frac{A_{44}}{2};$$

$$A_{47} = \sqrt{A_7}\,\mathrm{sech}(A_{11});$$

$$A_{48} = A_{18}\,A_{46};$$

$$A_{49} = \cosh(A_{10}) - \sinh(A_{10});$$

$$A_{50} = \sinh(A_{10}) - \cosh(A_{10});$$

$$A_{51} = A_{17}\,A_{50} + A_{18}\,A_{49};$$

$$A_{52} = A_{48} - A_{37};$$

$$A_{53} = A_{41}\,A_{51};$$

$$A_{54} = 64\,A_5\,A_{42};$$

$$A_{55} = A_{26}\,A_{41};$$

$$A_{56} = A_{11}^2\,A_{18};$$

$$A_{57} = \cosh(A_{11})\sinh(A_{11});$$

$$A_{58} = A_{33}\,\mathrm{sech}(A_{10});$$

$$A_{29} = A_{11}^2 \sinh(A_{11});$$

$$A_{30} = A_{28} - A_{29};$$

$$A_{31} = A_{11}^2 A_{18}^2$$

$$A_{32} = A_{19} A_{30};$$

$$A_{33} = A_9 (1 - C);$$

$$A_{34} = A_{16} \cosh^3(A_{11});$$

$$A_{65} = A_5 A_{55};$$

$$A_{66} == -4 A_{21} A_{23};$$

$$A_{67} = -4 A_{21} A_{30};$$

$$A_{68} = A_{65} + A_{66};$$

$$A_{69} = A_{65} + A_{67};$$

$$A_{70} = A_{22} A_{68} \sqrt{A_7};$$

$$A_{71} = A_{22} A_{69} \sqrt{A_7};$$

$$A_{59} = (4 A_{58} A_{52} - A_{53});$$

$$A_{60} = \frac{A_{58}}{4 A_{12}};$$

$$A_{61} = A_{47} - \gamma^2 \operatorname{sech}(A_{11});$$

$$A_{62} = A_{56} A_{59};$$

$$A_{63} = \frac{A_{33}}{4 A_{12}};$$

$$A_{64} = A_{63} \operatorname{sech}(A_{10});$$

$$A_{72} = 2 A_{38} + A_{39} + A_{42};$$

$$A_{73} = 128 A_{43} + A_{54};$$

$$A_{74} = 16 A_{72};$$

$$A_{75} = 64 A_{40};$$

$$A_{76} = A_{73} + A_{75};$$

$$A_{77} = A_5 A_{76}.$$

References

1. M. Farooq, M. T. Rahim, S. Islam, A. M. Siddiqui, Steady Poiseuille flow and heat transfer of Couple stress fluids between two parallel inclined plates with variable viscosity. Journal of Association of Arab Universities for Basic and Applied Sciences, 14 (2013) 9-18.
2. U. S. Mahabaleshwar, I. E. Sarris, A. Hill, G. Lorenzini, I. Pop, An MHD Couple stress fluid due to a perforated sheet undergoing linear stretching with heat transfer. International Journal of Heat and Mass Transfer, 105 (2017) 157–167.
3. H. Saad, E. A. Ashmawy, Unsteady plane Couette flow of an incompressible Couple stress fluid with slip boundary conditions. International Journal of Medical and Health Sciences, 3 (2016) 85-92.
4. S. Akhtar, N. A. Shah, Exact solutions for some unsteady flows of a Couple stress fluid between parallel plates. Ain Shams Engineering Journal, 9 (2018) 985–992.
5. N. A. Khan, H. Khan, S.A. Ali, Exact solutions for MHD flow of Couple stress fluid with heat transfer. Journal of Egyptian Mathematical Society, 24 (2016) 125–129.
6. S. Asghar, A. Ahmad, Unsteady Couette flow of viscous fluid under a non-uniform magnetic field. Applied Mathematics Letters, 25 (2012) 1953–1958.
7. W. Shaowei, X. Mingyu, Exact solution on unsteady Couette flow of generalized Maxwell fluid with fractional derivative. Acta Mechanica, 187 (2006)103–112.
8. A. S. Eegunjobi, O. D. Makinde, M. S. Tshehla, O. Franks, Irreversibility analysis of unsteady Couette flow with variable viscosity. Journal of Hydrodynamics, 27 (2015) 304–310.
9. R. Ellahi, X. Wang, M. Hameed, Effects of heat transfer and nonlinear slip on the steady flow of Couette fluid by means of Chebyshev Spectral Method. Zeitschrift fur Naturforschung A, 69 (2014) 1–8.
10. R. Ellahi, E. Shivanian, S. Abbasbandy, T. Hayat, Numerical study of magnetohydrodynamics generalized Couette flow of Eyring-Powell fluid with heat transfer and slip condition. International Journal of Numerical Methods of Heat Fluid Flows, 26 (2016) 1433–1445.
11. A. Zeeshan, N. Shehzad, R. Ellahi, Analysis of activation energy in Couette-Poiseuille flow of nanofluid in the presence of chemical reaction and convective boundary conditions. Results in Physics, 8 (2018) 502–512.

12. N. Shehzad, A. Zeeshan, R. Ellahi, Electroosmotic flow of MHD Power law Al2O3-PVC nanofluid in a horizontal channel: Couette-Poiseuille flow model. Communications in Theoratical Physics, 69(2018) 655–666.
13. F. Hussain, R. Ellahi, A. Zeeshan, K. Vafai, Modelling study on heated Couple stress fluid peristaltically conveying gold nanoparticles through coaxial tubes: A remedy for gland tumors and arthritis. Journal of Molecular Liquids, 268 (2018) 149–155.
14. R. Ellahi, A. Zeeshan, F. Hussain, A. Asadollahi, Peristaltic blood flow of Couple stress fluid suspended with nanoparticles under the influence of chemical reaction and activation energy. Symmetry, 11 (2019) 276-287.
15. R. Ellahi, M. M. Bhatti, C. Fetecau, K. Vafai, K. Peristaltic flow of Couple stress fluid in a non-uniform rectangular duct having compliant walls. Communications in Theoretical Physics, 65 (2016) 66–72.
16. V. Poply, P. Singh, A. K. Yadav, A study of temperature-dependent fluid properties on MHD free stream flow and heat transfer over a non-linearly stretching sheet. Procedia Engineering, 127 (2015) 391–397.
17. R. Ellahi, M. Raza, K. Vafai, Series solutions of non-Newtonian nanofluids with Reynolds model and Vogel's model by means of the homotopy analysis method. Mathematical and Computer Modelling, 55(2012) 1876–1891.
18. A. B. Disu, M. S. Dada, Reynolds model viscosity on radiative MHD flow in a porous medium between two vertical wavy walls. Journal of Taibah University for Sciences, 11(2017) 548–565.
19. S. Nadeem, M. Ali, Analytical solutions for pipe flow of a fourth-grade fluid with Reynolds and Vogel's models of viscosities. Communication in Nonlinear Science and Numerical Simulation, 14 (2009) 2073–2090.
20. R. Ellahi, A. Zeeshan, F. Hussain, T. Abbas, Thermally charged MHD bi-phase flow coatings with non-Newtonian nanofluid and Hafnium particles through slippery walls. Coatings, 9 (2019) 300-312.
21. M. A. Mahmoud, Chemical reaction and variable viscosity effects on flow and mass transfer of a non-Newtonian visco-elastic fluid past a stretching surface embedded in a porous medium. Meccanica, 45 (2010) 835–846.
22. O. D. Makinde, Laminar falling liquid film with variable viscosity along an inclined heated plate. Applied Mathematics and Computation, 175 (2006) 80–88.
23. M. Jawad, Z. Shah, S. Islam, J. Majdoubi, I. Tlili, W. Khan, I. Khan, Impact of nonlinear thermal radiation and the viscous dissipation effect on the unsteady three-dimensional

rotating flow of single-wall carbon nanotubes with aqueous suspensions. Symmetry, 11 (2019), 207-225.

24. R. Ellahi, A study on the convergence of series solution of non-Newtonian third grade fluid with variable viscosity: By means of homotopy analysis method. Advances in Mathematical Physics, (2012), 634925-935.
25. A. Karimipour, A. D. Orazio, M. S Shadloo, The effects of different nano particles of Al_2O_3 and Ag on the MHD nano fluid flow and heat transfer in a microchannel including slip velocity and temperature jump. Physics E, 86 (2017)146–153.
26. A. Zeeshan, N. Ijaz, T. Abbas, R. Ellahi, The sustainable characteristic of Bio bi-phase flow of peristaltic transport of MHD Jeffery fluid in human body, Sustainability, 10(8) (2017) 2671-2681.
27. H. Nasiri, M. Y. Jamalabadi, R. Sadeghi, M. R. Safaei, T. K. Nguyen, M. S. Shadloo, A smoothed particle hydrodynamics approach for numerical simulation of nano-fluid flows. Journal of Thermal Analysis and Calorimetry, (2018), 1–9.
28. M. R. Safaei, G. Ahmadi, M. S. Goodarzi, M. S. Shadloo, H. R. Goshayeshi, M. Dahari, Heat transfer and pressure drop in fully developed turbulent flows of graphene nanoplatelets–silver/water nanofluids. Fluids, 1 (2016) 20-29.
29. M. Marin, M. M. Maskeen, A. Zeeshan, O.U. Mehmood, M. Hassan, Hydromagnetic transport of iron nanoparticle aggregates suspended in water. Indian Journal of Physics, 93 (1) (2019) 53-59.
30. F. Garoosi, B. Rohani, M. M. Rashidi, Two-phase mixture modeling of mixed convection of nanofluids in a square cavity with internal and external heating. Powder Technology, 275 (2015) 304-321.
31. F. Selimefendigil, H. F. Öztop, Corrugated conductive partition effects on MHD free convection of CNT-water nanofluid in a cavity. International Journal of Heat and Mass Transfer, 129 (2019) 265-277.
32. M. Turkyilmazoglu, Exact solutions for two-dimensional laminar flow over a continuously stretching or shrinking sheet in an electrically conducting quiescent couple stress fluid. International Journal of Heat and Mass Transfer, 72 (2014) 1-8.
33. I. Pop, R. S. R. Gorla, M. Rashidi, The effect of variable viscosity on flow and heat transfer to a continuous moving flat plate. International Journal of Engineering Science, 30 (1) (1992) 1-6.

34. S. E. Charm, G. S. Kurland, Blood Flow and Microcirculation; Wiley: New York, USA, 1974.
35. R. Akhter, M. M. Ali, Md. B. Hossain, M. M. Miah, MHD free convection boundary layer flow over an inclined heated flat plate with thermal radiation effect, American Journal of Fluid Dynamics, 7(2017) 41-48.
36. N. F. M. Noor, S. Abbasbandy, I. Hashim, Heat and mass transfer of thermophoretic MHD flow over an inclined radiate isothermal permeable surface in the presence of heat source/sink, International Journal of Heat and Mass Transfer, 55 (2012) 2122-2128.
37. G. K. Ramesh, B. J. Gireesha, C. S. Bagewadi, Heat transfer in MHD dusty boundary layer flow over an inclined stretching sheet with Non-uniform heat source/sink. Advances in Mathematical Physics, (2012) 233-246.
38. P. Ganesan, G. Palani, Finite difference analysis of unsteady natural convection MHD flow past an inclined plate with variable surface heat and mass flux. International Journal of Heat and Mass Transfer, 47 (2004) 4449–4457.
39. H. Kumar, Heat and mass transfer on isothermal inclined porous plate in the presence of chemical reaction. International Journal of Pure and Applied Mathematics, 113 (5) (2017) 523-539.
40. A. Sh. Kherbeet, H. A. Mohammed, H. E. Ahmed, B. H. Salman, O. A. Alawi, M. R. Safaei, M. T. Khazaal, Mixed convection nanofluid flow over microscale forward-facing step-Effect of inclination and step heights. International Communication of Heat and Mass Transfer, 78 (2016) 145-154.
41. A. A Khan, F. Masood, R. Ellahi, M. M. Bhatti, Mass transport on chemicalized fourthgrade fluid propagating peristaltically through a curved channel with magnetic effects. Journal of Molecular Liquids, 258 (2018) 186-195.
42. M. Turkyilmazoglu, Heat and mass transfer of MHD second order slip flow. Computers and Fluids, 71 (30) (2013) 426-434
43. M. M. Rashidi, B. Rostami, N. Freidoonimehr, S. Abbasbandy, Free convective heat and mass transfer for MHD fluid flow over a permeable vertical stretching sheet in the presence of the radiation and buoyancy effects. Ain Shams Engineering Journal, 5 (3) (2014) 901-912.
44. M. Abdulhameed, D. Vieru, R. Roslan, Magnetohydrodynamic electroosmotic flow of Maxwell fluids with Caputo–Fabrizio derivatives through circular tubes. Computers and Mathematics with Applications, 74 (10) (2017) 2503-2519.

45. F. Selimefendigil, H. F. Oztop, A. J. Chamkha, MHD mixed convection in a nanofluid filled vertical lid-driven cavity having a flexible fin attached to its upper wall. Journal of Thermal Analysis and Calorimetry, 135 (1) (2019) 325–340.
46. K. A. Hakeem, S. Saranya, B. Ganga, Comparative study on Newtonian/non-Newtonian base fluids with magnetic/non-magnetic nanoparticles over a flat plate with uniform heat flux. Journal of Molecular Liquids, 230 (2017) 445–452.
47. A. Malvandi, M. R. Safaei, M. H. Kaffash, D. D. Ganji, MHD mixed convection in a vertical annulus filled with Al2O3–water nanofluid considering nanoparticle migration. Journal of Magnetism and Magnetic Materials, 382 (2015) 296–306.
48. R. Ellahi, M. H. Tariq, M. Hassan, K. Vafai, On boundary layer magnetic flow of nano-Ferroliquid under the influence of low oscillating over stretchable rotating disk. Journal of Molecular Liquids, 229 (2017) 339-345.
49. J. Prakash, D. Tripathi, Electroosmotic flow of Williamson ionic nanoliquids in a tapered microfluidic channel in presence of thermal radiation and peristalsis. Journal of Molecular Liquids, 256 (2018) 352-371.
50. D. Tripathi, R. Jhorar, O. A. Beg, A. Kadir, Electro-magneto-hydrodynamic peristaltic pumping of Couple stress biofluids through a complex wavy micro-channel. Journal of Molecular Liquids, 236 (2017) 358–367.
51. G. J. Reddy, M. Kumar, B. Kethireddy, A. J. Chamkha, Colloidal study of unsteady magnetohydrodynamic Couple stress fluid flow over an isothermal vertical flat plate with entropy heat generation. Journal of Molecular Liquids, 252 (2018) 169–179.
52. M. M. Rashidi, S. Abelman, N. F. Mehr, Entropy generation in steady MHD flow due to a rotating porous disk in a nanofluid. International Journal of Heat and Mass Transfer, 62 (2013) 515-525.
53. F. Selimefendigil, H. F. Öztop, Effects of an inner stationary cylinder having an elastic rod-like extension on the mixed convection of CNT-water nanofluid in a three dimensional vented cavity. International Journal of Heat and Mass Transfer, 137 (2019) 650-668.
54. C. S. Balla, N. Kishan, R. S. R. Gorla, B. J. Gireesha, MHD boundary layer flow and heat transfer in an inclined porous square cavity filled with nanofluids. Ain Shams Engineering Journal, 8 (2) (2017) 237-254.
55. M. Hassan, M. Marin, A. Alsharif, R. Ellahi, Convective heat transfer flow of nanofluid in a porous medium over wavy surface. Physics Letters A, 382 (38) (2018) 2749-2753.

56. B. J. Gireesha, R. S. R. Reddy. Gorla, B. Mahanthesh, Effect of suspended nanoparticles on three-dimensional MHD flow, heat and mass transfer of radiating Eyring-Powell fluid over a stretching sheet. Journal of Nanofluids, 4 (4) (2015) 474-484.

57. B. J. Gireesha, B. Mahanthesh, P. T. Manjunatha, R. S. R. Gorla, Numerical solution for hydromagnetic boundary layer flow and heat transfer past a stretching surface embedded in non-Darcy porous medium with fluid-particle suspension. Journal of the Nigerian Mathematical Society, 34 (3) (2015) 267-285.

58. M. H. Esfe, H. Rostamian, Non-Newtonian power-law behavior of TiO2/SAE 50 nanolubricant: An experimental report and new correlation. Journal of Molecular Liquids, 232 (2017) 219–225.

59. H. R. Goshayeshi, M. Goodarzi, M. R. Safaei, M. Dahari, Experimental study on the effect of inclination angle on heat transfer enhancement of a ferrofluid in a closed loop oscillating heat pipe under magnetic field. Experimental and Thermal Fluid Science, 74 (2016) 265–270.

60. F. Hussain, R. Ellahi, A. Zeeshan, Mathematical models of electro-magnetohydrodynamic multiphase flows synthesis with nano-sized Hafnium particles. Applied Sciences, 8 (2) (2018) 275-293.

61. R. L. Nichols, Viscosity of lava. Journal of Geology, 47 (3) (1939) 290-302.

62. O. Melnik and R. S. J. Sparks, Nonlinear dynamics of lava dome extrusion. Nature, 402 (1999) 37-41.

63. J. G. Moore, D. A. Clague, Volcano growth and evolution of the island of Hawaii. Geological Society of America Bulletin, 104 (1992) 1471-1484.

64. S. Diniega, S. E. Smrekar, S. Anderson, E. R. Stofan, The influence of temperature dependent viscosity on lava flow dynamics. Journal of Geophysical Research, 118 (2013) 1516-1532.

65. G. Palani, U. Srikanth, MHD flow past a semi-infinite vertical plate with mass transfer nonlinear analysis: Modelling and Control, 14(3) (2009) 345–356.

66. S. R. Kumar, Effect of Couple stress fluid flow on magnetohydrodynamic peristaltic blood flow with porous medium through inclined channel in the presence of slip effect - Blood flow model. International Journal of Bio-Science and Bio-Technology, 7(5) (2015) 65-84.

67. R. V. M. Kumar, G. V. Kumar, C. S. K. Raju, S. A. Shehzad, S. V. K. Varma, Analysis of Arrhenius activation energy in magnetohydrodynamic Carreau fluid flow through

improved theory of heat diffusion and binary chemical reaction. Journal of Physics Communication, 2 (2018) 35–49.

68. N. Murti, D. K. Sastry, P. K. Kameswaran, T. P. Kantha, Effects of mixed convection and double dispersion on semi-infinite vertical plate in presence of radiation. International Journal of Mathematical and Computational Sciences, 5(12) (2011) 56-66.
69. S. Ghosh, R. Usha, Stability of viscosity stratified flows down an incline: Role of miscibility and wall slip. Physics of Fluids, 28 (10) (2016) 36-42.
70. G. Bognar, I. Gombkoti, K. Hriczo, Power-law non-Newtonian fluid flow on an inclined plane. International Journal of Mathematical Models and Methods in Applied Sciences, 6 (1) (2012) 72-80.
71. A. Ganguly, M. Reza, A. S. Gupta, Thin-film flow of a Power-Law fluid down an inclined plane. Journal of Fluids Engineering, 134(4) (2012) 34-38.
72. M. J. Uddin, Convective flow of Micropolar fluids along an inclined flat plate with variable electric conductivity and uniform surface heat flux. Daffodil International University Journal of Science and Technology, 6(1) (2011) 69-79.
73. A. A. Khan, S. R. Bukhari, M. Marin, R. Ellahi, Effects of chemical reaction on third-grade MHD fluid flow under the influence of heat and mass transfer with variable reactive index. Heat Transfer Research, 50 (11) (2019) 1061-1080.
74. M. Sheikholeslami, K. Vajravelu, M. M. Rashidi, Forced convection heat transfer in a semi annulus under the influence of a variable magnetic field. International Journal of Heat and Mass Transfer, 92 (2016) 339-348.
75. M. M. Rashidi, M. Ali, N. Freidoonimehr, F. Nazari, Parametric analysis and optimization of entropy generation in unsteady MHD flow over a stretching rotating disk using artificial neural network and particle swarm optimization algorithm. Energy, 55 (15) (2013) 497-510.
76. M. Turkyilmazoglu, MHD fluid flow and heat transfer due to a stretching rotating disk. International Journal of Thermal Sciences, 51 (2012) 195-201.
77. D. Vieru, C. Fetecau, A. Sohail, Flow due to a plate that applies an accelerated shear to a second grade fluid between two parallel walls perpendicular to the plate. Zeitschrift für angewandte Mathematik und Physik, 62 (1) (2011) 161-172.
78. M. Turkyilmazoglu, Unsteady convection flow of some nanofluids past a moving vertical flat plate with heat transfer. Journal of Heat Transfer 136 (3) (2014) 0317041-7.

79. C. Fetecau, C. Fetecau, M. Kamran, D. Vieru, Exact solutions for the flow of a generalized Oldroyd-B fluid induced by a constantly accelerating plate between two side walls perpendicular to the plate. Journal of Non-Newtonian Fluid Mechanics 156 (3) (2009) 189-201.
80. M. Turkyilmazoglu, Unsteady MHD flow with variable viscosity: Applications of spectral scheme. International Journal of Thermal Sciences, 49 (3) (2010) 563-570.
81. K. L. Lakshmi, B. J. Gireesha, R. S. R. Gorla, B. Mahanthesh, Effects of diffusion-thermo and thermo-diffusion on two-phase boundary layer flow past a stretching sheet with fluid-particle suspension and chemical reaction: A numerical study. Journal of the Nigerian Mathematical Society, 35 (1) (2016) 66-81.
82. F. S,elimefendigil, H. F. Öztop, Effects of phase shift on the heat transfer characteristics in pulsating mixed convection flow in a multiple vented cavity. Applied Mathematical Modelling, 39 (13) (2015) 3666-3677.
83. A. Sohail, D. Vieru, M. A. Imran, Influence of side walls on the oscillating motion of a Maxwell fluid over an infinite plate. Mechanics, 19 (3) (2013) 269-276.
84. D. Vieru, C. Fetecau, M. Athar, C. Fetecau, Flow of a generalized Maxwell fluid induced by a constantly accelerating plate between two side walls. Zeitschrift für angewandte Mathematik und Physik 60 (2) (2009) 334-343.
85. F. S,elimefendigil, S. Föller, W. Polifke, Nonlinear identification of unsteady heat transfer of a cylinder in pulsating cross flow. Computers and Fluids, 53 (15) (2012) 1-14.
86. M. Hassan, M. Marin, R. Ellahi, S. Z. Alamri, Exploration of convective heat transfer and flow characteristics synthesis by Cu-Ag/water hybrid-nanofluids. Heat Transfer Research, 49 (18) (2018)1837-1848.
87. A. Majeed, A. Zeeshan, S. Z. Alamri, R. Ellahi, Heat transfer analysis in ferromagnetic viscoelastic fluid flow over a stretching sheet with suction. Neural Computing and Applications, 30 (6) (2018) 1947–1955.
88. M. Nawaz, A. Zeeshan, R. Ellahi, S. Abbasbandy, S. Rashidi, Joules heating effects on stagnation point flow over a stretching cylinder by means of genetic algorithm and Nelder-Mead method. International Journal of Numerical Methods for Heat and Fluid Flow, 25 (3) (2015) 665-684.
89. N. Shehzad, A. Zeeshan, R. Ellahi, Electroosmotic flow of MHD Power law Al2O3-90 PVC nanofluid in a horizontal channel: Couette-Poiseuille flow model. Communications in Theoretical Physics, 69 (6) (2018) 655-666.

90. K. M. Shirvan, M. Mamourian, S. Mirzakhanlari, A. B. Rahimi, R. Ellahi, Numerical study of surface radiation and combined natural convection heat transfer in a solar cavity receiver. International Journal of Numerical Methods for Heat and Fluid Flow, 27 (10) (2017) 2385-2399.
91. J. Umavathi, J. P. Kumar, I. Pop, M. Shekar, Flow and heat transfer of Couple stress fluid in a vertical channel in the presence of heat source/sink. International Journal of Numerical Methods for Heat and Fluid Flow, 27(4) (2017) 795-819.
92. S. U. S. Choi, J. A. Eastman, Enhancing thermal conductivity of fluids with nanoparticles, ASME-Publications- Fed. 231 (1995) 99–106.
93. M. Sheikholeslami, Numerical modeling of nano enhanced PCM solidification in an enclosure with metallic fin. Journal of Molecular Liquids, 259 (2018) 424–438.
94. R. U. Haq, Z.H. Khan, S.T. Hussain, Z. Hammouch, Flow and heat transfer analysis of water and ethylene glycol-based Cu nanoparticles between two parallel disks with suction/injection effects. Journal of Molecular Liquids, 221 (2016) 298–304.
95. J. Buongiorno, W. Hu, Nanofluid coolants for advanced nuclear power plant, Proceedings of ICAPP, 5705 (2005) 15–19.
96. J. Buongiorno, Convective transport in nanofluids. Journal of Heat Transfer, 128 (2006) 240–250.
97. H. Xu, T. Fan, I. Pop, Analysis of mixed convection flow of a nanofluid in a vertical channel with the Buongiorno mathematical model. International Communications in Heat and Mass Transfer, 44 (2013) 15–22.
98. K. Mekheimer, W. Hasona, R. E. Abo-Elkhair, A. Zaher, Peristaltic blood flow with gold nanoparticles as a third grade nanofluid in catheter: Application of Cancer Therapy. Physics Letters A, 382 (2018) 85–93.
99. S. U. Rehman, R. Ellahi, S. Nadeem, Q. M. Zaigham Zia, Simultaneous effects of nanoparticles and slip on Jeffrey fluid through tapered artery with mild stenosis. Journal of Molecular Liquids, 218 (2016) 484–493.
100. Z. Xu, C. Kleinstreuer, Direct nano-drug delivery for tumor targeting subject to shear-augmented diffusion in blood flow. Medical and Biological Engineering and Computing, 56 (2018) 1949–1958.
101. T. M. Nabil, N.T.M. El-dabe, G. M. Moatimid, M. A. Hassan, W. A. Godh, Wall properties of peristaltic MHD Nanofluid flow through porous channel. Fluid Mechanics Research International Journal, 2 (2018)19-38.

102. D. Tripathi, O. A. Beg, A study on peristaltic flow of nanofluids: Application in drug delivery systems. International Journal of Heat and Mass Transfer, 70 (2014) 61–70.
103. G. C. Shit, M. Roy, Hydromagnetic effect on inclined peristaltic flow of a Couple stress fluid, Hydromagnetic effect on inclined peristaltic flow of a Couple stress fluid. Alexandria Engineering Journal, 53 (2014) 949–958.
104. M. Y. A. Jamalabadi, M. Daqiqshirazi, H. Nasiri, M. R. Safaei, T. K. Nguyen, Modeling and analysis of biomagnetic blood Carreau fluid flow through a stenosis artery with magnetic heat transfer: A transient study. Plos One, 13 (2018) e0192138.
105. S. M. Hosseini, M. R. Safaei, M. Goodarzi, A. A. A. Alrashed, T. K. Nguyen, New temperature interfacial shell dependent dimensionless model for thermal conductivity of nanofluids. International Journal of Heat and Mass Transfer, 114 (2017) 207–210.
106. S. Rashidi, S. Akar, M. Bovand, R. Ellahi, Volume of fluid model to simulate the nanofluid flow and entropy generation in a single slope solar still. Renewable Energy, 115 (2018) 400–410.
107. A. Zeeshan, A. Majeed, R. Ellahi, Effect of magnetic dipole on viscous ferro-fluid past a stretching surface with thermal radiation. Journal of Molecular Liquids, 215 (2016) 549–554.
108. M. M. Bhatti, M. M. Rashidi, Effects of thermo-diffusion and thermal radiation on Williamson nanofluid over a porous shrinking/stretching sheet. Journal of Molecular Liquids, 221 (2016) 567–573.
109. R. Ellahi, M. Hassan, A. Zeeshan, Shape effects of spherical and non-spherical nanoparticles in mixed convection flow over a vertical stretching permeable sheet. Mechanics of Advanced Material and Structure, 24 (2017) 1231–1238.
110. R. Ellahi, A. Zeeshan, N. Shehzad, Sultan Z. Alamri, Structural impact of Kerosene-Al2O3 nanoliquids on MHD Poiseuille flow with variable thermal conductivity: application of cooling process. Journal of Molecular Liquids, 264 (2018) 607–615.
111. M. R. Safaei, G. Ahmadi, M. S. Goodarzi, M. S. Shadloo, H.R. Goshayeshi, M. Dahari, Heat transfer and pressure drop in fully developed turbulent flows of graphene nanoplatelets–silver/water nanofluids. Fluids, 1 (2016) 20-41.
112. S. T Mohyud-Din, U. Khan, N. Ahmed, S. M. Hassan, Magnetohydrodynamic flow and heat transfer of nanofluids in stretchable convergent/divergent channels. Applied Sciences, 5 (2015) 1639–1664.
113. A. J. Chamkha, F. Selimefendigil, F. Forced convection of pulsating nanofluid flow over a backward facing step with various particle shapes. Energies, 11 (2018) 3068.

114. M. M. Rashidi, M. Nasiri, M. S. Shadloo, Z. Yang, Entropy generation in a circular tube heat exchanger using nanofluids: Effects of different modeling approaches. Heat Transfer Engineering, 38 (2017) 853–866.

115. M. Marin, An approach of a heat-flux dependent theory for micropolar porous media. Meccanica, 51 (2016) 127–1133.

116. A. Zeeshan, N. Ijaz, T. Abbas, R. Ellahi, The sustainable characteristic of Bio-bi-phase flow of peristaltic transport of MHD Jeffery fluid in human body. Sustainability, 10(8) (2018) 1-17.

117. F. Hussain, R. Ellahi, A. Zeeshan, A. Mathematical models of electro magnetohydrodynamic multiphase flows synthesis with nanosized hafnium particles. Applied Sciences, 8 (2018) 275-293.

118. S. Anuradha, M. Yegammai, MHD radiative boundary layer flow of nanofluid past a vertical plate with effects of binary chemical reaction and activation energy. Journal of Pure and Applied Mathematics, 13 (2017) 6377–6392.

119. M. Mustafa, J. A. Khan, T. Hayat, A. Alsaedi, A. Buoyancy effects on the MHD nanofluid flow past a vertical surface with chemical reaction and activation energy. International Journal of Heat and Mass Transfer, 108 (2017) 1340–1346.

120. V. K. Stokes, *Theories of Fluids with Microstructure: An Introduction*, Springer-Verlag,1984.

121. N. Ashrafi, R. E. Khayat, A low-dimensional approach to nonlinear plane-Couette flow of viscoelastic fluids. Physics of Fluids, 12 (2000) 345–365.

122. L. M. Srivastava, V. P. Srivastava, Peristaltic transport of a particle-fluid suspension. Journal of Biomechanical Engineering, 111(1989) 157–165.

123. C. K. W. Tam, The drag on a cloud of spherical particles in a low Reynolds number flow. Journal of Fluid Mechanics, 38 (1969) 537–546.

124. R. Ellahi, The effects of MHD and temperature dependent viscosity on the flow of non-Newtonian nanofluid in a pipe: Analytical solutions. Applied Mathematical Modelling, 37 (2013) 1451–1457.

125. N. Nalinakshi, P. A. Dinesh, D. V. Chandrashekar, Shooting method to study mixed convection past a vertical heated plate with variable fluid properties and internal heat generation. Mapana Journal of Sciences, 13(3) (2014) 31-50.

126. O. D. Makinde, O. O. Onyejekwe, A numerical study of MHD generalized Couette flow and heat transfer with variable viscosity and electrical conductivity. Journal of Magnetism and Magnetic Materials, 323 (2011) 2757–2763.

127. B. V. Swarnalathamma, M. V. Krishna, Peristaltic hemodynamic flow of Couple stress fluid through a porous medium under the influence of magnetic field with slip effect. AIP Conference Proceedings, 1728 (2016) 0206031–0206039.

128. M. P. Coelho, J. S. Faria, On the generalized Brinkman number definition and its importance for Bingham fluids. Journal of Heat Transfer, 133 (2011) 545051–545055.

129. Kh. S. Mekheimer, Y. Abd Elmaboud, Peristaltic flow of a Couple stress fluid in an annulus: Application of an endoscope. Physica A, 387 (2008) 2403–2415.

130. B. J. Gireesha, B. Mahanthesh, G.T. Thammanna, P. B. Sampathkumar, Hall effects on dusty nanofluid two-phase transient flow past a stretching sheet using KVL model. Journal of Molecular Liquids, 256 (2018) 139-147.

131. Y. K. Chung, H. H. Chun, On the planning of a flat plate at high Froude numbers in a two-dimensional case, Ocean Engineering 35 (2008) 646-652.

132. D. Srinivasacharya, K. Kaladhar, Mixed convection flow of Couple stress fluid in a non-Darcy porous medium with Soret and Dufour effects. Journal of Applied Science and Engineering, 15 (4) (2012) 415-422.

133. R. A. Van Gorder, K. Vajravelu, On the selection of auxiliary functions, operators, and con-vergence control parameters in the application of the homotopy analysis method to nonlinear differential equations: a general approach. Communications in Nonlinear Science Numerical Simulation, 14 (2009) 4078–4089.

134. S. J. Liao, Beyond Perturbation: Introduction to homotopy analysis method, Chapman & Hall, Boca Raton, (2003).

135. Y. Zhao, S. Liao, HAM-based Mathematica package BVPh 2.0 for nonlinear boundary value problems, Advances in the homotopy analysis method World Scientific Press, (2013) 361.

136. N. T. Eldabe, A. M. Sedki, I. K. Youssef, Numerical solutions for boundary layer fluid flow with mass transfer over a moving permeable flat plate embedded in porous medium with variable wall concentration in presence of chemical reaction. American Journal of Computational and Applied Mathematics, 4 (4) (2014) 141-153.

Turnitin Originality Report

Study of Multiphase Flows Through Different Geometries by Farooq Hussain

From PhD Thesis (PhD Mathematics-1)

turnitin

- Processed on 05-Dec-2019 12:15 PKT
- ID: 1227564124
- Word Count: 23855

Similarity Index
13%
Similarity by Source

Internet Sources:
7%
Publications:
6%
Student Papers:
10%

Shakeel Ahmed
Superintendent
International Islamic University
Islamabad

sources:

1 1% match (student papers from 14-Dec-2018)
Class: PhD Mathematics
Assignment: Thesis
Paper ID: 1056936089

2 1% match (student papers from 13-Dec-2018)
Class: PhD Mathematics
Assignment: Thesis
Paper ID: 1056270579

3 1% match (Internet from 15-Nov-2019)
https://www.mdpi.com/2079-6412/9/5/300/htm

4 < 1% match (Internet from 27-Nov-2019)
https://www.emerald.com/insight/content/doi/10.1108/HFF-11-2018-0677/full/html

5 < 1% match (Internet from 31-Jul-2019)
https://www.mdpi.com/2073-8994/11/5/647

6 < 1% match (student papers from 22-Jul-2019)
Submitted to Higher Education Commission Pakistan on 2019-07-22

7 < 1% match (student papers from 03-Oct-2019)
Submitted to University of KwaZulu-Natal on 2019-10-03

8 < 1% match (student papers from 21-Dec-2015)